Universal phase-field mixture representation of thermodynamics and shock-wave mechanics in porous soft biologic continua

J. D. Clayton ◉*

Terminal Effects Division, DEVCOM ARL, Aberdeen Proving Ground, Maryland 21005-5066, USA

A continuum mixture theory is formulated for large deformations, thermal effects, phase interactions, and degradation of soft biologic tissues suitable at high pressures and low to very high strain rates. Tissues consist of one or more solid and fluid phases and can demonstrate nonlinear anisotropic elastic, viscoelastic, thermoelastic, and poroelastic physics. Under extreme deformations or shock loading, tissues may fracture, tear, or rupture. Existing models do not account for all physics simultaneously, and most poromechanics and soft-tissue models assume incompressibility of some or all constituents, generally inappropriate for modeling shock waves or extreme compressions. Motivated by these prior limitations, a thermodynamically consistent formulation that combines a continuum theory of mixtures, compressible nonlinear anisotropic thermoelasticity, viscoelasticity, and phase-field mechanics of fracture is constructed to resolve the pertinent physics. A metric tensor of generalized Finsler space supplies geometric insight on effects of rearrangements of microstructure, for example degradation, growth, and remodeling. Shocks are modeled as singular surfaces. Hugoniot states and shock decay are analyzed: Solutions account for concurrent viscoelasticity, fracture, and interphase momentum and energy exchange not all contained in previous analyses. Suitability of the framework for representing blood, skeletal muscle, and liver is demonstrated by agreement with experimental data and observations across a range of loading rates and pressures. Insight into previously unresolved physics is obtained, for example importance of rate sensitivity of damage and quantification of effects of dissipation from viscoelasticity and phase interactions on shock decay.

I. INTRODUCTION

Constitutive models describe the complex physics of soft biological tissue—for example, skin, muscle, connective tissue, blood vessels, and the internal organs—when subject to mechanical and thermal stimuli. These materials are often simultaneously nonlinear anisotropic elastic, viscoelastic, thermoelastic, and poroelastic [1,2]. Large deformations manifesting nonlinear mechanical response occur even under normal physiological activity. Medical events involving disease and surgery incur cutting or tearing (i.e., fracture) of the tissue. For traumatic scenarios involving dynamic impact or blast, even more extreme deformations and rapid loading rates arise [1,3–6].

Microstructures are often hierarchical and highly complex [1,2]. Materials consist of multiple solid- and fluidlike phases. The liver includes the spongy parenchyma, connective tissue, blood vessels and ducts plus blood and bile [7]. Skeletal and cardiac muscles contain fibers (i.e., cells), connective tissue, blood and interstitial fluid [2,8]. Skin includes dermal tissue layers, cells, and interstitial fluid [9]. Lung includes parenchyma (e.g., alveoli and ducts), air, and surfactant fluid, as well as stiffer elements of the bronchiole. structure [1]. Membraneous tissues (e.g., in skin) contain ground substance, elastin, and collagen fibers [10]. Blood has cells immersed in the extracellular plasma [2,11]. Cells themselves include solidlike walls and internal fluids [12].

Most constitutive treatments of mechanics of soft tissues focus on their nonlinear elastic response [8,13,14]. Effects of fluids are included implicitly in the energy densities and parameters, perhaps augmented with viscoelasticity or other dissipation elements [15,16]. Even in the nondissipative case, sophisticated models are needed to account for anisotropy and nonlinearity, for example due to collagen fiber distributions [17–19]. If tearing or degradation occur, then continuum damage mechanics theories are fairly standard [20,21], whereby a phenomenological kinetic equation is prescribed for an internal state variable measuring local loss of stress-bearing capacity.

In contrast to the former, the phase-field approach has been more recently advocated for modeling tearing of soft biologic tissues [22,23]. Diffuse-interface modeling has witnessed use over a broad application space; models with elasticity include phase changes, twinning, and dislocations in crystals [24–27]. The method appeared for brittle fracture around 25 years ago [28–30], typically for small-strain, isotropic elasticity theory. Finite-strain approaches for fracture appeared thereafter [31,32]. Fluid cavitation [33] and fluid injection [34] have been modeled.

Continuum mixture theories and porous media theories emerged in the mid-20th century [35–38]. Microstructure details are smeared, but these models distinguish stresses and deformations of each constituent and capture transfers

---

*Contact author: john.d.clayton1.civ@army.mil

of mass, momentum, and energy between phases. Mixture- and porous-media theories introduce length and timescales that are absent in single-phase viscoelasticity [39]. Although porous media models have been used for soft tissues [7,39–41], they have not been combined with the phase-field fracture approach for the class of soft biologic materials. Finite strain and thermal exchange [42] effects have, however, been considered for phase-field fracture modeling of brittle porous media.

The theory of porous media classically models a two-phase system of one solid and one fluid, though models with multiple fluids exist. The fully dense solid and fluid phases are usually treated as incompressible, but the mixture overall is compressible as fluid is locally squeezed out [7,39,40]. Solid and fluid are usually, but not always [43], treated as inviscid individually, but interactions of viscous origin between phases are captured by permeability and dissipation from fluid transport (e.g., Darcy's law). An effective stress principle [44] decomposes total stress into solid skeleton stress and pore pressure. Constitutive equations are supplied for the solid skeleton (i.e., drained material) and fully dense fluid rather than for partial stresses of mixture components. This method has proven successful for soil and rock mechanics in which the distinction between solid and fluid(s) is clear (e.g., water flowing through sand or porous rock), and it has been used elsewhere for porous tissues [39,40].

The effective stress principle with solid skeleton concept is not implemented here for several reasons. First, tissue may consist of multiple solid and fluid phases. For example, the liver has the parenchyma, blood vessels, and connective tissue (which might be tied or displace independently) and distinct fluids of blood and bile. Second, designation of a constituent as a "solid" or "fluid" may be ambiguous, for example, the extracellular matrix of tissue or blood demonstrating both viscous (fluidlike) and viscoelastic (solidlike) physics [11,45]. With no single true solid or fluid phase, the soil mechanics analogy is tenuous. Cracking in ambiguously soft materials also shows richer physics than in brittle elastic solids due to stochastic bond opening and closure (i.e., healing) [46].

A mixture theory similar to that of Refs. [37,47,48] is advocated here instead, with constituent energies formulated on a per-unit-mass basis. Complexity in thermodynamic derivations is reduced since partial stresses rather than effective stress and pore pressure are used. However, potential difficulty can arise in ascertaining properties of isolated phases as experiments might measure responses of only some (e.g., fluid) phase(s) and the mixture as a whole. This issue is rectified by example later.

Here the typical assumption of incompressibility of individual phases [7,39,40] is abandoned to resolve bulk sound waves and longitudinal shocks. Furthermore, in a two-phase nonreactive mixture of a solid and fluid, incompressibility of the "real" solid phase restricts local compression to not exceed the porosity (i.e., an initial fluid volume fraction) [49,50]. For biologic systems modeled later with porosities $\approx 10\%$, solid incompressibility is incompatible with strong shock loading [51]. If no interphase mass exchange occurs, then the system is closed (i.e., no mass flux across boundaries), and all constituents are truly incompressible, global volumetric compression is impossible.

Incompressibility is unrealistic if materials rupture or cavitate (i.e., tensile damage).

A unified framework is formulated in Secs. II and III, synthesizing continuum mixture theory, nonlinear anisotropic thermoelasticity, viscosity, viscoelasticity, and phase-field fracture mechanics for biologic systems. A universal, thermodynamically consistent theory containing all such features relevant to soft-tissue mechanics for intense rapid loading does not seem to exist. Another notable aspect is generalized Finsler geometry describing the material manifold with evolving microstructure [52].

Traditional continuum models are couched in ambient Euclidean three-space. Residual stresses from growth or remodeling have been considered via Riemannian geometry with a metric of nonvanishing curvature tensor [53–55]. A recent approach [56,57] accounts for effects of microstructure using a generalized Finslerian metric [58] as opposed to a Riemannian metric. In addition to residual stress and growth, the Finsler-geometric approach on the material manifold has been used to describe changes in local configurations of collagen fibers as tissues degrade and tear [52]. A Finsler metric was used elsewhere to quantify effects of fiber orientations on mechanical responses of soft tissues in a discrete bond-based model [59] rather than a continuum physics approach as herein. The Finsler-geometric theory has similarities to micropolar theory [60,61], but the former is more general [56]. Much past work focused on hard crystalline solids [62,63].

Shock waves in soft tissues are analyzed here with the mixture theory and constitutive frameworks. Hugoniot solutions and evolution equations are derived for compressive shocks, extending prior works [50,64–66] to simultaneously account for internal state variables (e.g., order parameters) and the Finsler metric that, in the present application, can be transformed to an osculating Riemannian metric [52,67,68]. Dissipation from viscoelasticity, momentum and energy transfer between phases, and degradation due to shear-induced tearing all potentially affect shock amplitudes over time. Treatment of shocks as singular surfaces of velocity differs from those of continuous waves in nonlinear materials [69]. Shock structures (e.g., shapes of continuous waves) are studied elsewhere in nonlinear solids and fluid mixtures [48].

Modeled in Sec. IV are three soft-tissue systems: skeletal muscle with interstitial fluid, liver with blood, and lung with air. Solutions to physical problems involving tension, compression, or shock-wave loading grant understanding of the physics demonstrated by these materials. Concluding remarks give closure in Sec. V.

II. GOVERNING EQUATIONS

The present theory builds on the finite-strain mixture theories of Refs. [37,38,50]. This framework of Bowen [37], with origins in the treatise of Truesdell and Toupin [36] and consistent with the rational thermodynamics philosophy of Truesdell *et al.* [70], is used as starting point for several reasons. First, this framework is of sufficient generality, on several augmentations discussed shortly, to describe all physical phenomena of present interest. Second, although other rigorous mixture theories exist and numerous generalizations and specializations of the Bowen-Truesdell framework have

been postulated, especially with regard to thermodynamics (see, e.g, discussion in Refs. [71,72], and references therein), the original theory was then, and still is, widely accepted as physically credible and mathematically "correct" [37].

To the same extent as the original theories [36,37,70], the present framework obeys the three principles of mixture theory emphasized in Ref. [70], paraphrased as follows: (1) All properties of the mixture are mathematically obtained from properties of its constituents, (2) each constituent's behaviors can be described by governing equations for that single constituent, provided these equations account for its interactions with other constituents; and (3) behavior of the mixture obeys governing equations of the same form as those for a single-constituent body. The third principle constrains interactions and suggests definitions for "average" quantities of the mixture as a whole. The latter are not unique [73], nor even all exist. For example, average (e.g., tensor-valued) quantities referred to "material" coordinates may not exist, there being no unique reference configuration of the mixed system when velocity histories of constituents differ or mass supplies exist [74,75]. Average temperature is not well defined in Ref. [37] unless all constituents share the same temperature, but it has been defined elsewhere [76].

Two main enhancements are incorporated here. First, time-dependent general internal state vectors are introduced. Elements of these vectors are associated with history dependent mechanisms in the material microstructure, namely viscoelasticity, active tension, and damage, all generally anisotropic. Dependence of energy potentials on internal state and gradients of internal state is permitted, with terms associated with internal state gradients incorporated in the balance of energy and boundary conditions. This enables a phase-field type representation if variables are interpreted as order parameters [24,26,77], suitable for modeling regularized fracture [23,31,32]. Second, metric tensors on spatial and material manifolds may depend on internal state and can be time dependent. Distances measured in the material can include remnant strains from dissipative processes, or biologic growth and remodeling if resolved by state variables. If internal-state dependence of metrics is explicit and distinct from coordinate dependence, then a generalized Finsler representation emerges [56,57]. If internal-state dependence is implicit and state vectors are (time-dependent) functions of position [78], then an osculating Riemannian geometry [52,68] is obtained. In the Riemannian setting, similarities exist with Refs. [53–55].

A mixture of $N \geqslant 1$ constituents is considered, where at time t, these occupy a shared infinitesimal control volume $d\Omega$ centered at spatial position $\mathbf{x}$. Motions are

$$\mathbf{x} = \boldsymbol{\chi}^\alpha(\mathbf{X}^\alpha, t). \tag{1}$$

Greek superscripts $\alpha = 1, \ldots, N$ label constituents having reference coordinates $\mathbf{X}^\alpha$; constituents coincident at $\mathbf{x}$ may occupy different $\mathbf{X}^\alpha$ due to diffusion, growth, etc.

A spatial manifold comprising the material body, parameterized by coordinate chart(s) $\{x^k\}$, is $\mathfrak{m}$. Referential manifold(s) $\mathfrak{M}^\alpha$ are parameterized by coordinate chart(s) $\{(X^\alpha)^K\}$ corresponding to reference positions of constituent α. Denote by $\{\boldsymbol{\xi}^\alpha(\mathbf{x}, t)\}$ and $\{\boldsymbol{\Xi}^\alpha(\mathbf{X}^\alpha, t)\}$ sets of internal state variables viewed as auxiliary coordinates over $\mathfrak{m}$ and $\mathfrak{M}^\alpha$,

respectively. Metric tensors $\mathbf{g}$ and $\mathbf{G}^\alpha$ with components g_{ij} and G^α_{IJ} are permitted to be coordinate and time dependent, of the forms

$$\mathbf{g} = \mathbf{g}(\mathbf{x}, t) = \tilde{\mathbf{g}}(\mathbf{x}, \{\boldsymbol{\xi}^\alpha(\mathbf{x}, t)\}), \tag{2}$$

$$\mathbf{G}^\alpha = \mathbf{G}^\alpha(\mathbf{X}^\alpha, t) = \tilde{\mathbf{G}}^\alpha(\mathbf{X}^\alpha, \{\boldsymbol{\Xi}^\alpha(\mathbf{X}^\alpha, t)\}). \tag{3}$$

The $\sim$ notation denotes the generalized Finsler description [56–58] of metrics on $\mathfrak{m}$ and $\mathfrak{M}^\alpha$, whereas unadorned versions are interpreted as osculating Riemannian metric tensors [52,67,68] at any fixed time t. Determinants are written $g = \det \mathbf{g}$ and $G^\alpha = \det \mathbf{G}^\alpha$. The partial time derivative at fixed $\mathbf{x}$ is $\partial_t(\cdot)$; the material time derivative at fixed $\mathbf{X}^\alpha$ is $D^\alpha_t(\cdot)$, related by

$$D^\alpha_t(\cdot) = \partial_t(\cdot) + \boldsymbol{\nabla}(\cdot) \cdot \boldsymbol{v}^\alpha, \quad (\upsilon^\alpha)^k = D^\alpha_t(\chi^\alpha)^k. \tag{4}$$

Particle velocity is $\boldsymbol{v}^\alpha$, and $\boldsymbol{\nabla}(\cdot)$ is the covariant derivative with respect to $\mathbf{x}$ where Christoffel symbols are those of the Levi-Civita connection derived from g_{ij}. The covariant derivative with respect to $\mathbf{X}^\alpha$ on $\mathfrak{M}^\alpha$ is $\boldsymbol{\nabla}^\alpha_0(\cdot)$.

Spatial and referential gradient operators obey

$$\boldsymbol{\nabla}(\cdot) = \partial(\cdot)/\partial x^k \otimes \mathbf{g}^k, \quad \boldsymbol{\nabla}^\alpha_0(\cdot) = \partial(\cdot)/\partial(X^\alpha)^K \otimes \mathbf{G}^K. \tag{5}$$

When used on typical scalars, vectors, and tensors, $\partial_t(\cdot)$ and $D^\alpha_t(\cdot)$ are performed with natural basis vectors $\mathbf{g}_k = \partial\mathbf{x}/\partial x^k$ and $\mathbf{G}^\alpha_K = \partial\mathbf{X}/\partial(X^\alpha)^K$ held fixed with respect to t at $\mathbf{x}$ and $\mathbf{X}^\alpha$, respectively, so $\partial_t\mathbf{g}_k$ and $D^\alpha_t\mathbf{G}^\alpha_K$ vanish in such circumstances. This produces commutation rules:

$$\boldsymbol{\nabla}[\partial_t(\cdot)] = \partial_t[\boldsymbol{\nabla}(\cdot)], \quad \boldsymbol{\nabla}^\alpha_0[D^\alpha_t(\cdot)] = D^\alpha_t[\boldsymbol{\nabla}^\alpha_0(\cdot)]. \tag{6}$$

The deformation gradient $\mathbf{F}^\alpha$ and Jacobian determinant J^α are defined as follows, giving a relation between reference and spatial gradient operators:

$$(F^\alpha)^i_J = \frac{\partial(\chi^\alpha)^i}{\partial(X^\alpha)^J}, \quad J^\alpha = \det\left[(F^\alpha)^i_J\right]\sqrt{g/G^\alpha}, \tag{7}$$

$$\mathbf{F}^\alpha = (F^\alpha)^i_J \mathbf{g}_i \otimes \mathbf{G}^J, \quad \boldsymbol{\nabla}^\alpha_0(\cdot) = \boldsymbol{\nabla}(\cdot)\mathbf{F}^\alpha. \tag{8}$$

The velocity gradient $\mathbf{l}^\alpha$ and its trace are

$$\mathbf{l}^\alpha = \boldsymbol{\nabla}\boldsymbol{v}^\alpha = D^\alpha_t\mathbf{F}^\alpha(\mathbf{F}^\alpha)^{-1}, \quad \boldsymbol{\nabla} \cdot \boldsymbol{v}^\alpha = \text{tr}\mathbf{l}^\alpha. \tag{9}$$

Spatial and material volume elements, $d\Omega$ and $d\Omega^\alpha_0$, obey

$$d\Omega(\mathbf{x}(\mathbf{X}^\alpha, t), t) = J^\alpha(\mathbf{X}^\alpha, t)d\Omega^\alpha_0(\mathbf{X}^\alpha, t). \tag{10}$$

Time derivatives of local volume elements allow for time dependence of metric tensors. Extending Refs. [54,55],

$$\partial_t(d\Omega) = \tfrac{1}{2}\text{tr}(\partial_t\mathbf{g})d\Omega = \partial_t(\ln\sqrt{g})d\Omega, \tag{11}$$

$$D^\alpha_t(d\Omega^\alpha_0) = \tfrac{1}{2}\text{tr}(D^\alpha_t\mathbf{G}^\alpha)d\Omega^\alpha_0 = D^\alpha_t(\ln\sqrt{G^\alpha})d\Omega^\alpha_0, \tag{12}$$

$$D^\alpha_t(d\Omega) = (D^\alpha_t J^\alpha + J^\alpha D^\alpha_t \ln\sqrt{G^\alpha})d\Omega^\alpha_0$$
$$= (\boldsymbol{\nabla} \cdot \boldsymbol{v}^\alpha + \partial_t \ln\sqrt{g})d\Omega. \tag{13}$$

In (13), $D^\alpha_t\sqrt{g/G^\alpha}$ is included in $D^\alpha_t J^\alpha$, and $\partial_t g = D^\alpha_t g$ since $\boldsymbol{\nabla}g$ vanishes for a Levi-Civita connection [79].

Define the following, all fields of $(\mathbf{x}, t)$: partial Cauchy stress tensor $\boldsymbol{\sigma}^\alpha$, traction vector $\mathbf{t}^\alpha = \boldsymbol{\sigma}^\alpha \cdot \mathbf{n}$, body force per unit mass $\mathbf{b}^\alpha$, partial internal energy per unit mass u^α, heat source per unit mass r^α, heat flux vector $\mathbf{q}^\alpha$,

mass exchange rate c^α, linear momentum exchange $\mathbf{h}^\alpha$, and energy exchange rate ϵ^α. The spatial mass density of constituent α is $\rho^\alpha(\mathbf{x}, t)$. Referential mass density at fixed time $t = t_0$ is $\rho_0^\alpha(\mathbf{X}^\alpha)$ with metric $\mathbf{G}_0^\alpha(\mathbf{X}^\alpha)$ and mass element $dm_0^\alpha(\mathbf{X}^\alpha) = \rho_0^\alpha \sqrt{G_0^\alpha/G^\alpha}\, d\Omega_0^\alpha$. At arbitrary t, the mass element is $dm^\alpha(\mathbf{X}^\alpha, t) = \rho^\alpha d\Omega = \rho^\alpha J^\alpha d\Omega_0^\alpha$.

A. Continuous processes

A global energy balance for each constituent is posited on a region of $\mathfrak{m}$ occupying transient control volume Ω, enclosed by oriented boundary $\partial\Omega$ with unit outward normal $\mathbf{n}$. Velocity and heat flux normal to $\partial\Omega$ are $\upsilon_n^\alpha = \boldsymbol{v}^\alpha \cdot \mathbf{n}$ and $q_n^\alpha = \mathbf{q}^\alpha \cdot \mathbf{n}$. The global balance per constituent extends Ref. [37] to account for working of generalized tractions $\{\mathbf{z}^\alpha\} = \{\boldsymbol{\zeta}^\alpha \cdot \mathbf{n}\}$ conjugate to rates of auxiliary variables $\{D_t^\alpha \boldsymbol{\xi}^\alpha\}$ on $\partial\Omega$, similarly to Ref. [77]:

$$\partial_t \int_\Omega \rho^\alpha \left(u^\alpha + \frac{1}{2}|\boldsymbol{v}^\alpha|^2\right) d\Omega + \oint_{\partial\Omega} \rho^\alpha \left(u^\alpha + \frac{1}{2}|\boldsymbol{v}^\alpha|^2\right) \upsilon_n^\alpha d\partial\Omega$$

$$= \oint_{\partial\Omega} \left(\mathbf{t}^\alpha \cdot \boldsymbol{v}^\alpha + \{\mathbf{z}^\alpha\} \cdot \{D_t^\alpha \boldsymbol{\xi}^\alpha\} - q_n^\alpha\right) d\partial\Omega$$

$$+ \int_\Omega \left[\rho^\alpha(\mathbf{b}^\alpha \cdot \boldsymbol{v}^\alpha + r^\alpha) + \mathbf{h}^\alpha \cdot \boldsymbol{v}^\alpha + \epsilon^\alpha\right.$$

$$\left. + c^\alpha \left(u^\alpha + \frac{1}{2}|\boldsymbol{v}^\alpha|^2\right)\right] d\Omega. \quad (14)$$

Angular momentum exchange between constituents [37] is omitted herein. When $\{\boldsymbol{\zeta}^\alpha\} \to \{\mathbf{0}\}$, (14) matches the Bowen-Truesdell theory [36,37]. Working of $\{\mathbf{z}^\alpha\}$ is necessary to enable derivation of Ginzburg-Landau (i.e., Allen-Cahn) kinetic laws for internal variables of gradient type [77,80]. Field variables in (14) are assumed sufficiently smooth on Ω such that the divergence theorem applies on $\mathfrak{m}$. Energy conservation under rigid motions (i.e., various time-dependent translations and rigid-body rotations [81,82]) of all constituents then furnishes local conservation laws for mass, momenta, and energy:

$$\partial_t \rho^\alpha + \nabla \cdot (\rho^\alpha \boldsymbol{v}^\alpha) = c^\alpha - \rho^\alpha \partial_t \ln\sqrt{g} = \hat{c}^\alpha, \quad (15)$$

$$\nabla \cdot \boldsymbol{\sigma}^\alpha + \rho^\alpha \mathbf{b}^\alpha + \mathbf{h}^\alpha = \rho^\alpha D_t^\alpha \boldsymbol{v}^\alpha, \quad \boldsymbol{\sigma}^\alpha = (\boldsymbol{\sigma}^\alpha)^\mathsf{T}, \quad (16)$$

$$\rho^\alpha D_t^\alpha u^\alpha = \boldsymbol{\sigma}^\alpha : \nabla \boldsymbol{v}^\alpha + \nabla \cdot \left(\{\boldsymbol{\zeta}^\alpha\} \cdot \{D_t^\alpha \boldsymbol{\xi}^\alpha\}\right)$$

$$- \nabla \cdot \mathbf{q}^\alpha + \rho^\alpha r^\alpha + \epsilon^\alpha. \quad (17)$$

Differentiation $\partial_t(\cdot)$ is at fixed coordinates $\{x^k\}$, but volume element $d\Omega(x^k, t)$ may vary with time due to time dependence of $\mathbf{g}$ in (2), producing (11) and $\partial_t \int(\cdot)d\Omega = \int[\partial_t(\cdot) + (\cdot)\partial_t \ln\sqrt{g}]d\Omega$. This yields the $\rho^\alpha \partial_t \ln\sqrt{g}$ term in (15). This term only explicitly enters (15) and not (16) or (17). It vanishes from the latter two according to steps in derivations of the local laws, where mass conservation is obtained first and then eliminated in the process of obtaining local momentum and energy balances [37]. All agree with invariance of the global energy balance under rigid-body motions [81], paralleling derivations in spatial coordinates in Ref. [82] and general treatments with transient material metrics for growth given in Refs. [54,55].

The c^α account for mass transfer between constituents when all internal variables $\{\boldsymbol{\xi}^\beta\}$, $\beta = 1, \ldots, N$ affecting the metric $\boldsymbol{g}$ through (2) are held fixed. The $\rho^\alpha \partial_t \ln\sqrt{g}$ measure density changes manifesting from rates of these internal variables, which could include growth or damage, the latter considered an opposite of remodeling. The net mass supply rate for both sources is $\hat{c}^\alpha = c^\alpha - \rho^\alpha \partial_t \ln\sqrt{g}$.

Denote by η^α the local entropy per unit mass and $\theta^\alpha > 0$ the absolute temperature of constituent α. As in Refs. [37,50], an entropy inequality for each constituent is avoided in lieu of an inequality for the whole mixture:

$$\partial_t \int_\Omega \sum_\alpha \rho^\alpha \eta^\alpha d\Omega + \oint_{\partial\Omega} \sum_\alpha \rho^\alpha \eta^\alpha \upsilon_n^\alpha d\partial\Omega$$

$$\geqslant \int_\Omega \sum_\alpha \frac{\rho^\alpha r^\alpha}{\theta^\alpha} d\Omega - \oint_{\partial\Omega} \sum_\alpha \frac{q_n^\alpha}{\theta^\alpha} d\partial\Omega. \quad (18)$$

Note that (18) is identical to Bowen-Truesdell theory [37,83]. From the divergence theorem, (15), and localization [84],

$$\sum_\alpha \left[\rho^\alpha D_t^\alpha \eta^\alpha + \frac{\nabla \cdot \mathbf{q}^\alpha}{\theta^\alpha} - \frac{\mathbf{q}^\alpha \cdot \nabla\theta^\alpha}{(\theta^\alpha)^2} - \frac{\rho^\alpha r^\alpha}{\theta^\alpha} + c^\alpha \eta^\alpha\right] \geqslant 0. \quad (19)$$

Let ψ^α be Helmholtz free energy per unit mass, whereby substitution of (17) into (19) yields

$$\psi^\alpha = u^\alpha - \theta^\alpha \eta^\alpha, \quad (20)$$

$$\sum_\alpha (1/\theta^\alpha)\left[\boldsymbol{\sigma}^\alpha : \nabla \boldsymbol{v}^\alpha + \nabla \cdot \left(\{\boldsymbol{\zeta}^\alpha\} \cdot \{D_t^\alpha \boldsymbol{\xi}^\alpha\}\right)\right.$$

$$- (\mathbf{q}^\alpha \cdot \nabla\theta^\alpha)/\theta^\alpha + \epsilon^\alpha + c^\alpha \theta^\alpha \eta^\alpha$$

$$\left. - \rho^\alpha\left(D_t^\alpha \psi^\alpha + \eta^\alpha D_t^\alpha \theta^\alpha\right)\right] \geqslant 0. \quad (21)$$

B. Singular surfaces

Now consider a propagating singular surface $\Sigma(t)$ in $\mathfrak{m}$, with image $\Sigma^\alpha(t)$ in $\mathfrak{M}^\alpha$. The Eulerian function ϕ defines this surface, from which the unit normal $\mathbf{n}$ and Eulerian speed $\mathcal{U} > 0$ in the direction of $\mathbf{n}$ follow:

$$\phi(\mathbf{x}, t) = 0, \quad \mathbf{n} = \nabla\phi/|\nabla\phi|, \quad \mathcal{U} = -\partial_t\phi/|\nabla\phi|. \quad (22)$$

Let $(\cdot)^+$ and $(\cdot)^-$ label limiting values of $(\cdot)$ as Σ is approached from either side; $\mathbf{n}$ is directed from the $(\cdot)^-$ side (behind Σ) to the $(\cdot)^+$ side. The jump across Σ is

$$[\![(\cdot)]\!] = (\cdot)^- - (\cdot)^+. \quad (23)$$

Across a shock front Σ, each $\boldsymbol{\chi}^\alpha$ is continuous, but space-time derivatives of $\boldsymbol{\chi}^\alpha$ are not necessarily so. Nor always are other field variables such as ρ^α, $\boldsymbol{\sigma}^\alpha$, θ^α, etc. With $\mathbf{n}$ defined per (22), the normal velocity, heat flux, and tractions are $\upsilon_n^\alpha = \boldsymbol{v}^\alpha \cdot \mathbf{n}$, $q_n^\alpha = \mathbf{q}^\alpha \cdot \mathbf{n}$, $\mathbf{t}^\alpha = \boldsymbol{\sigma}^\alpha \cdot \mathbf{n}$, and $\{\mathbf{z}^\alpha\} = \{\boldsymbol{\zeta}^\alpha \cdot \mathbf{n}\}$. Conservation laws for mass, linear momentum, and energy, and the entropy imbalance, across Σ are derived using principles set forth in Refs. [36,85].

Specifically, a closed region Ω of $\mathfrak{m}$ is partitioned by Σ at an instant in time into two sub-bodies, within which the local continuum balance laws (15)–(17) and (19) hold. These continuum laws are integrated over Ω and then over each sub-body, the latter accounting for possible boundary

contributions on Σ from tractions and heat flux. Integrals are assumed to be physically meaningful even if $\mathfrak{m}$ is non-Euclidean. The total mass rate, linear momentum rate, energy rate, and entropy production rate are required to be equal for Ω and the summed contributions of each sub-body with boundary Σ. Application of a form of Reynolds's transport theorem [85,86] derived from the divergence theorem and (13) then gives analogs of (15), (16), and (17) across Σ for each α:

$$\llbracket \rho^\alpha (\upsilon_n^\alpha - \mathcal{U}) \rrbracket = 0, \tag{24}$$

$$\llbracket \rho^\alpha \boldsymbol{v}^\alpha (\upsilon_n^\alpha - \mathcal{U}) \rrbracket = \llbracket \mathbf{t}^\alpha \rrbracket, \tag{25}$$

$$\llbracket \rho^\alpha (u^\alpha + \tfrac{1}{2}|\boldsymbol{v}^\alpha|^2)(\upsilon_n^\alpha - \mathcal{U}) \rrbracket$$
$$= \llbracket \mathbf{t}^\alpha \cdot \boldsymbol{v}^\alpha + \{\mathbf{z}^\alpha\} \cdot \{D_t^\alpha \boldsymbol{\xi}^\alpha\} - q_n^\alpha \rrbracket. \tag{26}$$

A jump equation for angular momentum can be derived, but it encompasses nothing beyond (25). Similarly, arguments in Ref. [85] applied to (19) furnish a local entropy inequality across Σ for the mixture:

$$\sum_\alpha \llbracket \rho^\alpha \eta^\alpha (\mathcal{U} - \upsilon_n^\alpha) - q_n^\alpha/\theta^\alpha \rrbracket \geqslant 0. \tag{27}$$

Now consider one-dimensional (1D) loading conditions: $n_k \to n_1 = 1$, $x^k \to x^1 = x$, $(\chi^\alpha)^k \to (\chi^\alpha)^1 = \chi^\alpha$, $(F^\alpha)_j^i \to (F^\alpha)_1^1 = \partial \chi^\alpha/\partial X^\alpha = F^\alpha$, $(\upsilon^\alpha)^k \to (\upsilon^\alpha)^1 = \upsilon_n^\alpha = \upsilon^\alpha$, $(t^\alpha)_k \to (t^\alpha)_1 = (\sigma^\alpha)_1^1 = t^\alpha$, $\{(z^\alpha)_k\} \to \{(z^\alpha)_1\} = \{(\zeta^\alpha)_1^1\} = \{z^\alpha\}$, $\{(\xi^\alpha)^k\} \to \{(\xi^\alpha)^1\} = \{\xi^\alpha\}$, and $(q^\alpha)^k \to (q^\alpha)^1 = q_n^\alpha = q^\alpha$. The shock is planar, with Eulerian speed $\mathcal{U}$. Eulerian forms of Rankine-Hugoniot equations (24)–(27) reduce to

$$\llbracket \rho^\alpha (\upsilon^\alpha - \mathcal{U}) \rrbracket = 0, \tag{28}$$

$$\llbracket \rho^\alpha \upsilon^\alpha (\upsilon^\alpha - \mathcal{U}) \rrbracket = \llbracket t^\alpha \rrbracket, \tag{29}$$

$$\left\llbracket \rho^\alpha \left(u^\alpha + \frac{1}{2}|\upsilon^\alpha|^2\right)(\upsilon^\alpha - \mathcal{U}) \right\rrbracket$$
$$= \llbracket t^\alpha \upsilon^\alpha + \{z^\alpha\}\{D_t^\alpha \xi^\alpha\} - q^\alpha \rrbracket, \tag{30}$$

$$\sum_\alpha \llbracket \rho^\alpha \eta^\alpha (\mathcal{U} - \upsilon^\alpha) - q^\alpha/\theta^\alpha \rrbracket \geqslant 0. \tag{31}$$

A Lagrangian description of a singular surface, denoted $\Sigma^\alpha(t)$ for each constituent α, is, analogously to (22),

$$\Phi^\alpha(\mathbf{X}^\alpha, t) = 0, \quad \mathbf{N}^\alpha = \nabla_0^\alpha \Phi^\alpha / |\nabla_0^\alpha \Phi^\alpha|,$$
$$\mathcal{U}^\alpha = -D_t^\alpha \Phi^\alpha / |\nabla_0^\alpha \Phi^\alpha|. \tag{32}$$

In 1D, Eulerian and Lagrangian shock speeds are [66]

$$\mathcal{U}(t) = d\Sigma(t)/dt, \quad \mathcal{U}^\alpha(t) = d\Sigma^\alpha(t)/dt. \tag{33}$$

From 1D inverse motion $X^\alpha(\chi^\alpha, t) = (\chi^\alpha)^{-1}(x, t)$ [66],

$$\Sigma^\alpha(t) = (\chi^\alpha)^{-1}(\Sigma(t), t) \Rightarrow \mathcal{U}^\alpha = (F^\alpha)^{-1}(\mathcal{U} - \upsilon^\alpha), \tag{34}$$

with $(F^\alpha)^{-1} = \partial(\chi^\alpha)^{-1}/\partial x$. Now assume a continuous referential density field $\rho_0^\alpha(X^\alpha)$ exists and can be related in 1D to any other spatial density field $\rho^\alpha(x, t)$ via $\rho_0^\alpha = F^\alpha \rho^\alpha$. Sufficient conditions for the latter consistent with mass conservation are $c^\alpha = \rho^\alpha \partial_t \ln \sqrt{g}$ with $g(\chi^\alpha(X^\alpha, t), t) = G^\alpha(X^\alpha, t)$.

In this case, (28) with (34) and $\llbracket \rho_0^\alpha \rrbracket = 0$ produces $\llbracket \mathcal{U}^\alpha \rrbracket = 0$. Thus, noting that $\mathcal{U}^\alpha$ is intrinsic and (34) should hold at all $(\cdot)^\pm$ states, the following Lagrangian forms of the 1D Rankine-Hugoniot equations are derived:

$$\rho_0^\alpha \mathcal{U}^\alpha \llbracket 1/\rho^\alpha \rrbracket = -\llbracket \upsilon^\alpha \rrbracket, \tag{35}$$

$$\rho_0^\alpha \mathcal{U}^\alpha \llbracket \upsilon^\alpha \rrbracket = -\llbracket t^\alpha \rrbracket, \tag{36}$$

$$\rho_0^\alpha \mathcal{U}^\alpha \left\llbracket u^\alpha + \frac{1}{2}|\upsilon^\alpha|^2 \right\rrbracket = -\llbracket t^\alpha \upsilon^\alpha + \{z^\alpha\}\{D_t^\alpha \xi^\alpha\} - q^\alpha \rrbracket, \tag{37}$$

$$\sum_\alpha \left(\rho_0^\alpha \mathcal{U}^\alpha \llbracket \eta^\alpha \rrbracket - \llbracket q^\alpha/\theta^\alpha \rrbracket \right) \geqslant 0. \tag{38}$$

Routine algebra produces velocity jumps and Lagrangian shock speeds in terms of jumps in stress and mass density:

$$\llbracket \upsilon^\alpha \rrbracket = (\llbracket t^\alpha \rrbracket \llbracket 1/\rho^\alpha \rrbracket)^{1/2}, \quad \rho_0^\alpha \mathcal{U}^\alpha = (\llbracket t^\alpha \rrbracket/\llbracket 1/\rho^\alpha \rrbracket)^{1/2}. \tag{39}$$

Also, since $\rho_0^\alpha/\rho^\alpha = F^\alpha$ by construction,

$$\llbracket \upsilon^\alpha \rrbracket = -\mathcal{U}^\alpha \llbracket F^\alpha \rrbracket, \quad \llbracket t^\alpha \rrbracket = \rho_0^\alpha (\mathcal{U}^\alpha)^2 \llbracket F^\alpha \rrbracket. \tag{40}$$

The Rankine-Hugoniot energy balance follows by eliminating particle and shock velocities from (37):

$$\llbracket u^\alpha \rrbracket = \langle t^\alpha \rangle \llbracket 1/\rho^\alpha \rrbracket - \frac{\llbracket \{z^\alpha\}\{D_t^\alpha \xi^\alpha\} - q^\alpha \rrbracket}{(\llbracket t^\alpha \rrbracket/\llbracket 1/\rho^\alpha \rrbracket)^{1/2}}, \tag{41}$$

where $\langle (\cdot) \rangle = \frac{1}{2}[(\cdot)^+ + (\cdot)^-]$ is the average across Σ^α.

The displacement derivative $\delta_t(\cdot)$ is defined as follows in 1D [36], consistently with (4) and (33):

$$\delta_t(\cdot) = \partial_t(\cdot) + \mathcal{U}\partial(\cdot)/\partial x = D_t^\alpha(\cdot) + \mathcal{U}^\alpha \partial(\cdot)/\partial X^\alpha. \tag{42}$$

This is the time derivative of a quantity measured by an observer moving with the shock front. Structured steady waves (e.g., of finite width) are addressed in Appendix A.

C. Total expressions for mixture

The spatial mass density of the mixture ρ, mean velocity of the mixture $\boldsymbol{v}$, and diffusion velocities $\boldsymbol{\mu}^\alpha$ are

$$\rho = \sum_\alpha \rho^\alpha, \quad \boldsymbol{v} = \frac{1}{\rho}\sum_\alpha \rho^\alpha \boldsymbol{v}^\alpha, \quad \boldsymbol{\mu}^\alpha = \boldsymbol{v}^\alpha - \boldsymbol{v}. \tag{43}$$

Note $\sum_\alpha \rho^\alpha \boldsymbol{\mu}^\alpha = \mathbf{0}$. Define the material time derivative of $\square$ with respect to the mixture as

$$\dot{\square} = \partial_t(\square) + \nabla(\square) \cdot \boldsymbol{v} \Rightarrow D_t^\alpha(\square) = \dot{\square} + (\nabla\square) \cdot \boldsymbol{\mu}^\alpha. \tag{44}$$

Recall from (15) that $\hat{c}^\alpha = c^\alpha - \rho^\alpha \partial_t \ln \sqrt{g}$. Summing (15) over α then gives the total mass balance for the mixture at space-time location $(\mathbf{x}, t)$:

$$\dot{\rho} + \rho \nabla \cdot \boldsymbol{v} = \hat{C}, \quad \hat{C} = \sum_\alpha \hat{c}^\alpha = \sum_\alpha c^\alpha - \rho \, \partial_t \ln \sqrt{g}. \tag{45}$$

Define, respectively, the total Cauchy stress tensor, total body force vector, total internal energy density, total entropy density, total heat supply, total heat flux, total internal state vector,

and total conjugate force vector:

$$\boldsymbol{\sigma} = \sum_\alpha (\boldsymbol{\sigma}^\alpha - \rho^\alpha \boldsymbol{\mu}^\alpha \otimes \boldsymbol{\mu}^\alpha), \quad \mathbf{b} = \frac{1}{\rho} \sum_\alpha \rho^\alpha \mathbf{b}^\alpha, \quad (46)$$

$$u = \frac{1}{\rho} \sum_\alpha \rho^\alpha \left[u^\alpha + \frac{1}{2} |\boldsymbol{\mu}^\alpha|^2 \right], \quad (47)$$

$$\eta = \frac{1}{\rho} \sum_\alpha \rho^\alpha \eta^\alpha, \quad r = \frac{1}{\rho} \sum_\alpha \rho^\alpha r^\alpha, \quad (48)$$

$$\mathbf{q} = \sum_\alpha \left(\mathbf{q}^\alpha - \boldsymbol{\sigma}^\alpha \cdot \boldsymbol{\mu}^\alpha + \rho^\alpha u^\alpha \boldsymbol{\mu}^\alpha + \frac{\rho^\alpha}{2} |\boldsymbol{\mu}^\alpha|^2 \boldsymbol{\mu}^\alpha \right), \quad (49)$$

$$\{\boldsymbol{\xi}\} = (\{\boldsymbol{\xi}\}^1, \dots, \{\boldsymbol{\xi}\}^N), \quad \{\boldsymbol{\zeta}\} = (\{\boldsymbol{\zeta}\}^1, \dots, \{\boldsymbol{\zeta}\}^N). \quad (50)$$

Imposed henceforth are the following constraints on mass, momentum, and energy supplies and exchanges:

$$\hat{C} = \sum_\alpha \hat{c}^\alpha = 0, \quad \sum_\alpha (\mathbf{h}^\alpha + \hat{c}^\alpha \boldsymbol{\mu}^\alpha) = \mathbf{0}, \quad (51)$$

$$\sum_\alpha \left[\epsilon^\alpha + \mathbf{h}^\alpha \cdot \boldsymbol{\mu}^\alpha + \hat{c}^\alpha \left(u^\alpha + \frac{1}{2} |\boldsymbol{\mu}^\alpha|^2 \right) \right] = 0. \quad (52)$$

In classical mixture theory [37], the body consisting of all $\alpha = 1, \dots, N$ phases is viewed as a closed system in Euclidean space, $\partial_t \ln \sqrt{g} = 0$, and c^α account exclusively for exchange of mass between phases, locally summing to zero. In many theoretical models of biologic growth and remodeling, the material body is analyzed as an open system [54,87,88]: Mass can be injected or extracted due to chemical-biological interactions with a background environment. In that open-system interpretation, even in a single-phase body, $\sum_\alpha \hat{c}^\alpha(\mathbf{x}, t)$ can be nonzero. Here, per the first of (51), a closed-system viewpoint is accepted: total mass comprised by all phases is constant, so $\hat{C} = 0$.

Given (43)–(50) with constraints (51) and (52), the total balances of mass, linear momentum, angular momentum, and energy and the dissipation inequality are obtained by accumulating (15), (16), (17), and (19) over $\alpha = 1, \dots, N$, following steps detailed by Bowen [37], with the addition of work contributions from (50) whose individual entries are defined as orthogonal:

$$\dot{\rho} + \rho \boldsymbol{\nabla} \cdot \boldsymbol{\upsilon} = 0, \quad \boldsymbol{\nabla} \cdot \boldsymbol{\sigma} + \rho \mathbf{b} = \rho \dot{\boldsymbol{\upsilon}}, \quad \boldsymbol{\sigma} = \boldsymbol{\sigma}^\mathsf{T}, \quad (53)$$

$$\rho \dot{u} = \boldsymbol{\sigma} : \boldsymbol{\nabla} \boldsymbol{\upsilon} + \boldsymbol{\nabla} \cdot (\{\boldsymbol{\zeta}\} \cdot \{\boldsymbol{\xi}'\}) - \boldsymbol{\nabla} \cdot \mathbf{q} + \rho r$$
$$+ \sum_\alpha \rho^\alpha \mathbf{b}^\alpha \cdot \boldsymbol{\mu}^\alpha, \quad \{\boldsymbol{\xi}'\} = \{\dot{\boldsymbol{\xi}}\} + \sum_\alpha \{\boldsymbol{\nabla} \boldsymbol{\xi}^\alpha \cdot \boldsymbol{\mu}^\alpha\}, \quad (54)$$

$$\rho \dot{\eta} + \boldsymbol{\nabla} \cdot \sum_\alpha \left(\frac{\mathbf{q}^\alpha}{\theta^\alpha} + \rho^\alpha \eta^\alpha \boldsymbol{\mu}^\alpha \right) - \sum_\alpha \frac{\rho^\alpha r^\alpha}{\theta^\alpha} \geqslant 0. \quad (55)$$

For the particular case when $\theta^\alpha = \theta$ is uniform among constituents at $(\mathbf{x}, t)$, then (55) simplifies to

$$\rho \dot{\eta} + \boldsymbol{\nabla} \cdot (\hat{\mathbf{q}}/\theta) - \rho r/\theta \geqslant 0, \quad \hat{\mathbf{q}} = \sum_\alpha (\mathbf{q}^\alpha + \theta \rho^\alpha \eta^\alpha \boldsymbol{\mu}^\alpha).$$
$$(56)$$

The quantity $\{\boldsymbol{\zeta}\} \cdot \{\boldsymbol{\xi}'\}$ in (54) can be identified with an interstitial flux vector of Ref. [89] in a broad sense, but the present theory does not later incorporate higher-order deformation or density gradients in energy potentials as in that work. Notice that the entropy fluxes in the divergence terms of (55) and

(56) are generally different than what would be obtained from the mixture heat flux $\mathbf{q}$ of (49) entering (54). The difference is well known [73] and consistent with Bowen and Truesdell [37,70]. It emerges naturally if spatial form of second law in (18) is accepted as fundamental. If a global form of (55) is used as a starting point, then different energy or entropy fluxes in first and second laws must be prescribed *a priori* [37].

Jump conditions across singular surfaces can be derived from (53), (54), and (56) using the methods already discussed for constituent α. Let $\mathcal{U}$ now be the Eulerian shock speed for the mixture as a whole. Analogs of (24)–(27) are, with an obvious change of notation,

$$[\![\rho(\upsilon_n - \mathcal{U})]\!] = 0, \quad [\![\rho \boldsymbol{\upsilon}(\upsilon_n - \mathcal{U})]\!] = [\![\mathbf{t}]\!], \quad (57)$$

$$[\![\rho(u + \tfrac{1}{2}|\boldsymbol{\upsilon}|^2)(\upsilon_n - \mathcal{U})]\!] = [\![\mathbf{t} \cdot \boldsymbol{\upsilon} + \{\mathbf{z}\} \cdot \{\boldsymbol{\xi}'\} - \hat{q}_n]\!], \quad (58)$$

$$[\![\rho \eta(\mathcal{U} - \upsilon_n) - \hat{q}_n/\theta]\!] \geqslant 0. \quad (59)$$

Eulerian equations for the 1D case follow trivially. Lagrangian equations for the 1D case are obtained by defining Lagrangian speed $\mathcal{U}_0$, deformation mapping F, and space-time continuous reference mass density ρ_0 to obey

$$\mathcal{U}_0 = F^{-1}(\mathcal{U} - \upsilon), \quad F = \rho_0/\rho. \quad (60)$$

Given ρ_0, υ, and $\mathcal{U}$, F and $\mathcal{U}_0$ are well defined. Analogs of (35)–(38) are then derived as, with $t_k \to t_1 = \sigma$,

$$\rho_0 \mathcal{U}_0 [\![1/\rho]\!] = -[\![\upsilon]\!], \quad \rho_0 \mathcal{U}_0 [\![\upsilon]\!] = -[\![\sigma]\!], \quad (61)$$

$$\rho_0 \mathcal{U}_0 [\![u + \tfrac{1}{2}\upsilon^2]\!] = -[\![\sigma \upsilon + \{z\}\{\xi'\} - \hat{q}]\!], \quad (62)$$

$$\rho_0 \mathcal{U}_0 [\![\eta]\!] - [\![\hat{q}/\theta]\!] \geqslant 0. \quad (63)$$

Equations fully analogous to (39)–(41) can be derived summarily with the obvious substitutions.

If invertibility and integrability of the second of (60) hold, then a 1D deformation gradient $F = \partial x/\partial X$ and Lagrangian coordinate X for the mixture exist whereby

$$\dot{F} = (\partial \upsilon/\partial x)F = \partial \upsilon/\partial X, \quad (64)$$

$$X(x, t) = \chi^{-1}(x, t) = \int_{x_0}^x F^{-1}(\tilde{x}, t)d\tilde{x}. \quad (65)$$

The analog of the displacement derivative of (42) for the entire mixture is then

$$\delta_t(\Box) = \partial_t(\Box) + \mathcal{U}\partial(\Box)/\partial x = (\dot{\Box}) + \mathcal{U}_0 \partial(\Box)/\partial X. \quad (66)$$

Returning to the general 3D case, diffusion problems are often analyzed using dimensionless measures of local amounts of each constituent. Recall ρ^α is the local mass of α per unit total spatial volume of mixture. The spatial volume fraction n^α is the ratio of volume occupied by α to that of the mixture, while the "real" mass density ρ_R^α is the local mass of α per unit spatial volume occupied by α (i.e., ρ_R^α is mass density of the isolated, fully dense constituent). The spatial mass concentration m^α is the mass of α per total mass of the mixture. Equations are

$$n^\alpha(\mathbf{x}, t) = \frac{\rho^\alpha(\mathbf{x}, t)}{\rho_R^\alpha(\mathbf{x}, t)}, \quad \sum_\alpha n^\alpha = 1, \quad (67)$$

$$m^\alpha(\mathbf{x}, t) = \frac{\rho^\alpha(\mathbf{x}, t)}{\rho(\mathbf{x}, t)}, \quad \sum_\alpha m^\alpha = 1. \quad (68)$$

At a reference $t = t_0$ when all particles occupy positions $\mathbf{X}^\alpha$, reference volume and mass fractions are $n_0^\alpha(\mathbf{X}^\alpha) = \rho_0^\alpha(\mathbf{X}^\alpha)/\rho_{R0}^\alpha(\mathbf{X}^\alpha)$ and $m_0^\alpha(\mathbf{X}^\alpha) = \rho_0^\alpha(\mathbf{X}^\alpha)/\rho_0(\mathbf{X}^\alpha)$.

III. CONSTITUTIVE THEORY

Thermodynamic identities are derived in Sec. III A by appealing to the local balance of energy and entropy inequality. Pragmatic and thermodynamically admissible energy functions, metric tensors, and kinetic relations are posited in respective Secs. III B, III C, and III D. The comprehensive model, and certain specializations used afterwards in Sec. IV, are summarized in Sec. III E.

A. Thermodynamics

Helmholtz free energy per unit mass and entropy density are of the following functional forms, each depending only on state variables for its particular constituent α and not others β when $\beta \neq \alpha$:

$$\psi^\alpha = \psi^\alpha\big(\mathbf{F}^\alpha, \theta^\alpha, \{\boldsymbol{\xi}^\alpha\}, \{\boldsymbol{\nabla}_0^\alpha\boldsymbol{\xi}^\alpha\}, \mathbf{X}^\alpha\big), \tag{69}$$

$$\eta^\alpha = \eta^\alpha\big(\mathbf{F}^\alpha, \theta^\alpha, \{\boldsymbol{\xi}^\alpha\}, \{\boldsymbol{\nabla}_0^\alpha\boldsymbol{\xi}^\alpha\}, \mathbf{X}^\alpha\big). \tag{70}$$

Partial stress consists of elastic $\bar{\boldsymbol{\sigma}}^\alpha$ and viscous $\hat{\boldsymbol{\sigma}}^\alpha$ parts:

$$\begin{aligned}\boldsymbol{\sigma}^\alpha = {} & \bar{\boldsymbol{\sigma}}^\alpha\big(\mathbf{F}^\alpha, \theta^\alpha, \{\boldsymbol{\xi}^\alpha\}, \{\boldsymbol{\nabla}_0^\alpha\boldsymbol{\xi}^\alpha\}, \mathbf{X}^\alpha\big)\\ & + \hat{\boldsymbol{\sigma}}^\alpha\big(\mathbf{F}^\alpha, \theta^\alpha, \{\boldsymbol{\xi}^\alpha\}, \{\boldsymbol{\nabla}_0^\alpha\boldsymbol{\xi}^\alpha\}, D_t^\alpha\mathbf{F}^\alpha, \mathbf{X}^\alpha\big). \end{aligned} \tag{71}$$

Relations (69)–(71) are justified as the standard for ideal thermoelastic mixtures [37,50,90] with three additions. First, internal state variables are added to represent dissipative processes such as viscoelasticity and damage mechanisms [5,91,92] and growth and remodeling [93,94]. Second, state variable gradients are added to represent surface energies or phase boundaries [31,32] and support derivation of Ginzburg-Landau kinetics for these variables [49,77,80]. Last, viscous stress [95] is added to address (e.g., Newtonian or another admissible) viscosity, important in biologic fluids such as blood [2].

Arguments in (2) and (3) connect at time t via [52,57]

$$\{\boldsymbol{\Xi}^\alpha\}(t) = \{\boldsymbol{\Xi}^\alpha(\{\boldsymbol{\xi}^\alpha\}, \mathbf{X}^\alpha, \mathbf{x})\}(t). \tag{72}$$

Thus, all dependence of response functions on metrics $(\mathbf{g}, \mathbf{G}^\alpha)$ and states $\{\boldsymbol{\Xi}^\alpha\}$ is implicitly included via arguments $\{\boldsymbol{\xi}^\alpha\}$. Kinetic equations for heat flux, internal state, and interphase mass, momentum, and energy exchange are more general, allowing for dependence on all constituents $\beta = 1, \ldots, N$ including $\alpha = \beta$ and $\alpha \neq \beta$:

$$\mathbf{q}^\alpha = \mathbf{q}^\alpha\big(\mathbf{F}^\beta, \boldsymbol{\nabla}\mathbf{F}^\beta, \theta^\beta, \boldsymbol{\nabla}\theta^\beta, \boldsymbol{\xi}^\beta, \boldsymbol{\nabla}_0^\beta\boldsymbol{\xi}^\beta, \boldsymbol{v}^\beta, \rho^\beta\big), \tag{73}$$

$$\mathbf{h}^\alpha = \mathbf{h}^\alpha\big(\mathbf{F}^\beta, \boldsymbol{\nabla}\mathbf{F}^\beta, \theta^\beta, \boldsymbol{\nabla}\theta^\beta, \boldsymbol{\xi}^\beta, \boldsymbol{\nabla}_0^\beta\boldsymbol{\xi}^\beta, \boldsymbol{v}^\beta, \rho^\beta\big), \tag{74}$$

$$c^\alpha = c^\alpha\big(\mathbf{F}^\beta, \boldsymbol{\nabla}\mathbf{F}^\beta, \theta^\beta, \boldsymbol{\nabla}\theta^\beta, \boldsymbol{\xi}^\beta, \boldsymbol{\nabla}_0^\beta\boldsymbol{\xi}^\beta, \boldsymbol{v}^\beta, \rho^\beta\big), \tag{75}$$

$$\epsilon^\alpha = \epsilon^\alpha\big(\mathbf{F}^\beta, \boldsymbol{\nabla}\mathbf{F}^\beta, \theta^\beta, \boldsymbol{\nabla}\theta^\beta, \boldsymbol{\xi}^\beta, \boldsymbol{\nabla}_0^\beta\boldsymbol{\xi}^\beta, \boldsymbol{v}^\beta, \rho^\beta\big), \tag{76}$$

$$\begin{aligned}D_t^\alpha\{\boldsymbol{\xi}^\alpha\} = {} & D_t^\alpha\{\boldsymbol{\xi}^\alpha\}\big(\mathbf{F}^\beta, \boldsymbol{\nabla}\mathbf{F}^\beta, \theta^\beta, \boldsymbol{\nabla}\theta^\beta, \cdots\\ & \cdots\boldsymbol{\xi}^\beta, \boldsymbol{\nabla}_0^\beta\boldsymbol{\xi}^\beta, \boldsymbol{v}^\beta, \rho^\beta\big). \end{aligned} \tag{77}$$

Notation $\{\cdot\}$ on $\boldsymbol{\xi}^\alpha$ and admissible explicit dependence on $\mathbf{X}^\alpha$ for heterogeneous phases α are omitted in arguments of (73)–(77) for brevity. Particular forms of (73)–(76) must satisfy principles of spatial invariance for objective spatial vectors $\mathbf{q}^\alpha$ and $\mathbf{h}^\alpha$ and scalars c^α and ϵ^α. Evolution equations (77) must also be objective. Invariance under rigid translation of the mixture as a whole necessitates that dependence on velocities $\boldsymbol{v}^\alpha$ is at most only on the $N-1$ velocity differences $\boldsymbol{v}^1 - \boldsymbol{v}^N, \ldots, \boldsymbol{v}^{N-1} - \boldsymbol{v}^N$. See Ref. [37]. Diffusion velocities $\boldsymbol{\mu}^\alpha = \boldsymbol{\mu}^\alpha(\boldsymbol{v}^\beta, \rho^\beta)$ of (43) fulfill this requirement. Spatial invariance of (69) and (70) is obtained via dependence on $\mathbf{F}^\alpha$ through symmetric deformation tensor $\mathbf{C}^\alpha$:

$$\mathbf{C}^\alpha = (\mathbf{F}^\alpha)^\mathsf{T}\mathbf{F}^\alpha, \quad (C^\alpha)_J^K = (G^\alpha)^{KI}(F^\alpha)_I^i g_{ij}(F^\alpha)_J^j; \tag{78}$$

$$\partial\psi^\alpha/\partial\mathbf{F}^\alpha = 2\mathbf{F}^\alpha\partial\psi^\alpha/\partial\mathbf{C}^\alpha, \quad J^\alpha = \sqrt{\det\mathbf{C}^\alpha}; \tag{79}$$

$$D_t^\alpha\mathbf{C}^\alpha = 2(\mathbf{F}^\alpha)^\mathsf{T}\mathbf{d}^\alpha\mathbf{F}^\alpha, \quad 2\mathbf{d}^\alpha = \mathbf{l}^\alpha + (\mathbf{l}^\alpha)^\mathsf{T}. \tag{80}$$

The spatial deformation rate is $\mathbf{d}^\alpha$, and $D_t^\alpha\mathbf{C}^\alpha$ is taken with $(G^\alpha)^{IJ}$ and g_{ij} fixed with respect to t in (80).

Expanding $D_t^\alpha\psi$ using the chain rule on (69) and inserting the result and (71) into (21) gives

$$\begin{aligned}\sum_\alpha \frac{1}{\theta^\alpha}\bigg\{&\bigg[\bar{\boldsymbol{\sigma}}^\alpha(\mathbf{F}^\alpha)^{-\mathsf{T}} - 2\rho^\alpha\mathbf{F}^\alpha\frac{\partial\psi^\alpha}{\partial\mathbf{C}^\alpha}\bigg] : D_t^\alpha\mathbf{F}^\alpha\\ & - \rho^\alpha[\eta^\alpha + \partial\psi^\alpha/\partial\theta^\alpha]D_t^\alpha\theta^\alpha\\ & + \bigg[\{(\mathbf{F}^\alpha)^{-1}\boldsymbol{\zeta}^\alpha\} - \rho^\alpha\frac{\partial\psi^\alpha}{\partial\{\boldsymbol{\nabla}_0\boldsymbol{\xi}^\alpha\}}\bigg] : \big\{D_t^\alpha(\boldsymbol{\nabla}_0\boldsymbol{\xi}^\alpha)\big\}\\ & + \bigg[\{(\mathbf{F}^\alpha)^{-1} : \boldsymbol{\nabla}_0^\alpha\boldsymbol{\zeta}^\alpha\} - \rho^\alpha\frac{\partial\psi^\alpha}{\partial\{\boldsymbol{\xi}^\alpha\}}\bigg] \cdot \big\{D_t^\alpha\boldsymbol{\xi}^\alpha\big\}\\ & + \hat{\boldsymbol{\sigma}}^\alpha : \mathbf{d}^\alpha - (\mathbf{q}^\alpha\cdot\boldsymbol{\nabla}\theta^\alpha)/\theta^\alpha + \epsilon^\alpha + c^\alpha\theta^\alpha\eta^\alpha\bigg\} \geqslant 0. \end{aligned} \tag{81}$$

Identities from (6) and (8) have been used to obtain

$$\begin{aligned}\boldsymbol{\nabla}\cdot\big(\{\boldsymbol{\zeta}^\alpha\}\cdot\big\{D_t^\alpha\boldsymbol{\xi}^\alpha\big\}\big) = {} & (\boldsymbol{\nabla}\cdot\{\boldsymbol{\zeta}^\alpha\})\cdot\big\{D_t^\alpha\boldsymbol{\xi}^\alpha\big\}\\ & + \{(\mathbf{F}^\alpha)^{-1}\boldsymbol{\zeta}^\alpha\} : \big\{D_t^\alpha\big(\boldsymbol{\nabla}_0^\alpha\boldsymbol{\xi}^\alpha\big)\big\}. \end{aligned} \tag{82}$$

From standard arguments [32,77,95,96] and (69)–(77), the first three sets of terms in (81) should vanish for admissibility under general thermodynamic processes, leading to the following constitutive equalities:

$$\bar{\boldsymbol{\sigma}}^\alpha = 2\rho^\alpha\mathbf{F}^\alpha\frac{\partial\psi^\alpha}{\partial\mathbf{C}^\alpha}(\mathbf{F}^\alpha)^\mathsf{T}, \quad \eta^\alpha = -\frac{\partial\psi^\alpha}{\partial\theta^\alpha}, \tag{83}$$

$$\{\boldsymbol{\zeta}^\alpha\} = \rho^\alpha\big\{\mathbf{F}^\alpha\partial\psi^\alpha/\partial\boldsymbol{\nabla}_0^\alpha\boldsymbol{\xi}^\alpha\big\} = \rho^\alpha\frac{\partial\psi^\alpha}{\partial\{\boldsymbol{\nabla}\boldsymbol{\xi}^\alpha\}}, \tag{84}$$

$$\{\boldsymbol{\pi}^\alpha\} = \rho^\alpha\partial\psi^\alpha/\partial\{\boldsymbol{\xi}^\alpha\}, \tag{85}$$

where (85) defines a conjugate force to internal state variables or order parameters. Then (81) reduces to

$$\begin{aligned}\sum_\alpha \frac{1}{\theta^\alpha}\big[&(\{\boldsymbol{\nabla}\cdot\boldsymbol{\zeta}^\alpha\} - \{\boldsymbol{\pi}^\alpha\})\cdot\big\{D_t^\alpha\boldsymbol{\xi}^\alpha\big\}\\ & + \hat{\boldsymbol{\sigma}}^\alpha : \mathbf{d}^\alpha - (\mathbf{q}^\alpha\cdot\boldsymbol{\nabla}\theta^\alpha)/\theta^\alpha + \epsilon^\alpha + c^\alpha\theta^\alpha\eta^\alpha\big] \geqslant 0. \end{aligned} \tag{86}$$

Applying the Legendre transformation from (20) with

$$u^\alpha = u^\alpha\big(\mathbf{F}^\alpha, \eta^\alpha, \{\boldsymbol{\xi}^\alpha\}, \{\boldsymbol{\nabla}_0^\alpha\boldsymbol{\xi}^\alpha\}, \mathbf{X}^\alpha\big), \tag{87}$$

$$\theta^\alpha = \theta^\alpha\big(\mathbf{F}^\alpha, \eta^\alpha, \{\boldsymbol{\xi}^\alpha\}, \{\boldsymbol{\nabla}_0^\alpha\boldsymbol{\xi}^\alpha\}, \mathbf{X}^\alpha\big), \tag{88}$$

in conjunction with (83) and (84), gives

$$\bar{\boldsymbol{\sigma}}^\alpha = 2\rho^\alpha\mathbf{F}^\alpha\frac{\partial u^\alpha}{\partial\mathbf{C}^\alpha}(\mathbf{F}^\alpha)^\mathsf{T}, \quad \theta^\alpha = \frac{\partial u^\alpha}{\partial\eta^\alpha}, \tag{89}$$

$$\{\boldsymbol{\pi}^\alpha\} = \rho^\alpha\frac{\partial u^\alpha}{\partial\{\boldsymbol{\xi}^\alpha\}}, \quad \{\boldsymbol{\zeta}^\alpha\} = \rho^\alpha\frac{\partial u^\alpha}{\partial\{\boldsymbol{\nabla}\boldsymbol{\xi}^\alpha\}}. \tag{90}$$

Define specific heat per unit mass at constant strain c_ϵ^α, thermal stress coefficients $\boldsymbol{\beta}^\alpha$, and Grüneisen tensor $\boldsymbol{\gamma}^\alpha$:

$$c_\epsilon^\alpha = \theta^\alpha\partial\eta^\alpha/\partial\theta^\alpha = -\theta^\alpha\,\partial^2\psi^\alpha/\partial(\theta^\alpha)^2, \tag{91}$$

$$\boldsymbol{\beta}^\alpha = \rho^\alpha c_\epsilon^\alpha\boldsymbol{\gamma}^\alpha = -2\rho^\alpha\,\partial^2\psi^\alpha/\partial\theta^\alpha\partial\mathbf{C}^\alpha. \tag{92}$$

Define the intrinsic dissipation for constituent α:

$$\mathfrak{D}^\alpha = (\{\boldsymbol{\nabla}\cdot\boldsymbol{\zeta}^\alpha\} - \{\boldsymbol{\pi}^\alpha\})\cdot\big\{D_t^\alpha\boldsymbol{\xi}^\alpha\big\} + \hat{\boldsymbol{\sigma}}^\alpha : \mathbf{d}^\alpha. \tag{93}$$

Expand the rate of η^α using (70), (83), (91), and (92):

$$\begin{aligned} \rho^\alpha\theta^\alpha D_t^\alpha\eta^\alpha = {}& \rho^\alpha c_\epsilon^\alpha D_t^\alpha\theta^\alpha + \tfrac{1}{2}\theta^\alpha\boldsymbol{\beta}^\alpha : D_t^\alpha\mathbf{C}^\alpha \\ & - \rho^\alpha\theta^\alpha\big[(\partial^2\psi/\partial\theta^\alpha\partial\{\boldsymbol{\xi}^\alpha\})\cdot\big\{D_t^\alpha\boldsymbol{\xi}^\alpha\big\} \\ & + (\partial^2\psi/\partial\theta^\alpha\partial\{\boldsymbol{\nabla}\boldsymbol{\xi}^\alpha\}) : \big\{\boldsymbol{\nabla}\big(D_t^\alpha\boldsymbol{\xi}^\alpha\big)\big\}\big]. \end{aligned} \tag{94}$$

From (17), time differentiation of (20), and (83) and (84):

$$\rho^\alpha\theta^\alpha D_t^\alpha\eta^\alpha = \mathfrak{D}^\alpha - \boldsymbol{\nabla}\cdot\mathbf{q}^\alpha + \rho^\alpha r^\alpha + \epsilon^\alpha. \tag{95}$$

Temperature rates then are, combining (94) and (95),

$$\begin{aligned} \rho^\alpha c_\epsilon^\alpha D_t^\alpha\theta^\alpha = {}& \mathfrak{D}^\alpha - \tfrac{1}{2}\theta^\alpha\boldsymbol{\beta}^\alpha : D_t^\alpha\mathbf{C}^\alpha \\ & + \rho^\alpha\theta^\alpha\big[(\partial^2\psi/\partial\theta^\alpha\partial\{\boldsymbol{\xi}^\alpha\})\cdot\big\{D_t^\alpha\boldsymbol{\xi}^\alpha\big\} \\ & + (\partial^2\psi/\partial\theta^\alpha\partial\{\boldsymbol{\nabla}\boldsymbol{\xi}^\alpha\}) : \big\{\boldsymbol{\nabla}\big(D_t^\alpha\boldsymbol{\xi}^\alpha\big)\big\}\big] \\ & - \boldsymbol{\nabla}\cdot\mathbf{q}^\alpha + \rho^\alpha r^\alpha + \epsilon^\alpha. \end{aligned} \tag{96}$$

An alternative formulation using a strain measure independent of non-Euclidean parts of Finsler metric tensors is discussed in Appendix B. Though not needed for 1D problems of Sec. IV, this construction has found utility in applications on crystals [57,62] and biologic tissue [52].

B. Energy functions

Internal state variables $\{\boldsymbol{\xi}^\alpha\}$ consist of three sets: configurational variables associated with viscoelastic processes $\{\boldsymbol{\Gamma}^\alpha\}$, damage variables associated with degradation processes $\{\mathbf{D}^\alpha\}$, and electrochemical activation (e.g., muscle contraction) variables $\{\boldsymbol{\Delta}^\alpha\}$ [16,20,23,52]:

$$\{\boldsymbol{\xi}^\alpha\}(\mathbf{x}, t) = (\{\boldsymbol{\Gamma}^\alpha\}, \{\mathbf{D}^\alpha\}, \{\boldsymbol{\Delta}^\alpha\})(\mathbf{x}, t). \tag{97}$$

In the present work, as in phase-field and related theories [23,52], free and internal energy functions can depend on spatial gradients of damage variables, which are viewed as order parameters, but not on spatial gradients of viscoelastic and tissue activation variables. The present formulation is separate order parameters for degradation of matrix and each fiber family. Prior models [22,23] used but a single order parameter for the whole solid. Here, since strain energies of matrix

and fibers are separately resolved, and since strain energies are driving forces for fracture, physics suggest distinct order parameters be assigned for degradation of matrix and fibers. This enables delineation of mechanisms that can be compared with experimental observation. In addition, the current approach is realistic in the sense that unstretched and unsheared fibers should not witness any ruptures. Use of distinct order parameters for fiber families is similar to assigning separate parameters for fractures on discrete cleavage planes in crystal models [80].

Denote by ς_V^α and ς_S^α degradation functions associated with loss of strength due to changes in bulk and deviatoric strain energies, respectively. These scalar functions obey

$$\begin{aligned} \varsigma_V^\alpha &= \varsigma_V^\alpha(\{\mathbf{D}^\alpha\}, \mathbf{C}^\alpha) \in [0, 1], \\ \varsigma_S^\alpha &= \varsigma_S^\alpha(\{\mathbf{D}^\alpha\}) \in [0, 1], \end{aligned} \tag{98}$$

$$\partial\varsigma_V^\alpha/\partial\mathbf{C}^\alpha(\{\mathbf{D}^\alpha\}, \mathbf{C}^\alpha) = \mathbf{0} \ \forall\ \mathbf{C}^\alpha \neq \mathbf{1}. \tag{99}$$

A degradation operator for fibrous energy contributions with similar properties is $\varsigma_F^\alpha(\{\mathbf{D}^\alpha\})$.

Let $\Psi^\alpha = \rho_{R0}^\alpha\psi^\alpha$ and $U^\alpha = \rho_{R0}^\alpha u^\alpha$ be free and internal energies per unit reference volume of individual phases. Pragmatic functional forms consist of the following sums:

$$\begin{aligned} \Psi^\alpha\big(&\mathbf{C}^\alpha, \theta^\alpha, \{\boldsymbol{\xi}^\alpha\}, \{\boldsymbol{\nabla}_0^\alpha\mathbf{D}^\alpha\}\big) \\ = {}& \varsigma_V^\alpha(\{\mathbf{D}^\alpha\}, \mathbf{C}^\alpha)\Psi_V^\alpha(J^\alpha, \theta^\alpha) \\ & + \varsigma_S^\alpha(\{\mathbf{D}^\alpha\})\big[\Psi_S^\alpha(\mathbf{C}^\alpha) + \Psi_\Gamma^\alpha(\mathbf{C}^\alpha, \{\boldsymbol{\Gamma}^\alpha\})\big] \\ & + \varsigma_F^\alpha(\{\mathbf{D}^\alpha\})\circ\big[\Psi_F^\alpha(\mathbf{C}^\alpha) + \Psi_\Phi^\alpha(\mathbf{C}^\alpha, \{\boldsymbol{\Gamma}^\alpha\})\big] \\ & + \Psi_A^\alpha(\mathbf{C}^\alpha, \{\boldsymbol{\Delta}^\alpha\}) + \Psi_\theta^\alpha(\theta^\alpha) \\ & + \Psi_\sigma^\alpha(J^\alpha) + \Psi_D^\alpha\big(\{\boldsymbol{\xi}^\alpha\}, \{\boldsymbol{\nabla}_0^\alpha\mathbf{D}^\alpha\}\big), \end{aligned} \tag{100}$$

$$\begin{aligned} U^\alpha\big(&\mathbf{C}^\alpha, \eta^\alpha, \{\boldsymbol{\xi}^\alpha\}, \{\boldsymbol{\nabla}_0^\alpha\mathbf{D}^\alpha\}\big) \\ = {}& \varsigma_V^\alpha(\{\mathbf{D}^\alpha\}, \mathbf{C}^\alpha)U_V^\alpha(J^\alpha, \eta^\alpha) \\ & + \varsigma_S^\alpha(\{\mathbf{D}^\alpha\})\big[U_S^\alpha(\mathbf{C}^\alpha) + U_\Gamma^\alpha(\mathbf{C}^\alpha, \{\boldsymbol{\Gamma}^\alpha\})\big] \\ & + \varsigma_F^\alpha(\{\mathbf{D}^\alpha\})\circ\big[U_F^\alpha(\mathbf{C}^\alpha) + U_\Phi^\alpha(\mathbf{C}^\alpha, \{\boldsymbol{\Gamma}^\alpha\})\big] \\ & + U_A^\alpha(\mathbf{C}^\alpha, \{\boldsymbol{\Delta}^\alpha\}) + U_\theta^\alpha(\eta^\alpha) \\ & + U_\sigma^\alpha(J^\alpha) + U_D^\alpha\big(\{\boldsymbol{\xi}^\alpha\}, \{\boldsymbol{\nabla}_0^\alpha\mathbf{D}^\alpha\}\big). \end{aligned} \tag{101}$$

In Ψ^α, volumetric equilibrium free energy for the entire constituent α is Ψ_V^α, including isotropic thermoelastic coupling. Deviatoric equilibrium energy of the isotropic matrix is Ψ_S^α. Viscoelastic configurational energy of the isotropic matrix is Ψ_Γ^α. Anisotropic deviatoric equilibrium free energy from fibrous microstructures is Ψ_F^α. Configurational energy, often but not always anisotropic, from fibers is Ψ_Φ^α. Energy from fiber activation is Ψ_A^α. Thermal energy of specific heat is Ψ_θ^α. Energy from a nonzero reference pressure is Ψ_σ^α. Surface energy from fractures, tears, and other damage is contained in Ψ_D^α.

Fully analogous descriptors apply to internal energy contributions in U^α. Forms (100) and (101) are not the most mathematically and physically general, but they are sufficient for soft tissue materials of present interest given the scope of available data on their properties and response. A few, or even most, terms vanish for certain classes of materials (e.g.,

isotropic solids, viscoelastic fluids, gas phases, and so forth). All functions in (100) and (101) in materials with heterogeneous properties can further depend explicitly on $\mathbf{X}^\alpha$, omitted in the arguments for brevity. Dependence of state-dependent metric tensors is implicit, for example in J^α and scalar functions of certain vectors and tensors.

1. Ideal gas equation of state

For gaseous fluids such as air in the lung, an ideal gas model [50] is sufficient. For the ideal gas, $\psi^\alpha = (\Psi_V^\alpha + \Psi_\theta^\alpha)/\rho_{R0}^\alpha$ and $u^\alpha = (U_V^\alpha + U_\theta^\alpha)/\rho_{R0}^\alpha$. At a reference state, the following conditions hold: $J^\alpha = 1$, $\theta^\alpha = \theta_0^\alpha$, $\eta^\alpha = \eta_0^\alpha$, $\rho_0^\alpha = n_0^\alpha \rho_{R0}^\alpha$, $p_V^\alpha = p_0^\alpha = n_0^\alpha p_{R0}^\alpha$, and $c_\epsilon^\alpha = c_{\epsilon 0}^\alpha$. Quantities with zero subscripts are constants; $p_V^\alpha = -\frac{1}{3}\mathrm{tr}\bar{\boldsymbol{\sigma}}^\alpha$ is the partial inviscid pressure. From the identity $\partial J^\alpha/\partial \mathbf{C}^\alpha = \frac{1}{2}J^\alpha(\mathbf{C}^\alpha)^{-1}$, the stress contribution is spherical: $\bar{\boldsymbol{\sigma}}^\alpha = -p_V^\alpha \mathbf{1}$. The ideal gas constant is $\mathfrak{R}^\alpha$. Equation of state (EOS) and internal energy function are

$$p_V^\alpha = \rho^\alpha \mathfrak{R}^\alpha \theta^\alpha, \quad u^\alpha = c_{\epsilon 0}^\alpha \theta^\alpha. \tag{102}$$

From (102) and $\psi^\alpha = u^\alpha + \theta^\alpha(\partial \psi^\alpha/\partial \theta^\alpha)$, it follows that

$$\psi^\alpha(J^\alpha, \theta^\alpha) = -\mathfrak{R}^\alpha \theta^\alpha \ln J^\alpha - c_{\epsilon 0}^\alpha \theta^\alpha \big[\ln\big(\theta^\alpha/\theta_0^\alpha\big) - 1\big], \tag{103}$$

$$u^\alpha(J^\alpha, \eta^\alpha) = c_{\epsilon 0}^\alpha \theta_0^\alpha (J^\alpha)^{-\gamma_0^\alpha} \exp\big(\eta^\alpha/c_{\epsilon 0}^\alpha\big), \tag{104}$$

noting $\eta_0^\alpha = 0$ and $\gamma_0^\alpha = \mathfrak{R}^\alpha/c_{\epsilon 0}^\alpha$. Thermal stress tensor is $\boldsymbol{\beta}^\alpha = \rho^\alpha \mathfrak{R}^\alpha(\mathbf{C}^\alpha)^{-1}$ in (92), and $c_\epsilon^\alpha = c_{\epsilon 0}^\alpha$ in (91). The ideal gas model is justified as standard for shock compression of air [50]. Other models [41,97] could be substituted if consistent with (100) and (101).

2. Condensed matter EOS

For solid and liquid tissue phases, an EOS combining the third-order logarithmic form used for high-pressure physics [98,99] with an exponential form for tissue mechanics [100] is sufficiently general for the present applications. This model is chosen for its ability to capture bulk stiffening at high pressure as well as tensile stiffening observed in dilatation of some soft tissues [2,100]. It requires relatively few parameters, and its accuracy for depicting shock Hugoniot data for water, blood, and muscle is demonstrated in Sec. IV A.

Thermoelastic coupling is linear and isotropic with constant volumetric expansion coefficient A^α, and specific heat c_ϵ^α is constant. Reference temperature is θ_0^α, and reference pressure is p_{R0}^α. The reference isothermal bulk modulus is B_θ^α, and the pressure derivative of the isothermal bulk modulus in the reference state is $B_{\theta p}^\alpha$. Analogously, the isentropic bulk modulus and pressure derivative are B_η^α and $B_{\eta p}^\alpha$. Denote a constant controlling exponential stiffening by k_V^α. Free energies per unit initial volume of constituent α are

$$\Psi_V^\alpha = \frac{B_\theta^\alpha}{2}\left[\frac{\exp\{k_V^\alpha(\ln J^\alpha)^2\} - 1}{k_V^\alpha} - \frac{(B_{\theta p}^\alpha - 2)(\ln J^\alpha)^3}{3}\right]$$
$$- A^\alpha B_\theta^\alpha \big(\theta^\alpha - \theta_0^\alpha\big)\ln J^\alpha, \quad \Psi_\sigma^\alpha = -p_{R0}^\alpha \ln J^\alpha, \tag{105}$$

$$\Psi_\theta^\alpha = -\rho_{R0}^\alpha c_\epsilon^\alpha \big[\theta^\alpha \ln\big(\theta^\alpha/\theta_0^\alpha\big) - \big(\theta^\alpha - \theta_0^\alpha\big)\big]. \tag{106}$$

The contribution to stress $\bar{\boldsymbol{\sigma}}^\alpha$ from Ψ_V^α and Ψ_σ^α is spherical, with Cauchy pressure

$$p_V^\alpha = -\frac{\rho^\alpha}{\rho_{R0}^\alpha}\frac{\partial\big(\Psi_V^\alpha + \Psi_\sigma^\alpha\big)}{\partial \ln J^\alpha}$$
$$= -\frac{\rho^\alpha}{\rho_{R0}^\alpha}B_\theta^\alpha \ln J^\alpha\left[\exp\{k_V^\alpha(\ln J^\alpha)^2\} - \frac{1}{2}\big(B_{\theta p}^\alpha - 2\big)\ln J^\alpha\right]$$
$$+ \frac{\rho^\alpha}{\rho_{R0}^\alpha}A^\alpha B_\theta^\alpha\big(\theta^\alpha - \theta_0^\alpha\big) + \frac{\rho^\alpha}{\rho_{R0}^\alpha}p_{R0}^\alpha. \tag{107}$$

From (15), if $c^\alpha = \rho^\alpha \partial_t \ln\sqrt{g}$, $\partial_t \ln\sqrt{g} = D_t^\alpha \ln\sqrt{G^\alpha}$, and $\rho_0^\alpha = \rho_0^\alpha(\mathbf{X}^\alpha)$, then $\rho_0^\alpha = \rho^\alpha J^\alpha \Rightarrow \rho^\alpha/\rho_{R0}^\alpha = n_0^\alpha/J^\alpha$.

The thermal stress tensor and Grüneisen tensor are

$$\boldsymbol{\beta}^\alpha = \frac{\rho^\alpha}{\rho_{R0}^\alpha}A^\alpha B_\theta^\alpha(\mathbf{C}^\alpha)^{-1}, \quad \boldsymbol{\gamma}^\alpha = \frac{A^\alpha B_\theta^\alpha}{\rho_{R0}^\alpha c_\epsilon^\alpha}(\mathbf{C}^\alpha)^{-1}. \tag{108}$$

The scalar Grüneisen constant is $\gamma_0^\alpha = A^\alpha B_\theta^\alpha/(\rho_{R0}^\alpha c_\epsilon^\alpha)$.

Internal energy complementary to (105) and (106) is

$$U_V^\alpha = \frac{B_\eta^\alpha}{2}\left[\frac{\exp\{k_V^\alpha(\ln J^\alpha)^2\} - 1}{k_V^\alpha} - \frac{(B_{\eta p}^\alpha - 2)(\ln J^\alpha)^3}{3}\right]$$
$$- \rho_{R0}^\alpha \theta_0^\alpha \gamma_0^\alpha \eta^\alpha \ln J^\alpha, \quad U_\sigma^\alpha = -p_{R0}^\alpha \ln J^\alpha, \tag{109}$$

$$U_\theta^\alpha = \rho_{R0}^\alpha \theta_0^\alpha \eta^\alpha \big[1 + \eta^\alpha/\big(2c_\epsilon^\alpha\big)\big]. \tag{110}$$

Pressure and temperature from (109) and (110) are

$$p_V^\alpha = -\frac{\rho^\alpha}{\rho_{R0}^\alpha}\frac{\partial\big(U_V^\alpha + U_\sigma^\alpha\big)}{\partial \ln J^\alpha}$$
$$= -\frac{\rho^\alpha}{\rho_{R0}^\alpha}B_\eta^\alpha \ln J^\alpha\left[\exp\{k_V^\alpha(\ln J^\alpha)^2\} - \frac{1}{2}\big(B_{\eta p}^\alpha - 2\big)\ln J^\alpha\right]$$
$$+ \rho^\alpha \theta_0^\alpha \gamma_0^\alpha \eta^\alpha + \rho^\alpha p_{R0}^\alpha/\rho_{R0}^\alpha, \tag{111}$$

$$\theta^\alpha = \frac{1}{\rho_{R0}^\alpha}\frac{\partial\big(U_V^\alpha + U_\theta^\alpha\big)}{\partial \eta^\alpha} = \theta_0^\alpha\left[1 + \frac{\eta^\alpha}{c_\epsilon^\alpha} - \gamma_0^\alpha \ln J^\alpha\right]. \tag{112}$$

Bulk moduli B_θ^α and B_η^α are non-negative, and k_V^α should be non-negative for stiffening under large strain typical of soft tissues, compressive or tensile. If $B_{\theta p}^\alpha > 2$, then the material stiffens in compression and softens in tension, and vice versa for $B_{\theta p}^\alpha < 2$. Similar statements hold for $B_{\eta p}^\alpha$. Energy functions (105) and (109) are not (poly)convex in J^α. Polyconvexity is appealing for existence of unique solutions to boundary value problems [101] but is not essential. If $\varsigma_V^\alpha < 1$, then p_V^α contributions from Ψ_V^α and U_V^α (i.e., all terms except rightmost in (107) and (111) with p_{R0}^α) require multiplication by ς_V^α, as do $\boldsymbol{\beta}^\alpha$, $\boldsymbol{\gamma}^\alpha$, and γ_0^α.

3. Deviatoric matrix equilibrium

Deviatoric deformation gradient and deformation tensor are, with $f = f(\tilde{\mathbf{C}}^\alpha)$ a generic differentiable function of its argument,

$$\tilde{\mathbf{F}}^\alpha = (J^\alpha)^{-1/3}\mathbf{F}^\alpha, \quad \tilde{\mathbf{C}}^\alpha = (J^\alpha)^{-2/3}\mathbf{C}^\alpha, \tag{113}$$

$$\frac{\partial f}{\partial \mathbf{C}^\alpha} = (J^\alpha)^{-2/3}\left[\frac{\partial f}{\partial \tilde{\mathbf{C}}^\alpha} - \frac{1}{3}\left(\frac{\partial f}{\partial \tilde{\mathbf{C}}^\alpha} : \mathbf{C}^\alpha\right)(\mathbf{C}^\alpha)^{-1}\right]. \tag{114}$$

Let $\mu_S^\alpha \geqslant 0$ be a shear modulus. Energy is [101]

$$\Psi_S^\alpha = U_S^\alpha = \tfrac{1}{2}\mu_S^\alpha(\mathrm{tr}\,\tilde{\mathbf{C}}^\alpha - 3). \quad (115)$$

From (114), the contribution of (115) to Cauchy stress is

$$\boldsymbol{\sigma}_S^\alpha = 2\frac{\rho^\alpha}{\rho_{R0}^\alpha}\mathbf{F}^\alpha\frac{\partial \Psi_S^\alpha}{\partial \mathbf{C}^\alpha}(\mathbf{F}^\alpha)^\mathsf{T} = 2\frac{\rho^\alpha}{\rho_{R0}^\alpha}\mathbf{F}^\alpha\frac{\partial U_S^\alpha}{\partial \mathbf{C}^\alpha}(\mathbf{F}^\alpha)^\mathsf{T}$$

$$= \frac{\rho^\alpha}{\rho_{R0}^\alpha}\mu_S^\alpha\left[\tilde{\mathbf{B}}^\alpha - \tfrac{1}{3}(\mathrm{tr}\tilde{\mathbf{B}}^\alpha)\mathbf{1}\right], \quad \tilde{\mathbf{B}}^\alpha = \tilde{\mathbf{F}}^\alpha(\tilde{\mathbf{F}}^\alpha)^\mathsf{T}. \quad (116)$$

This contribution is linear in spatial deformation tensor $\tilde{\mathbf{B}}^\alpha$, traceless, and ultimately scaled by ς_S^α. Further nonlinearity can be furnished by Ψ_F^α and U_F^α. Function (115) is polyconvex [101] and isotropic. Many strain energy functions have been proposed for soft-tissue elasticity [14]. The present form (115) is used because it requires only one parameter, is simple to implement, and is widely used [101]. It is also compatible with (69), (100), and the fiber elastic model that follows next.

4. Fiber equilibrium

Let index k denote a fiber family of reference alignment by unit vector ι_k^α. Let $\kappa_k^\alpha \in [0, \tfrac{1}{3}]$ be dispersion constants. Structure tensors [17] are

$$\mathbf{H}_k^\alpha = \kappa_k^\alpha\mathbf{1} + (1 - 3\kappa_k^\alpha)\iota_k^\alpha \otimes \iota_k^\alpha. \quad (117)$$

Strain energy contributions are of functional forms

$$\Psi_F^\alpha = \Psi_F^\alpha\big(\tilde{\mathbf{C}}^\alpha, \mathbf{H}_k^\alpha(\mathbf{X}^\alpha)\big) = U_F^\alpha\big(\tilde{\mathbf{C}}^\alpha, \mathbf{H}_k^\alpha(\mathbf{X}^\alpha)\big), \quad (118)$$

with $\mathbf{H}_k^\alpha$ time independent at $\mathbf{X}^\alpha$ (i.e., not transient state variables). Depending on the number of fiber families k and their orientations, different scalar invariants entering (118) are possible. For the current presentation, one invariant per fiber family is sufficient: $I_k^\alpha = \tilde{\mathbf{C}}^\alpha : \mathbf{H}_k^\alpha$. The particular form of (118) is polyconvex [8,13,52,101]:

$$\Psi_F^\alpha = \sum_k \Psi_{Fk}^\alpha$$

$$= \sum_k \frac{\mu_k^\alpha}{4k_k^\alpha}\big\{\exp\big[k_k^\alpha(I_k^\alpha - 1)^2\big] - 1\big\}H(I_k^\alpha - 1). \quad (119)$$

A fiber modulus and stiffening coefficient are $\mu_k^\alpha \geqslant 0$ and $k_k^\alpha > 0$. Optional right-continuous Heaviside function is $H(\cdot)$; this disables fiber stiffness for buckling in compression along ι_k^α. Contributions to stress are traceless:

$$\boldsymbol{\sigma}_F^\alpha = 2\frac{\rho^\alpha}{\rho_{R0}^\alpha}\mathbf{F}^\alpha\frac{\partial \Psi_F^\alpha}{\partial \mathbf{C}^\alpha}(\mathbf{F}^\alpha)^\mathsf{T} = 2\frac{\rho^\alpha}{\rho_{R0}^\alpha}\mathbf{F}^\alpha\frac{\partial U_F^\alpha}{\partial \mathbf{C}^\alpha}(\mathbf{F}^\alpha)^\mathsf{T}$$

$$= \frac{\rho^\alpha}{\rho_{R0}^\alpha}\sum_k \mu_k^\alpha(I_k^\alpha - 1)\exp\big[k_k^\alpha(I_k^\alpha - 1)^2\big]H(I_k^\alpha - 1)\tilde{\mathbf{h}}_k^\alpha,$$

$$\tilde{\mathbf{h}}_k^\alpha = \tilde{\mathbf{F}}^\alpha\mathbf{H}_k^\alpha(\tilde{\mathbf{F}}^\alpha)^\mathsf{T} - \frac{1}{3}\mathrm{tr}\big[\tilde{\mathbf{F}}^\alpha\mathbf{H}_k^\alpha(\tilde{\mathbf{F}}^\alpha)^\mathsf{T}\big]\mathbf{1}. \quad (120)$$

Family k is isotropic as $\kappa_k^\alpha \to \tfrac{1}{3}$. Fiber compressibility is encompassed by the condensed matter EOS for phase α rather than distinct energetic terms. Stress contributions from (120) are affected by ς_F^α if fibers are damaged. Many other anisotropic elasticity models for soft tissues exist [14]. The framework of (117)–(120) is implemented here because it is widely used (e.g., based on seminal works of Holzapfel,

Ogden, and Gasser [8,13,17]) and can account for energies and anisotropies induced by any number of fiber families of arbitrary orientations.

5. Matrix viscoelasticity

The viscoelastic formulation combines features from prior works [91,92,100,102,103] in a thermodynamically consistent manner. Let $\{\boldsymbol{\Gamma}^\alpha\} \to \{\boldsymbol{\Gamma}_{Vl}^\alpha, \boldsymbol{\Gamma}_{Sm}^\alpha, \boldsymbol{\Gamma}_{\Phi k,n}^\alpha\}$ be internal strainlike configurational variables for constituent α. Index l spans a set of discrete relaxation time constants $\tau_{Vl}^\alpha = \tau_{V1}^\alpha, \dots$ for viscoelastic relaxation processes associated with volumetric deformation of the matrix. Index m spans times τ_{Sm}^α associated with deviatoric (shear) deformation of the matrix. Index n spans times $\tau_{\Phi k,n}^\alpha$ associated with fiber family k discussed in the next subsection. Internal stresses $\{\mathbf{Q}_{Vl}^\alpha, \mathbf{Q}_{Sm}^\alpha\}$ conjugate to the matrix internal strains, in coordinates referred to $\mathfrak{M}^\alpha$, obey [92,102]

$$\mathbf{Q}_{Vl}^\alpha = -\frac{\partial \Psi_\Gamma^\alpha}{\partial \boldsymbol{\Gamma}_{Vl}^\alpha} = 2\frac{\partial \Psi_{Vl}^\alpha}{\partial \mathbf{C}^\alpha}, \quad \mathbf{Q}_{Sm}^\alpha = -\frac{\partial \Psi_\Gamma^\alpha}{\partial \boldsymbol{\Gamma}_{Sm}^\alpha} = 2\frac{\partial \Psi_{Sm}^\alpha}{\partial \mathbf{C}^\alpha}, \quad (121)$$

$$\Psi_\Gamma^\alpha = U_\Gamma^\alpha = \sum_l \Psi_{Vl}^\alpha\big(\boldsymbol{\Gamma}_{Vl}^\alpha, \mathbf{C}^\alpha\big) + \sum_m \Psi_{Sm}^\alpha\big(\boldsymbol{\Gamma}_{Sm}^\alpha, \mathbf{C}^\alpha\big)$$

$$= \sum_l \int \frac{1}{2}\mathbf{Q}_{Vl}^\alpha : d\mathbf{C}^\alpha + \sum_m \int \frac{1}{2}\mathbf{Q}_{Sm}^\alpha : d\mathbf{C}^\alpha. \quad (122)$$

Indefinite integrals (122) are not needed explicitly. Evolution equations for internal stresses are

$$D_t^\alpha\mathbf{Q}_{Vl}^\alpha + \mathbf{Q}_{Vl}^\alpha/\tau_{Vl}^\alpha = 2D_t^\alpha\big(\partial\hat{\Psi}_{Vl}^\alpha/\partial\mathbf{C}^\alpha\big), \quad (123)$$

$$D_t^\alpha\mathbf{Q}_{Sm}^\alpha + \mathbf{Q}_{Sm}^\alpha/\tau_{Sm}^\alpha = 2D_t^\alpha\big(\partial\hat{\Psi}_{Sm}^\alpha/\partial\mathbf{C}^\alpha\big), \quad (124)$$

$$\hat{\Psi}_{Vl}^\alpha = \tfrac{1}{2}\beta_{Vl}^\alpha B_\theta^\alpha(\ln J^\alpha)^2, \quad (125)$$

$$\hat{\Psi}_{Sm}^\alpha = \tfrac{1}{2}\beta_{Sm}^\alpha\mu_S^\alpha(\mathrm{tr}\,\tilde{\mathbf{C}}^\alpha - 3). \quad (126)$$

Dimensionless factors are $\beta_{Vl}^\alpha \geqslant 0$, $\beta_{Sm}^\alpha \geqslant 0$. Initial conditions and convolution solutions to (123) and (124) are

$$\mathbf{Q}_{Vl0}^\alpha = 2\partial\hat{\Psi}_{Vl}^\alpha/\partial\mathbf{C}^\alpha, \quad \mathbf{Q}_{Sm0}^\alpha = 2\partial\hat{\Psi}_{Sm}^\alpha/\partial\mathbf{C}^\alpha, \quad (127)$$

$$\mathbf{Q}_{Vl}^\alpha(t) = \mathbf{Q}_{Vl0}^\alpha\exp\big[-t/\tau_{Vl}^\alpha\big]$$
$$+ \int_{0+}^t \exp\big[-(t - s)/\tau_{Vl}^\alpha\big]D_s^\alpha\big(2\partial\hat{\Psi}_{Vl}^\alpha/\partial\mathbf{C}^\alpha\big)ds, \quad (128)$$

$$\mathbf{Q}_{Sm}^\alpha(t) = \mathbf{Q}_{Sm0}^\alpha\exp\big[-t/\tau_{Sm}^\alpha\big]$$
$$+ \int_{0+}^t \exp\big[-(t - s)/\tau_{Sm}^\alpha\big]D_s^\alpha\big(2\partial\hat{\Psi}_{Sm}^\alpha/\partial\mathbf{C}^\alpha\big)ds. \quad (129)$$

Cauchy stress contributions are sums over l, m:

$$\boldsymbol{\sigma}_\Gamma^\alpha = 2\frac{\rho^\alpha}{\rho_{R0}^\alpha}\mathbf{F}^\alpha\frac{\partial \Psi_\Gamma^\alpha}{\partial \mathbf{C}^\alpha}(\mathbf{F}^\alpha)^\mathsf{T} = 2\frac{\rho^\alpha}{\rho_{R0}^\alpha}\mathbf{F}^\alpha\frac{\partial U_\Gamma^\alpha}{\partial \mathbf{C}^\alpha}(\mathbf{F}^\alpha)^\mathsf{T}$$

$$= \frac{\rho^\alpha}{\rho_{R0}^\alpha}\sum_l \mathbf{F}^\alpha\mathbf{Q}_{Vl}^\alpha(\mathbf{F}^\alpha)^\mathsf{T} + \frac{\rho^\alpha}{\rho_{R0}^\alpha}\sum_m \mathbf{F}^\alpha\mathbf{Q}_{Sm}^\alpha(\mathbf{F}^\alpha)^\mathsf{T}. \quad (130)$$

As $t/\tau^\alpha_{Vl} \to 0$ and $t/\tau^\alpha_{Sm} \to 0$, $\boldsymbol{\sigma}^\alpha_\Gamma$ in (130) sums to the instantaneous (glassy) viscoelastic stresses

$$2\frac{\rho^\alpha}{\rho^\alpha_{R0}} \sum_l \mathbf{F}^\alpha \frac{\partial \hat{\Psi}^\alpha_{Vl}}{\partial \mathbf{C}^\alpha}(\mathbf{F}^\alpha)^\mathsf{T} + 2\frac{\rho^\alpha}{\rho^\alpha_{R0}} \sum_m \mathbf{F}^\alpha \frac{\partial \hat{\Psi}^\alpha_{Sm}}{\partial \mathbf{C}^\alpha}(\mathbf{F}^\alpha)^\mathsf{T}$$

$$= \frac{\rho^\alpha}{\rho^\alpha_{R0}} \sum_l \beta^\alpha_{Vl} B^\alpha_\theta (\ln J^\alpha)\mathbf{1}$$

$$+ \frac{\rho^\alpha}{\rho^\alpha_{R0}} \sum_m \beta^\alpha_{Sm} \mu^\alpha_S \left[\tilde{\mathbf{B}}^\alpha - \frac{1}{3}(\mathrm{tr}\tilde{\mathbf{B}}^\alpha)\mathbf{1} \right]. \qquad (131)$$

As $t/\tau^\alpha_{Vl} \to \infty$ and $t/\tau^\alpha_{Sm} \to \infty$, $\mathbf{Q}^\alpha_{Vl} \to \mathbf{0}$ and $\mathbf{Q}^\alpha_{Sm} \to \mathbf{0}$ so that $\boldsymbol{\sigma}^\alpha_\Gamma \to \mathbf{0}$ in (130) for relaxed equilibrium response. Numerous viscoelastic theories for soft materials exist [2,5]. The framework of (121)–(131) is used here because its internal variable formalism is compatible with (69), (77), (100), and (115). Algorithms for updating viscoelastic stress contributions are robust and efficient [92] and have been used elsewhere for soft tissues [16].

6. Fiber viscoelasticity

Dissipative response of fiber families $k = 1, \dots$ is dictated by internal variables $\boldsymbol{\Gamma}^\alpha_{\Phi k,n}$ each with $n = 1, \dots$ relaxation times $\tau^\alpha_{\Phi k,n}$ and conjugate internal stresses $\mathbf{Q}^\alpha_{\Phi k,n}$. Internal stresses and energies are

$$\mathbf{Q}^\alpha_{\Phi k,n} = -\partial \Psi^\alpha_\Phi / \partial \boldsymbol{\Gamma}^\alpha_{\Phi k,n} = 2\partial \Psi^\alpha_{\Phi k,n} / \partial \mathbf{C}^\alpha, \qquad (132)$$

$$\Psi^\alpha_\Phi = U^\alpha_\Phi = \sum_k \Psi^\alpha_{\Phi k} = \sum_k \sum_n \Psi^\alpha_{\Phi k,n}(\boldsymbol{\Gamma}^\alpha_{\Phi k,n}, \mathbf{C}^\alpha)$$

$$= \sum_k \sum_n \int \frac{1}{2}\mathbf{Q}^\alpha_{\Phi k,n} : d\mathbf{C}^\alpha. \qquad (133)$$

Evolution equations and stored viscoelastic energies are

$$D^\alpha_t \mathbf{Q}^\alpha_{\Phi k,n} + \mathbf{Q}^\alpha_{\Phi k,n} / \tau^\alpha_{\Phi k,n} = 2D^\alpha_t (\partial \hat{\Psi}^\alpha_{\Phi k,n} / \partial \mathbf{C}^\alpha), \qquad (134)$$

$$\hat{\Psi}^\alpha_{\Phi k,n} = \frac{\beta^\alpha_{\Phi k,n} \mu^\alpha_k}{4k^\alpha_k} \left\{ \exp\left[k^\alpha_k (I^\alpha_k - 1)^2 \right] - 1 \right\} H(I^\alpha_k - 1), \qquad (135)$$

with $\beta^\alpha_{\Phi k,n} \geqslant 0$. Initial conditions and solutions (convolution integrals), followed by Cauchy stress terms, are

$$\mathbf{Q}^\alpha_{\Phi k,n0} = 2\partial \hat{\Psi}^\alpha_{\Phi k,n} / \partial \mathbf{C}^\alpha, \qquad (136)$$

$$\mathbf{Q}^\alpha_{\Phi k,n}(t) = \mathbf{Q}^\alpha_{\Phi k,n0} \exp\left[-t/\tau^\alpha_{\Phi k,n} \right]$$

$$+ \int^t_{0+} \exp\left[-(t-s)/\tau^\alpha_{\Phi k,n} \right] D^\alpha_s \left(2\partial \hat{\Psi}^\alpha_{\Phi k,n} / \partial \mathbf{C}^\alpha \right) ds, \qquad (137)$$

$$\boldsymbol{\sigma}^\alpha_\Phi = 2\frac{\rho^\alpha}{\rho^\alpha_{R0}} \mathbf{F}^\alpha \frac{\partial \Psi^\alpha_\Phi}{\partial \mathbf{C}^\alpha}(\mathbf{F}^\alpha)^\mathsf{T} = 2\frac{\rho^\alpha}{\rho^\alpha_{R0}} \mathbf{F}^\alpha \frac{\partial U^\alpha_\Phi}{\partial \mathbf{C}^\alpha}(\mathbf{F}^\alpha)^\mathsf{T}$$

$$= \frac{\rho^\alpha}{\rho^\alpha_{R0}} \sum_k \sum_n \mathbf{F}^\alpha \mathbf{Q}^\alpha_{\Phi k,n}(\mathbf{F}^\alpha)^\mathsf{T}. \qquad (138)$$

As $t/\tau^\alpha_{\Phi k,n} \to 0$, $\boldsymbol{\sigma}^\alpha_\Phi$ in (138) becomes the glassy stress

$$2\frac{\rho^\alpha}{\rho^\alpha_{R0}} \sum_k \sum_n \mathbf{F}^\alpha \frac{\partial \hat{\Psi}^\alpha_{\Phi k,n}}{\partial \mathbf{C}^\alpha}(\mathbf{F}^\alpha)^\mathsf{T}$$

$$= \frac{\rho^\alpha}{\rho^\alpha_{R0}} \sum_k \sum_n \left\{ \beta^\alpha_{\Phi k,n} \mu^\alpha_k (I^\alpha_k - 1) \exp\left[k^\alpha_k (I^\alpha_k - 1)^2 \right] \right.$$

$$\left. \times H(I^\alpha_k - 1)\tilde{\mathbf{h}}^\alpha_k \right\}. \qquad (139)$$

As $t/\tau^\alpha_{\Phi k,n} \to \infty$, $\mathbf{Q}^\alpha_{\Phi k,n} \to \mathbf{0}$ leading to $\boldsymbol{\sigma}^\alpha_\Phi \to \mathbf{0}$ in (138). This viscoelastic fiber model of Holzapfel *et al.* [16,92,102] is used for like reasons as and consistency with the prior framework for the soft-tissue matrix.

7. Active tension

Electrochemistry of soft tissue cellular activation [104] is beyond the present scope. A phenomenological approach is used instead, generalizing other continuum models [20,105,106]. Let $\{\boldsymbol{\Delta}^\alpha\} \to \{\Delta^\alpha_k\}(\mathbf{X}^\alpha, t)$ be a set of scalar internal variables associated with potentially active fiber families k in phase α. These variables can include internal strains in contractile elements and time-dependent switching functions. Define the fiber orientation tensors $\mathbf{H}^\alpha_k$ as in (117). In many models, cells are fully aligned such that $k = 1$ and $\kappa^\alpha_1 = 0$ [20,105], but this is inessential [106]. Stretch in the fiber direction is $\lambda^\alpha_k = \sqrt{I^\alpha_k}$. A generic energy function is

$$\Psi^\alpha_A = U^\alpha_A = \sum_k \Psi^\alpha_{Ak} = \sum_k \left[\Lambda^\alpha_k(\lambda^\alpha_k, \{\Delta^\alpha_k\}) + \chi^\alpha_k(\{\Delta^\alpha_k\}) \right]. \qquad (140)$$

Strain energy functions Λ^α_k furnish active stress terms

$$\boldsymbol{\sigma}^\alpha_A = 2\frac{\rho^\alpha}{\rho^\alpha_{R0}} \mathbf{F}^\alpha \frac{\partial \Psi^\alpha_A}{\partial \mathbf{C}^\alpha}(\mathbf{F}^\alpha)^\mathsf{T} = \frac{\rho^\alpha}{\rho^\alpha_{R0}} \sum_k \frac{1}{\lambda^\alpha_k} \frac{\partial \Lambda^\alpha_k}{\partial \lambda^\alpha_k} \tilde{\mathbf{h}}^\alpha_k. \qquad (141)$$

Energy functions χ^α_k ensure non-negative net dissipation. Stresses $\boldsymbol{\sigma}^\alpha_A$ should vanish for passive conditions. General form (140) is sufficient to embody successful models of muscle contraction [20,105,106]. It is physically justified by coupling of (muscle) fiber stretch to activation energy and active stress. For example, (140) and (141) do not involve deformation of the matrix since the matrix is deemed a passive element of muscle [105,106].

8. Damage

Internal variables $\{\mathbf{D}^\alpha\} \to \{\bar{D}^\alpha, D^\alpha_k\}$. Scalar damage measures in the isotropic matrix or fluid are $\bar{D}^\alpha \in [0, 1]$, and $D^\alpha_k \in [0, 1]$ are scalar functions for each fiber family k. All are akin to order parameters in phase-field fracture theory [23,31]. Degradation functions in (98)–(101) are, with $\bar{\vartheta}^\alpha \in [0, \infty)$, $\vartheta^\alpha_k \in [0, \infty)$ constants,

$$\varsigma^\alpha_V = [1 - \bar{D}^\alpha H(\ln J^\alpha)]^{\bar{\vartheta}^\alpha}, \qquad \varsigma^\alpha_S = (1 - \bar{D}^\alpha)^{\bar{\vartheta}^\alpha}, \qquad (142)$$

$$\varsigma^\alpha_F \circ (\cdot) = \varsigma^\alpha_F \circ \sum_k (\cdot)_k = \sum_k \varsigma^\alpha_{Fk}(\cdot)_k = \sum_k \left(1 - D^\alpha_k \right)^{\vartheta^\alpha_k}(\cdot)_k,$$

$$\varsigma^\alpha_{Fk} = \left(1 - D^\alpha_k \right)^{\vartheta^\alpha_k}. \qquad (143)$$

The Heaviside function in ς^α_V prevents degradation in compression so the bulk modulus is maintained [31,80]. Operator

ς_F^α in (100) and (101) is applied to a sum of energetic contributions (i.e., hyperelastic and viscoelastic) over all families k via (143). Partial stress less viscous stress of constituent α is $\bar{\boldsymbol{\sigma}}^\alpha = \boldsymbol{\sigma}^\alpha - \hat{\boldsymbol{\sigma}}^\alpha$. For an ideal gas, $\bar{D}^\alpha = \bar{\vartheta}^\alpha = 0 \to \varsigma_V^\alpha = 1$, so $\bar{\boldsymbol{\sigma}}^\alpha = -\rho^\alpha \mathfrak{R}^\alpha \theta^\alpha \mathbf{1}$ by (102). For solid and liquid α, applying (100), this stress is the sum of (107), (116), (120), (130), (138), and (141) scaled by one or more functions in (142) and (143):

$$\bar{\boldsymbol{\sigma}}^\alpha = \frac{\rho^\alpha}{\rho_{R0}^\alpha}[1 - \bar{D}^\alpha H(\ln J^\alpha)]^{\bar{\vartheta}^\alpha} B_\theta^\alpha$$
$$\times \left\{ \ln J^\alpha \left[\exp\{k_V^\alpha(\ln J^\alpha)^2\} - \frac{1}{2}\left(B_{\theta p}^\alpha - 2\right)\ln J^\alpha \right] \right.$$
$$\left. - A^\alpha\left(\theta^\alpha - \theta_0^\alpha\right)\right\}\mathbf{1} - \left(\rho^\alpha/\rho_{R0}^\alpha\right)p_{R0}^\alpha\mathbf{1}$$
$$+ \frac{\rho^\alpha}{\rho_{R0}^\alpha}(1 - \bar{D}^\alpha)^{\bar{\vartheta}^\alpha}\mu_S^\alpha\left[\tilde{\mathbf{B}}^\alpha - \frac{1}{3}(\text{tr}\tilde{\mathbf{B}}^\alpha)\mathbf{1}\right]$$
$$+ \frac{\rho^\alpha}{\rho_{R0}^\alpha}\sum_k \left(1 - D_k^\alpha\right)^{\vartheta_k^\alpha}\mu_k^\alpha\left(I_k^\alpha - 1\right)$$
$$\times \exp\left[k_k^\alpha\left(I_k^\alpha - 1\right)^2\right]H\left(I_k^\alpha - 1\right)\tilde{\mathbf{h}}_k^\alpha$$
$$+ \frac{\rho^\alpha}{\rho_{R0}^\alpha}(1 - \bar{D}^\alpha)^{\bar{\vartheta}^\alpha}\sum_l \mathbf{F}^\alpha\mathbf{Q}_{Vl}^\alpha(\mathbf{F}^\alpha)^\mathsf{T}$$
$$+ \frac{\rho^\alpha}{\rho_{R0}^\alpha}(1 - \bar{D}^\alpha)^{\bar{\vartheta}^\alpha}\sum_m \mathbf{F}^\alpha\mathbf{Q}_{Sm}^\alpha(\mathbf{F}^\alpha)^\mathsf{T}$$
$$+ \frac{\rho^\alpha}{\rho_{R0}^\alpha}\sum_k \left[\left(1 - D_k^\alpha\right)^{\vartheta_k^\alpha}\sum_n \mathbf{F}^\alpha\mathbf{Q}_{\Phi k,n}^\alpha(\mathbf{F}^\alpha)^\mathsf{T}\right]$$
$$+ \frac{\rho^\alpha}{\rho_{R0}^\alpha}\sum_k \frac{1}{\lambda_k^\alpha}\frac{\partial\Lambda_k^\alpha}{\partial\lambda_k^\alpha}\tilde{\mathbf{h}}_k^\alpha. \tag{144}$$

To preclude damage induced by normal muscle contraction, the final term is decoupled from $\{\mathbf{D}^\alpha\}$ consistently with (100) and (101). If (109) is used instead of (105), then spherical terms in (144) should appeal to (111) rather than (107). Equation (144) is compatible with the second law since it follows from (83), where the latter is deduced from the local dissipation inequality (81) using the "Coleman-Noll-Gurtin" procedure [95,96].

Let $\Psi_D^\alpha = U_D^\alpha$ comprise cohesive and surface energies of fracture per unit referential volume scaled by contributions of dimensionless Finsler-type metric $\hat{G}^\alpha$ in (B2) [52,57], where $\hat{G}^\alpha = \hat{G}^\alpha(\{\boldsymbol{\xi}^\alpha\}, \mathbf{X}^\alpha, \mathbf{x})$ via (72). Extending usual single-parameter phase-field theories, quadratic forms for matrix $[(\bar{\cdot})]$ and fiber $[(\cdot)_k]$ contributions are

$$\hat{\Psi}_D^\alpha = \Psi_D^\alpha/\sqrt{\hat{G}^\alpha} = \bar{E}_C^\alpha|\bar{D}^\alpha|^2 + \bar{\Upsilon}^\alpha\bar{l}_R^\alpha|\boldsymbol{\nabla}_0^\alpha\bar{D}^\alpha|^2$$
$$+ \sum_k \left[E_{Ck}^\alpha|D_k^\alpha|^2 + \Upsilon_k^\alpha l_{Rk}^\alpha|\boldsymbol{\nabla}_0^\alpha D_k^\alpha|^2\right]. \tag{145}$$

In (145), cohesive energies per unit volume are $\bar{E}_C^\alpha$ and E_{Ck}^α, surface energies are $\bar{\Upsilon}^\alpha$ and Υ_k^α, and gradient regularization lengths are $\bar{l}_R^\alpha = \bar{\alpha}^\alpha\bar{l}^\alpha$ and $l_{Rk}^\alpha = \alpha_k^\alpha l_k^\alpha$, all non-negative constants. For solids, typically $\bar{E}_C^\alpha = \bar{\Upsilon}^\alpha/\bar{l}^\alpha$ and $E_{Ck}^\alpha = \Upsilon_k^\alpha/l_k^\alpha$. Dimensionless factors $\bar{\alpha}^\alpha \in [0, \infty)$ and $\alpha_k^\alpha \in [0, \infty)$ allow

independent cohesive energies and gradient regularization lengths [80]. For cavitation of a fluid, gradient terms can be dropped [33] (i.e., $\bar{\alpha}^\alpha \to 0$); cohesion energy $\bar{E}_C^\alpha$ will capture fracture of the fluid for tensile pressure. Isotropic surface energies are assumed for gradient terms of (145). These could be extended to anisotropic contributions [23] if data exist. However, $\{D_k^\alpha\}$ furnish stress-damage anisotropy regardless.

When $\hat{G}^\alpha \to 1$, corresponding to a classical Euclidean material metric, (145) is justified as a standard model of phase-field fracture mechanics [31,32,80]. In the classical case ($\bar{\alpha}^\alpha \to 1$), only two parameters are needed for matrix and each fiber family, with physical meaning (i.e., cohesive energy and surface energy). Noteworthy is scaling of energy by $|\hat{G}^\alpha|^{1/2}$. Physically, as justified by studies of hard [57,63] and soft [52] solids, this scaling accounts for increases in internal free surface area of the material with microstructure as cavities enlarge or cracks slide and open. This in turn increases the material's resistance to fracture. Given the metric tensors of Sec. III C, $\hat{G}^\alpha \geqslant 1$ for the physically rational case of positive remnant strain. The increase in toughness due to remnant strain or collagen fiber sliding and remodeling [10] is akin to toughening of an elastic-plastic solid from plasticity at a crack tip.

C. Finsler metrics

Coordinate forms of metric splits in (B1) and (B2) are

$$\mathbf{g}(\mathbf{x}, t) = \bar{g}_{ik}(\mathbf{x})\hat{g}_j^k(\{\boldsymbol{\xi}^\alpha(\mathbf{x}, t)\})\mathbf{g}^i \otimes \mathbf{g}^j, \tag{146}$$

$$\mathbf{G}^\alpha(\mathbf{X}^\alpha, t) = (\bar{G}^\alpha)_{IK}(\mathbf{X}^\alpha)(\hat{G}^\alpha)_J^K(\{\boldsymbol{\Xi}^\alpha(\mathbf{X}^\alpha, t)\})(\mathbf{G}^\alpha)^I \otimes (\mathbf{G}^\alpha)^J. \tag{147}$$

Canonical transformations [52,57,63] between representations of state variables on $\mathfrak{m}$ and $\mathfrak{M}^\alpha$ are used for (72):

$$\{\boldsymbol{\Xi}^\alpha(\mathbf{X}^\alpha, t)\} = \{\boldsymbol{\xi}^\alpha(\mathbf{x}, t)\} \circ \boldsymbol{\chi}^\alpha(\mathbf{X}^\alpha, t). \tag{148}$$

Though other relationships are admissible, the analogous transformation law [52] between components of $\hat{\mathbf{G}}^\alpha$ and $\hat{\mathbf{g}}$ is prescribed here, with δ_j^i Kronecker's delta symbols:

$$(\hat{G}^\alpha)_J^I(\mathbf{X}^\alpha, t) = \delta_i^I\delta_J^j\hat{g}_j^i(\boldsymbol{\chi}^\alpha(\mathbf{X}^\alpha, t), t). \tag{149}$$

Only $\{\boldsymbol{\xi}^\alpha\}$ and $\hat{g}_j^i(\{\boldsymbol{\xi}^\alpha\})$ are defined constitutively, with (148) and (149) yielding $\{\boldsymbol{\Xi}^\alpha\}$ and $(\hat{G}^\alpha)_J^I(\{\boldsymbol{\Xi}^\alpha\})$, or vice versa if referential versions are defined instead.

Dependence of $\hat{\mathbf{g}}$ on $\{\boldsymbol{\xi}^\alpha\}$ is henceforth restricted to dependence on damage parameters ($\{\bar{D}^\alpha\}, \{D_k^\alpha\}$); (148) is $\bar{D}^\alpha(\mathbf{X}^\alpha, t) = \bar{D}^\alpha(\boldsymbol{\chi}^\alpha(\mathbf{X}^\alpha, t), t) \circ \boldsymbol{\chi}_t^\alpha$ and so on for $\{D_k^\alpha\}$. If the geometric framework is extended to describe biologic growth [54,55] and remodeling [107], then $\{\boldsymbol{\xi}^\alpha\}$ can be expanded with internal state variable(s) associated with such processes, for which kinetics of (77) are needed. For theories like Refs. [54,55], $\hat{\mathbf{G}}^\alpha$ should depend on some additional (e.g., growth) function(s), $\hat{g}_j^i \to \delta_j^i$, but (149) is not enforced, so $\mathfrak{m}$ is Euclidean but $\mathfrak{M}^\alpha$ need not be.

In the current application, as tears and commensurate fiber rearrangements arise in constituents of the mixture, the body manifold can expand and shear [52]. In applications of Sec. IV, the present specialization is restricted to a mixture having a single solid constituent. Fluids are devoid of microstructure that would affect metric tensors; any effects of

fluid cavitation, irrelevant in later calculations, are omitted. Metric forms can be expanded with additional products to allow for contributions from more constituents as shown below. Mixed-variant tensor $\hat{\mathbf{g}}$ is a product of matrix and fiber terms:

$$\hat{g}^i_j(\{\bar{D}^\alpha\}, \{D^\alpha_k\}) = \bar{\gamma}^i_k(\{\bar{D}^\alpha\})\tilde{\gamma}^k_j(\{D^\alpha_k\}). \tag{150}$$

Contributions from isotropic matrix damage $\{\bar{D}^\alpha\}$ in $\bar{\gamma}^i_j$ are assumed spherical (e.g., Weyl-type scaling [56]), measured by determinants $\bar{\gamma}^\alpha = \bar{\gamma}^\alpha(\bar{D}^\alpha)$. Spherical contributions of phases $\alpha = 1, \ldots, N$ are merged multiplicatively in $\hat{\mathbf{g}}$ since their sequence is irrelevant. Forms are

$$\bar{\gamma}^i_j = \delta^i_j \prod_\alpha (\bar{\gamma}^\alpha)^{1/3}, \quad \bar{\gamma}^\alpha = \exp\left[\frac{2n^\alpha_0 \bar{\kappa}^\alpha}{\bar{r}^\alpha}(\bar{D}^\alpha)^{\bar{r}^\alpha}\right]. \tag{151}$$

Recall $n^\alpha_0(\mathbf{X}^\alpha) \in [0, 1]$ is a reference volume fraction of phase α, and $\bar{r}^\alpha > 0$ and $\bar{\kappa}^\alpha$ are constants, the latter positive for dilatant damage. Remnant volumetric strain [52] at $\bar{D}^\alpha = 1$ is the ratio of constants $\bar{\epsilon}^\alpha = n^\alpha_0 \bar{\kappa}^\alpha/\bar{r}^\alpha$.

Fiber contributions from constituents α and families k are merged additively into $\hat{\mathbf{g}}$ since these terms are generally anisotropic [52,57]. Defining $(H^\alpha_k)^i_j = \delta^i_I \delta^J_j (H^\alpha_k)^I_J$ with $(H^\alpha_k)^I_J = \kappa^\alpha_k \delta^I_J + (1 - 3\kappa^\alpha_k)(\iota^\alpha_k)^I(\iota^\alpha_k)_J$ from (117),

$$\tilde{\gamma}^i_j = \delta^i_j + \sum_\alpha \sum_k (H^\alpha_k)^i_j \left\{ \exp\left[\frac{2n^\alpha_0 \tilde{\kappa}^\alpha_k}{\tilde{r}^\alpha_k}(D^\alpha_k)^{\tilde{r}^\alpha_k}\right] - 1 \right\}. \tag{152}$$

Constants $\tilde{r}^\alpha_k > 0$ and $\tilde{\kappa}^\alpha_k$ measure the logarithmic remnant strain contributions $\tilde{\epsilon}^\alpha_k = n^\alpha_0 \tilde{\kappa}^\alpha_k/\tilde{r}^\alpha_k$ at $D^\alpha_k = 1$.

Noting $\hat{G}^\alpha = \det \hat{\mathbf{G}}^\alpha = \det \hat{\mathbf{g}} = \hat{g}$ are related through (149), derivatives in conjugate forces (165) and (170) are found from (151) and (152) as

$$\partial(\ln \sqrt{\hat{G}^\alpha})/\partial\bar{D}^\alpha = n^\alpha_0 \bar{\kappa}^\alpha(\bar{D}^\alpha)^{\bar{r}^\alpha - 1}, \tag{153}$$

$$\frac{\partial(\ln \sqrt{\hat{G}^\alpha})}{\partial D^\alpha_k} = \exp\left[\frac{2n^\alpha_0 \tilde{\kappa}^\alpha_k}{\tilde{r}^\alpha_k}(D^\alpha_k)^{\tilde{r}^\alpha_k}\right]$$
$$\times (\tilde{\gamma}^{-1})^i_j(H^\alpha_k)^j_i n^\alpha_0 \tilde{\kappa}^\alpha_k (D^\alpha_k)^{\tilde{r}^\alpha_k - 1}. \tag{154}$$

Values $\bar{r}^\alpha \in (0, 1)$ and $\tilde{r}^\alpha_k \in (0, 1)$ produce nonsingular $\hat{\mathbf{g}}$ and admit solutions to some equilibrium problems [52]. However, these ranges can result in singularities at $\bar{D}^\alpha = 0$ and $D^\alpha_k = 0$ in (153) and (154). Such singularities can be avoided by choosing $\bar{r}^\alpha \geqslant 1$ and $\tilde{r}^\alpha_k \geqslant 1$. Stronger conditions $\bar{r}^\alpha > 1$ and $\tilde{r}^\alpha_k > 1$ usefully ensure (153), (154) vanish at (e.g., initial) states having $\bar{D}^\alpha = 0$, $D^\alpha_k = 0$. Partitions in (146) and (147) and exponential forms in (151) and (152) are chosen based on successful use in prior work [52,54]. The latter are convenient for deriving analytical solutions to problems since Christoffel symbols (i.e., derivatives) are of relatively simple form. Only a few parameters are required to fit data [52], physically related to measurable remnant strains in the case of degradation.

D. Kinetics

1. Viscous stress

Isotropic Newtonian behavior is usually adequate for each constituent α, with $\hat{B}^\alpha(\theta^\alpha) \geqslant 0$ and $\hat{\mu}^\alpha(\theta^\alpha) \geqslant 0$ possibly temperature-dependent bulk and shear viscosities. Viscous stresses and dissipation are

$$\hat{\boldsymbol{\sigma}}^\alpha = n^\alpha_0\left[\hat{B}^\alpha - \tfrac{2}{3}\hat{\mu}^\alpha\right]\text{tr}(\mathbf{d}^\alpha)\mathbf{1} + 2n^\alpha_0\hat{\mu}^\alpha\mathbf{d}^\alpha, \tag{155}$$

$$\hat{\mathfrak{D}}^\alpha = \hat{\boldsymbol{\sigma}}^\alpha : \mathbf{d}^\alpha = n^\alpha_0\hat{B}^\alpha|\text{tr}(\mathbf{d}^\alpha)|^2$$
$$+ 2n^\alpha_0\hat{\mu}^\alpha\left|\mathbf{d}^\alpha - \tfrac{1}{3}\text{tr}(\mathbf{d}^\alpha)\mathbf{1}\right|^2 \geqslant 0. \tag{156}$$

Viscous pressure and shear are $\hat{p}^\alpha = -n^\alpha_0\hat{B}^\alpha\nabla\cdot\boldsymbol{v}^\alpha$ and $\hat{\boldsymbol{\sigma}}^\alpha_S$, whereby $\hat{\boldsymbol{\sigma}}^\alpha = -\hat{p}^\alpha\mathbf{1} + \hat{\boldsymbol{\sigma}}^\alpha_S$. Relations (155) and (156) are standard, simple models used for relevant viscous fluids including air, water, and blood plasma [2,41,108], requiring only two measurable parameters. Another viscosity model obeying (71) and $\hat{\mathfrak{D}}^\alpha \geqslant 0$ could be used (e.g., for whole blood) if justified by rheology [2].

2. Viscoelasticity

Viscoelastic internal state variables are the subset of $\{\boldsymbol{\xi}^\alpha\}$ consisting of $\{\boldsymbol{\Gamma}^\alpha_{Vl}, \boldsymbol{\Gamma}^\alpha_{Sm}, \boldsymbol{\Gamma}^\alpha_{\Phi k,n}\}$. Conjugate forces entering (93) are a subset of $\{\boldsymbol{\pi}^\alpha\}$:

$$\boldsymbol{\pi}^\alpha_{Vl} = -\varsigma^\alpha_S \frac{\rho^\alpha}{\rho^\alpha_{R0}}\mathbf{Q}^\alpha_{Vl}, \quad \boldsymbol{\pi}^\alpha_{Sm} = -\varsigma^\alpha_S \frac{\rho^\alpha}{\rho^\alpha_{R0}}\mathbf{Q}^\alpha_{Sm},$$

$$\boldsymbol{\pi}^\alpha_{\Phi k,n} = -\varsigma^\alpha_{Fk} \frac{\rho^\alpha}{\rho^\alpha_{R0}}\mathbf{Q}^\alpha_{\Phi k,n}. \tag{157}$$

Kinetic laws for internal variables [91,92,100] are

$$D^\alpha_t\boldsymbol{\Gamma}^\alpha_{Vl} = \frac{\mathbf{Q}^\alpha_{Vl}}{\beta^\alpha_{Vl}B^\alpha_\theta\tau^\alpha_{Vl}}, \quad D^\alpha_t\boldsymbol{\Gamma}^\alpha_{Sm} = \frac{\mathbf{Q}^\alpha_{Sm}}{\beta^\alpha_{Sm}\mu^\alpha_S\tau^\alpha_{Sm}},$$

$$D^\alpha_t\boldsymbol{\Gamma}^\alpha_{\Phi k,n} = \frac{\mathbf{Q}^\alpha_{\Phi k,n}}{\beta^\alpha_{\Phi k,n}\mu^\alpha_k\tau^\alpha_{\Phi k,n}}. \tag{158}$$

Dissipation from viscoelasticity is non-negative in (93):

$$\mathfrak{D}^\alpha_\Gamma = \frac{\rho^\alpha}{\rho^\alpha_{R0}}\sum_l \frac{\varsigma^\alpha_S\mathbf{Q}^\alpha_{Vl} : \mathbf{Q}^\alpha_{Vl}}{\beta^\alpha_{Vl}B^\alpha_\theta\tau^\alpha_{Vl}}$$
$$+ \frac{\rho^\alpha}{\rho^\alpha_{R0}}\sum_m \frac{\varsigma^\alpha_S\mathbf{Q}^\alpha_{Sm} : \mathbf{Q}^\alpha_{Sm}}{\beta^\alpha_{Sm}\mu^\alpha_S\tau^\alpha_{Sm}}$$
$$+ \frac{\rho^\alpha}{\rho^\alpha_{R0}}\sum_k\sum_n \frac{\varsigma^\alpha_{Fk}\mathbf{Q}^\alpha_{\Phi k,n} : \mathbf{Q}^\alpha_{\Phi k,n}}{\beta^\alpha_{\Phi k,n}\mu^\alpha_k\tau^\alpha_{\Phi k,n}} \geqslant 0. \tag{159}$$

Initial conditions for state variables are $\boldsymbol{\Gamma}^\alpha_{Vl0} = \mathbf{0}$, $\boldsymbol{\Gamma}^\alpha_{Sm} = \mathbf{0}$, and $\boldsymbol{\Gamma}^\alpha_{\Phi k,n} = \mathbf{0}$. For energies, $\Psi^\alpha_{Vl}(\mathbf{0}, \mathbf{C}^\alpha) = \hat{\Psi}^\alpha_{Vl}(\mathbf{C}^\alpha)$, $\Psi^\alpha_{Sm}(\mathbf{0}, \mathbf{C}^\alpha) = \hat{\Psi}^\alpha_{Sm}(\mathbf{C}^\alpha)$, $\Psi^\alpha_{\Phi k,n}(\mathbf{0}, \mathbf{C}^\alpha) = \hat{\Psi}^\alpha_{\Phi k,n}(\mathbf{C}^\alpha)$. Configurational energies are integrated over time as

$$\Psi^\alpha_\Gamma = \sum_l\left[\hat{\Psi}^\alpha_{Vl} - \int_0^t \mathbf{Q}^\alpha_{Vl} : D^\alpha_s\boldsymbol{\Gamma}^\alpha_{Vl}\,ds\right]$$
$$+ \sum_m\left[\hat{\Psi}^\alpha_{Sm} - \int_0^t \mathbf{Q}^\alpha_{Sm} : D^\alpha_s\boldsymbol{\Gamma}^\alpha_{Sm}\,ds\right], \tag{160}$$

$$\Psi^\alpha_\Phi = \sum_k\sum_n\left[\hat{\Psi}^\alpha_{\Phi k,n} - \int_0^t \mathbf{Q}^\alpha_{\Phi k,n} : D^\alpha_s\boldsymbol{\Gamma}^\alpha_{\Phi k,n}\,ds\right]. \tag{161}$$

Viscoelastic kinetics are consistent with (121)–(139) and Refs. [91,92,100]. This theory is further justified by its need for only two parameters for each mode $(\cdot)^\alpha_{k,n}$: glassy factor β and relaxation time τ. In Sec. IV B, this framework depicts

compression and tension data well on liver and muscle across a wide range of loading rates.

3. Active tension

Internal state variables in $\{\boldsymbol{\xi}^\alpha\}$ are the scalar functions $\{\Delta_k^\alpha\}$ with k the fiber family number. Kinetic equations with initial conditions are imposed directly [20,105,106] rather than by more sophisticated electrochemical physics [104] outside the present scope:

$$D_t^\alpha \{D_t^\alpha \Delta_k^\alpha\} = \{D_t^\alpha \Delta_k^\alpha\}(\mathbf{X}^\alpha, t),$$
$$\{\Delta_k^\alpha\}(\mathbf{X}^\alpha, 0) = \{\Delta_{k0}^\alpha\}(\mathbf{X}^\alpha). \tag{162}$$

Evolution equations (162) should implicitly be affected by local states; for example, the history of fiber damage $\{D_k^\alpha\}$, if severe, should limit maximum contractile stress. Conjugate forces in (93) are the following parts of $\{\boldsymbol{\pi}^\alpha\}$:

$$\{\pi_{Ak}^\alpha\}(\lambda_k^\alpha, \{\Delta_k^\alpha\})$$
$$= \varsigma_{Fk}^\alpha \frac{\rho^\alpha}{\rho_{R0}^\alpha} \frac{\partial}{\partial\{\Delta_k^\alpha\}}\left[\Lambda_k^\alpha(\lambda_k^\alpha, \{\Delta_k^\alpha\}) + \chi_k^\alpha(\{\Delta_k^\alpha\})\right]. \tag{163}$$

Dissipation from activation or passivation should be non-negative, to be ensured by storage-release functions χ_k^α:

$$\mathfrak{D}_A^\alpha = -\sum_k \{\pi_{Ak}^\alpha\} \cdot \{D_t^\alpha \Delta_k^\alpha\} \geqslant 0. \tag{164}$$

The framework (162)–(164) is justified by compatibility with (100), (140), and (141), and non-negative dissipation. A specialization in Sec. IV B provides validation in the context of experimental data [20,109].

4. Damage

From (100) and (145), conjugate forces to damage measures for the matrix in $\{\boldsymbol{\pi}^\alpha\}$ and $\{\boldsymbol{\zeta}^\alpha\}$ are

$$\bar{\pi}_D^\alpha = \rho^\alpha \frac{\partial \psi^\alpha}{\partial \bar{D}^\alpha} = \frac{\rho^\alpha}{\rho_{R0}^\alpha} \frac{\partial}{\partial \bar{D}^\alpha}\left[\sqrt{\hat{G}^\alpha} \hat{\Psi}_D^\alpha\right.$$
$$\left. + \varsigma_V^\alpha \Psi_V^\alpha + \varsigma_S^\alpha(\Psi_S^\alpha + \Psi_\Gamma^\alpha)\right]$$
$$= \frac{\rho^\alpha}{\rho_{R0}^\alpha}\left[2\sqrt{\hat{G}^\alpha}\bar{E}_C^\alpha \bar{D}^\alpha + \Psi_D^\alpha \frac{\partial}{\partial \bar{D}^\alpha}\ln\sqrt{\hat{G}^\alpha}\right]$$
$$- \frac{\rho^\alpha}{\rho_{R0}^\alpha}\bar{\vartheta}^\alpha[1 - \bar{D}^\alpha H(\ln J^\alpha)]^{\bar{\vartheta}^\alpha - 1} H(\ln J^\alpha)\Psi_V^\alpha$$
$$- \frac{\rho^\alpha}{\rho_{R0}^\alpha}\bar{\vartheta}^\alpha[1 - \bar{D}^\alpha]^{\bar{\vartheta}^\alpha - 1}(\Psi_S^\alpha + \Psi_\Gamma^\alpha), \tag{165}$$

$$\bar{\zeta}_D^\alpha = \rho^\alpha \mathbf{F}^\alpha \frac{\partial \psi^\alpha}{\partial \nabla_0^\alpha \bar{D}^\alpha} = \frac{\rho^\alpha}{\rho_{R0}^\alpha}\sqrt{\hat{G}^\alpha}\mathbf{F}^\alpha \frac{\partial \hat{\Psi}_D^\alpha}{\partial \nabla_0 \bar{D}^\alpha}$$
$$= 2\frac{\rho^\alpha}{\rho_{R0}^\alpha}\sqrt{\hat{G}^\alpha}\bar{\Upsilon}^\alpha \bar{l}_R^\alpha \mathbf{F}^\alpha[(\nabla \bar{D}^\alpha)\mathbf{F}^\alpha]. \tag{166}$$

Define total conjugate force to damage in the matrix:

$$\bar{F}_D^\alpha = -\bar{\pi}_D^\alpha + \nabla \cdot \bar{\zeta}_D^\alpha. \tag{167}$$

Define viscosity $\bar{v}_D^\alpha \geqslant 0$. A Ginzburg-Landau kinetic law and non-negative dissipation for the matrix in (93) are

$$n_0^\alpha \bar{v}_D^\alpha D_t^\alpha \bar{D}^\alpha = \bar{F}_D^\alpha, \tag{168}$$

$$\bar{\mathfrak{D}}_D^\alpha = \bar{F}_D^\alpha D_t^\alpha \bar{D}^\alpha = n_0^\alpha \bar{v}_D^\alpha |D_t^\alpha \bar{D}^\alpha|^2 \geqslant 0. \tag{169}$$

To render the damage rate always non-negative, (168) can be modified to $n_0^\alpha \bar{v}_D^\alpha D_t^\alpha \bar{D}^\alpha = \bar{F}_D^\alpha H(\bar{F}_D^\alpha)$. Damage kinetics are suppressed for $\bar{v}_D^\alpha \to \infty$ and rate independent for $\bar{v}_D^\alpha \to 0$ with equilibrium condition $\bar{F}_D^\alpha = 0$. For rate insensitivity, irreversibility is enforced by setting $\bar{D}^\alpha(t)$ to the maximum of the argument of $\bar{F}_D^\alpha(\bar{D}^\alpha; \cdot)(t) = 0$ and $\bar{D}^\alpha(s)\,\forall\, s < t$, where the latter renders $D_t^\alpha \bar{D}^\alpha(t^-) \to 0$. Usual, but inessential, initial conditions are $\bar{D}_0^\alpha = 0$.

When $\hat{G}^\alpha \to 1$, this theory reduces to Ginzburg-Landau or Allen-Cahn kinetics [77], justified as standard for phase-field modeling of fracture [32,80]. The nondissipative simplification $\bar{v}_D^\alpha \to 0$ is popular for quasistatics [23,31]. The formulation has been used elsewhere for arterial rupture [22,23]. As remarked following (145), noteworthy is the factor $\hat{G}^\alpha > 1$, which increases fracture resistance due to microstructure changes associated with remnant strain, for example nonaffine collagen fiber deformations and fibril-matrix sliding [10]. This feature was instrumental for modeling skin tearing [52]. Factors proportional to Ψ_D^α in (165) and later (170) contribute to dissipation in a similar way as the spherical part of the Eshelby stress, proportional to Helmholtz free energy, in finite plasticity theory [110] and growth mechanics [111].

Damage in fiber families k is treated analogously. Viscosities are $v_{Dk}^\alpha \geqslant 0$. Conjugate thermodynamic forces and dissipative Ginzburg-Landau kinetics are

$$\pi_{Dk}^\alpha = \rho^\alpha \frac{\partial \psi^\alpha}{\partial D_k^\alpha} = \frac{\rho^\alpha}{\rho_{R0}^\alpha} \frac{\partial}{\partial D_k^\alpha}\left[\sqrt{\hat{G}^\alpha}\hat{\Psi}_D^\alpha + \varsigma_{Fk}^\alpha(\Psi_{Fk}^\alpha + \Psi_{\Phi k}^\alpha)\right]$$
$$= \frac{\rho^\alpha}{\rho_{R0}^\alpha}\left[2\sqrt{\hat{G}^\alpha}E_{Ck}^\alpha D_k^\alpha + \Psi_D^\alpha \frac{\partial}{\partial D_k^\alpha}\ln\sqrt{\hat{G}^\alpha}\right]$$
$$- \frac{\rho^\alpha}{\rho_{R0}^\alpha}\vartheta_k^\alpha[1 - D_k^\alpha]^{\vartheta_k^\alpha - 1}(\Psi_{Fk}^\alpha + \Psi_{\Phi k}^\alpha), \tag{170}$$

$$\zeta_{Dk}^\alpha = \rho^\alpha \mathbf{F}^\alpha \frac{\partial \psi^\alpha}{\partial \nabla_0^\alpha D_k^\alpha} = \frac{\rho^\alpha}{\rho_{R0}^\alpha}\sqrt{\hat{G}^\alpha}\mathbf{F}^\alpha \frac{\partial \hat{\Psi}_D^\alpha}{\partial \nabla_0 D_k^\alpha}$$
$$= 2\frac{\rho^\alpha}{\rho_{R0}^\alpha}\sqrt{\hat{G}^\alpha}\Upsilon_k^\alpha l_{Rk}^\alpha \mathbf{F}^\alpha[(\nabla D_k^\alpha)\mathbf{F}^\alpha], \tag{171}$$

$$F_{Dk}^\alpha = -\pi_{Dk}^\alpha + \nabla \cdot \zeta_{Dk}^\alpha, \tag{172}$$

$$n_0^\alpha v_{Dk}^\alpha D_t^\alpha D_k^\alpha = F_{Dk}^\alpha, \tag{173}$$

$$\mathfrak{D}_{DF}^\alpha = \sum_k \mathfrak{D}_{Dk}^\alpha = \sum_k F_{Dk}^\alpha D_t^\alpha D_k^\alpha$$
$$= n_0^\alpha \sum_k v_{Dk}^\alpha |D_t^\alpha D_k^\alpha|^2 \geqslant 0. \tag{174}$$

To forbid healing, $n_0^\alpha v_{Dk}^\alpha D_t^\alpha D_k^\alpha = F_{Dk}^\alpha H(F_{Dk}^\alpha)$ in lieu of (173). For rate insensitivity, $v_{Dk}^\alpha \to 0 \Rightarrow F_{Dk}^\alpha = 0$ with possible irreversibility constraints analogous to those for $\bar{D}^\alpha(t)$. Usual initial conditions are $D_{k0}^\alpha = 0$.

5. Heat conduction

Fourier conduction is usually sufficient for each bulk constituent α, with isotropic conductivity $\kappa_\theta^\alpha(\theta, \{\boldsymbol{\xi}^\alpha\}) \geqslant 0$, often temperature and internal-state dependent. It could degrade

with damage via, e.g., $\kappa_\theta^\alpha \approx \varsigma_V^\alpha \kappa_{\theta 0}^\alpha$. Heat flux and entropy production are

$$\mathbf{q}^\alpha = -n_0^\alpha \kappa_\theta^\alpha \boldsymbol{\nabla}\theta^\alpha, \quad \mathfrak{D}_q^\alpha = -(\mathbf{q}^\alpha \cdot \boldsymbol{\nabla}\theta^\alpha)/\theta^\alpha$$

$$= (n_0^\alpha \kappa_\theta^\alpha/\theta^\alpha)|\boldsymbol{\nabla}\theta^\alpha|^2 \geqslant 0. \tag{175}$$

Such textbook isotropic Fourier conduction has been used elsewhere for soft tissue [112]. Realism may improve with anisotropic conductivity, if measured. Any other model obeying (73) and $\mathfrak{D}_q^\alpha \geqslant 0$ could be substituted.

6. Momentum transfer

Momentum exchange includes Darcy-like contributions from velocity differences $\boldsymbol{v}^\alpha - \boldsymbol{v}^\beta = \boldsymbol{\mu}^\alpha - \boldsymbol{\mu}^\beta$ [48,50] and mass exchange to satisfy (51):

$$\mathbf{h}^\alpha = -\sum_\beta [\lambda^{\alpha\beta}(\boldsymbol{\mu}^\alpha - \boldsymbol{\mu}^\beta)] - \hat{c}^\alpha \boldsymbol{\mu}^\alpha. \tag{176}$$

The inverse hydraulic-type conductivity matrix is $\lambda^{\alpha\beta} = \lambda^{\beta\alpha}$. Summing (176) over α, total contributions to linear momentum from the first sum on the right of (176) vanish, producing (51), consistent with Ref. [37] and the mixture momentum balance in the second of (53). Forces $\mathbf{h}^\alpha$ do not necessarily sum to zero if mass supplies $\hat{c}^\alpha$ are nonzero. Entries $\lambda^{\alpha\beta} \geqslant 0$ can depend on temperature and volume of each phase (e.g., to account for changes in interphase viscosity with temperature and in permeability with porosity [41]) and degrade with damage [42]:

$$\lambda^{\alpha\beta}(J^\alpha, J^\beta, \theta^\alpha, \theta^\beta, \bar{D}^\alpha, \bar{D}^\beta)$$

$$= \bar{\lambda}^{\alpha\beta}(J^\alpha, J^\beta, \theta^\alpha, \theta^\beta)\sqrt{\varsigma_V^\alpha \varsigma_V^\beta}. \tag{177}$$

Relation (176) is justified as follows. As discussed by Bowen [37,66], $\mathbf{h}^\alpha$ must be an odd function of phase velocity differences and conserve total momentum per (51). The first sum, linear in velocity differences, is a simple expression that fulfills the first requirement. The second sum in (176) is the simplest that can enforce the second requirement. Higher-order (e.g., cubic) terms could be added at the expense of more parameters. Only the linear terms affect weak-shock solutions derived in Sec. IV C. In the absence of mass supplies, (176) is standard for poromechanics, including biology [41,50,97].

7. Energy transfer

Energy exchange includes heat transfer from temperature differences $\theta^\alpha - \theta^\beta$ as well as momentum and mass exchange terms to satisfy (52):

$$\epsilon^\alpha = -\sum_\beta [\omega^{\alpha\beta}(\theta^\alpha - \theta^\beta)] - m^\alpha \sum_\beta \mathbf{h}^\beta \cdot \boldsymbol{\mu}^\beta$$

$$- m^\alpha \sum_\beta \hat{c}^\beta \left(u^\beta + \frac{1}{2}|\boldsymbol{\mu}^\beta|^2\right), \tag{178}$$

recalling mass concentration $m^\alpha = \rho^\alpha/\rho$ from (68). The matrix of heat transfer coefficients $\omega^{\alpha\beta} = \omega^{\beta\alpha} \geqslant 0$ can depend on state variables and damage [42] like (177):

$$\omega^{\alpha\beta}(J^\alpha, J^\beta, \theta^\alpha, \theta^\beta, \bar{D}^\alpha, \bar{D}^\beta)$$

$$= \bar{\omega}^{\alpha\beta}(J^\alpha, J^\beta, \theta^\alpha, \theta^\beta)\sqrt{\varsigma_V^\alpha \varsigma_V^\beta}. \tag{179}$$

In compression, contact among fully broken constituents permits momentum and heat transfer in respective (177) and (179) even if $\bar{D}^\alpha \to 1$ or $\bar{D}^\beta \to 1$. Damage dependence differing from basic illustrations (177) and (179) (e.g., Ref. [42]) could be substituted. The form of (178) is motivated as follows. The linear term in temperature differences is standard for heat exchange in soft tissues [112,113]. The second and third sums are simple additions that can be used to satisfy mixture energy conservation in (52) and (54). These are even functions of velocities per known thermodynamic restrictions [37,66].

8. Mass transfer

Terms $\hat{c}^\alpha$ sum to zero in (51); they account for mass supply and transfer rates between constituents. In biology, these could relate to growth, for example, nutrients dissolved in a fluid to support growth of new solid tissue. Thermodynamic constraints emerge from (86) with (176) and stipulation that the rightmost two sums in (86) should be non-negative in concert:

$$\sum_\alpha \left[\frac{\epsilon^\alpha}{\theta^\alpha} + c^\alpha \eta^\alpha\right] = \sum_\alpha \sum_\beta \frac{\omega^{\alpha\beta}(\theta^\alpha - \theta^\beta)^2}{2\theta^\alpha\theta^\beta}$$

$$+ \sum_\alpha \frac{m^\alpha}{2\theta^\alpha} \sum_\beta \lambda^{\alpha\beta}|\boldsymbol{\mu}^\alpha - \boldsymbol{\mu}^\beta|^2$$

$$+ \sum_\alpha \frac{m^\alpha}{\theta^\alpha} \sum_\beta \hat{c}^\beta \left[\frac{|\boldsymbol{\mu}^\beta|^2}{2} - u^\beta\right]$$

$$+ \sum_\alpha \hat{c}^\alpha \eta^\alpha + \rho\eta\, \partial_t \ln\sqrt{g} \geqslant 0. \tag{180}$$

The first two double sums in (180) are always non-negative. When all $\epsilon^\alpha = 0$ and $\hat{c}^\alpha = 0$ (i.e., no energy exchanges or net mass supplies), (180) becomes, with (B1), $\eta\, \partial_t \hat{g} \geqslant 0$. Then when $\rho\eta = \sum_\alpha \rho^\alpha \eta^\alpha > 0$, the non-Euclidean part of the metric tensor $\hat{\mathbf{g}}$ should only be dilating, which is consistent with non-negative remnant strains from matrix and fiber degradation in Sec. III C.

Differentiating m^α of (68) and using (15), (43), (44), and (51), mass concentration rates $\dot{m}^\alpha$ relate to $\hat{c}^\alpha$ [37]:

$$\hat{c}^\alpha = \rho\dot{m}^\alpha + \boldsymbol{\nabla} \cdot (\rho^\alpha \boldsymbol{\mu}^\alpha), \quad \sum_\alpha \dot{m}^\alpha = 0. \tag{181}$$

Kinetic equations for $\dot{m}^\alpha$ or $D_t^\alpha m^\alpha$ could be prescribed in lieu of $\hat{c}^\alpha$. Detailed constitutive equations for growth and remodeling are beyond the present scope. Example functions such as $\hat{c}^\alpha$ pertinent to reactive tissues, respecting total mass conservation, are found in Refs. [75,114,115].

The Allen-Cahn equation has been used for kinetics of remodeling processes that do not affect mass density [49]. This equation, in bare form, is likely unsuitable for $\dot{m}^\alpha$ and $\hat{c}^\alpha$ since it need not respect (51), (180), and (181). A variation on the Cahn-Hilliard equation with source term $\hat{c}^\alpha$ might be admitted for $\dot{m}^\alpha$ by allowing energy density to depend on mass concentration and concentration gradients and accounting for work of the latter in the energy balance [77]. The Cahn-Hilliard equation is classically used to simulate spinodal decomposition [116]. The current theory is unable to predict

spinodal decomposition; aforementioned adaptations could permit this, but spontaneous agglomeration of phases might not be realistic for tissues, depending on their microstructures.

E. Summary

Total stress $\boldsymbol{\sigma}^\alpha$ for constituent α is the sum of (144) and (155). Total stress for the mixture $\boldsymbol{\sigma}$ is (46). Total constituent dissipation $\mathfrak{D}^\alpha$ entering (93) is the sum of (156), (159), (164), (169), (174), and (175), each individually non-negative:

$$\mathfrak{D}^\alpha - (\mathbf{q}^\alpha \cdot \nabla\theta^\alpha)/\theta^\alpha = \hat{\mathfrak{D}}^\alpha + \mathfrak{D}_\Gamma^\alpha + \mathfrak{D}_A^\alpha$$
$$+ \bar{\mathfrak{D}}_D^\alpha + \mathfrak{D}_{DF}^\alpha + \mathfrak{D}_q^\alpha \geqslant 0. \quad (182)$$

The total dissipation inequality of (86) is then

$$\sum_\alpha \left[\frac{\mathfrak{D}^\alpha + \mathfrak{D}_q^\alpha}{\theta^\alpha} \right] + \sum_\alpha \left[\frac{\epsilon^\alpha}{\theta^\alpha} + c^\alpha \eta^\alpha \right] \geqslant 0. \quad (183)$$

From (14), boundary conditions are required for each constituent $\alpha = 1, \ldots, N$. Mechanical conditions are prescribed histories of traction $\mathbf{t}^\alpha$ or velocity $\boldsymbol{v}^\alpha$ on $\partial\Omega$. Thermal conditions are histories of flux q_n^α or temperature θ^α on $\partial\Omega$. For internal variables $\{\boldsymbol{\xi}^\alpha\}$ with gradient energetic dependence (e.g., order parameters for damage), histories of fluxes $\{\mathbf{z}^\alpha\} = (\rho^\alpha \partial\psi^\alpha/\partial\{\nabla\boldsymbol{\xi}\}^\alpha) \cdot \mathbf{n}$ or conjugate rates $D_t^\alpha \boldsymbol{\xi}^\alpha$ are needed on $\partial\Omega$. Histories of body force $\mathbf{b}^\alpha$ and heat source r^α are prescribed over Ω.

The constitutive framework of Sec. III is now summarized. The mixture consists of one or more coexisting phases $\alpha = 1, \ldots, N$. The total free and internal energies of each α are (100) and (101). A single phase can include any or all of the following features: EOS (ideal gas or condensed matter), matrix elasticity, fiber elasticity, matrix viscoelasticity, fiber viscoelasticity, active fiber tension, damage (fluid cavitation, matrix and/or fiber fractures), non-Euclidean (e.g., Finsler or Riemannian) metric tensor contribution, Newtonian viscosity, and Fourier conduction. When $N > 1$, the material is further described by momentum, energy, and mass exchanges among (all) phases. Typically, as is in Sec. IV, a subset of features is sufficient to describe a real material over a given loading regime. For example, an EOS is all that is needed for modeling the shock Hugoniot of isolated fluids. Active tension is intended for muscle contraction and is not relevant for passive constituents. In all applications of Sec. IV, $\hat{c}^\alpha = 0 \, \forall \alpha = 1, \ldots, N$ is imposed since growth and remodeling usually require much longer timescales than prescribed loading durations [93]. Governing equations of Sec. II and constitutive theory of Sec. III are used for all applications in Sec. IV. No new theories or models are introduced, only material parameters and specialized forms of some equations of Secs. II and III.

IV. SOFT-TISSUE PHYSICS

A. Shock Hugoniot response

1. Fluids

The theory is first exercised for three fluids that comprise the majority of soft tissues: water, extracellular fluid (ECF, representative of blood plasma [2] and interstitial fluid in skeletal muscle and skin), and whole blood, the latter with

TABLE I. Physical properties or model parameters for water, ECF, human blood, and porcine skeletal muscle (cells and matrix, $\alpha = k = 1$, vol. fract. $n_0^1 = 0.9$).

Property	Water	ECF	Human blood	Porcine muscle
ρ_{R0}^α (g/cm^3)	1.00	1.03	1.06	1.10
B_η^α (GPa)	2.10	2.20	2.64	3.28
c_ϵ^α (J/g K)	4.15	3.96	3.58	3.25
γ_0^α (–)	0.120	0.132	0.160	0.313
$B_{\eta p}^\alpha$ (–)	6.96	6.96	12.0	8.0
k_V^α (–)	7.0	7.0	0.0	6.0
$\hat{B}^\alpha$ (mPa s)	2.1	...	...	...
$\hat{\mu}^\alpha$ (mPa s)	0.8	1.2	5.0	...
μ_S^α (kPa)	...	...	...	1.0
μ_k^α (kPa)	...	...	...	1.0
k_k^α (–)	...	...	...	10.0
β_S^α (–)	...	...	...	1.0×10^5
$\beta_{\Phi k}^\alpha$ (–)	...	...	...	1.0×10^5
J_C (kJ/m^2)	...	...	...	0.84
l^α (mm)	...	...	...	0.88
ϑ^α (–)	...	...	...	2.0
ϵ_r^α (–)	...	...	...	0.2
$\bar{r}^\alpha = \tilde{r}_k^\alpha$ (–)	...	...	...	2.0

a realistic hematocrit of 0.4. Shock responses are modeled via theory of Sec. II B with each fluid a single-phase material ($\alpha = N = 1$, superscript henceforth suppressed). Planar (1D) impact is along the $x = x^1$ direction. Fluid is quiescent upstream, at density ρ_0, temperature θ_0, and ambient pressure $p_0 = p_{R0} = 1$ atm. Eulerian and Lagrangian shock speeds are identical, labeled $\mathcal{U}$. Particle velocity in Hugoniot states is $v^- = v$. In Hugoniot (i.e., downstream shocked) $(\cdot)^-$ states,

$$\rho = \rho_0/J, \quad J = F_1^1 = F = \partial\chi/\partial X, \quad (184)$$

$$u = U/\rho_0, \quad t_1 = \sigma_1^1 = -P = -p, \quad (185)$$

where U is energy per unit reference volume and P is longitudinal Cauchy stress, positive in compression. Since volume fraction $n_0^1 = n^1 = 1$, $\rho_{R0} = \rho_0$, and $\rho_R = \rho$.

To calculate the material response, J is decremented from unity. At each decrement, the constitutive model, here the condensed matter EOS for U_V and p_V in (109)–(111), is solved concurrently with Hugoniot energy equation (41) for P and η. With macroscopically adiabatic conditions assumed and $\{z\} = 0$, the latter reduces to

$$U = \frac{1}{2}(P + p_0)(1 - J) \quad (186)$$

since $U_0 = 0$ and $J = 1$ upstream. Then v, $\mathcal{U}$, and θ are found from (39) and (112). For single-phase materials, $\boldsymbol{\mu}^\alpha = \mathbf{0}$, $\mathbf{h}^\alpha = \mathbf{0}$, $\epsilon^\alpha = 0$, and here $\hat{c}^\alpha = 0$. For compression, fluid cavitation is omitted, so no damage is modeled. Hence, all metrics are Euclidean: $g = G = \hat{g} = \hat{G} = 1$.

Properties entering the EOS are listed in Table I. All are obtained or estimated from experimental literature [2,108,117–120] with the exception of nonlinear bulk stiffening parameters $B_{\eta p}$ and k_V that are fit to the experimental Hugoniot data. The ambient bulk modulus is related to the bulk sound velocity $c_B = \sqrt{(B_\eta + p_0)/\rho_0}$. For water, the usual relationship $B_{\eta p} = 4S - 1$ is used, where S is the slope of a linear
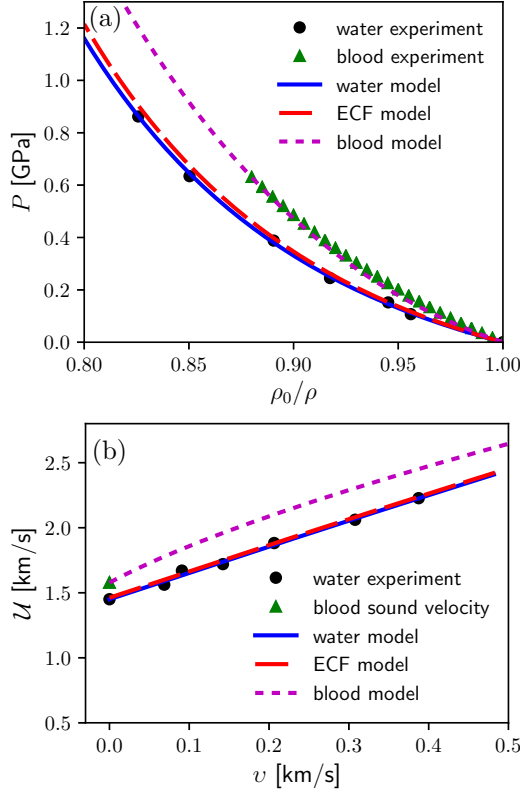
FIG. 1. Model results and shock data [118,122] for (a) Hugoniot stress vs mass density and (b) shock velocity vs particle velocity in water, ECF, and human blood.

fit to the $\mathcal{U}$-υ Hugoniot [69]. Since shock compression data are apparently unavailable for ECF, $B_{\eta p}$ and k_V for water are assigned. Newtonian viscosities $\hat{B}$, $\hat{\mu}$ are listed for completeness [2,108], where $\hat{\mu}$ for blood is for high rates [2] and bulk viscosity is supplied only for water [108]. These do not enter the present analysis. Newtonian viscosity (155) and Fourier conduction (175) are omitted; both are incompatible with treatment of shocks as singular surfaces [121].

Compared in Fig. 1(a) are P-ρ Hugoniot predictions and experimental data on water ($\theta_0 = 297$ K) [118] and human blood ($\theta_0 \approx 310$ K) [122]. Shock data on ECF do not seem to exist; predictions are for $\theta_0 = 310$ K. Compared in Fig. 1(b) are $\mathcal{U}$-υ data for water [118] and predictions for all three fluids; shock velocity data were not reported for blood in Ref. [122]. The c_B value for blood, $\mathcal{U} \to c_B$ as $\upsilon \to 0$, is from Ref. [120].

Only two EOS parameters need be fitted. Results in Fig. 1 confirm validity of the EOS of Sec. III B for water and human blood. The latter is stiffer than ECF, which is stiffer than water. Neither vaporization nor solidification is modeled here; the EOS would need modification to account for latent heats and differing properties of solid, liquid, and gas phases. Temperature rise predicted at 20% compression is on the order of 20 K, by which water should remain in its liquid phase according to the P-θ phase diagram in Ref. [118]. Solid-liquid-gas phase diagrams of ECF and blood appear to be unknown at high pressures, but neither experiments nor the EOS in Ref. [122] indicate any phase transition occurs.

2. Skeletal muscle

Planar shock response of skeletal muscle is predicted next. Properties and loading conditions replicate impact experiments of Wilgeroth *et al.* [4,51] on porcine muscle tissue. The material is modeled as a mixture of two coexisting phases ($\alpha = 1, 2$): a "solid" tissue of initial volume fraction $n_0^1 = 0.9$ [123] and an interstitial fluid depicted by the ECF, comprising remaining fraction $n_0^2 = 0.1$. The first phase consists of the muscle cells (i.e., fibers), collagenous connective tissues, and ground substance between and encasing the cells (i.e., the extracellular matrix). Muscle cells contain significant internal fluid whose physical properties are included implicitly in the constitutive model for the first phase.

Experiments [51] show a single-wave structure with steep shock front (rise time on the order of μs or smaller) rather than multiple waveforms that would be expected if shock and particle velocities among the phases differed significantly [50,66]. This suggests inverse hydraulic conductivity is very large (e.g., $\lambda^{\alpha\beta} \vec{\to} \infty$) at these high-pressure dynamic conditions, and diffusion velocities $\boldsymbol{\mu}^\alpha$ are negligible. It is thus assumed particle velocity histories match in each phase: $\upsilon^\alpha(x, t) = \upsilon^1(x, t) = \upsilon^2(x, t) = \upsilon(x, t)$. Therefore, $J(x, t) = F(x, t) = \partial\chi/\partial X$ is identical in each constituent. Microsecond scales are too brief for biologic mass exchange: $\hat{c}^\alpha = 0$. Shock compression is adiabatic: $q^\alpha \to 0$. Heat transfer in ϵ^α of (178) is likewise assumed null in Hugoniot states: $\theta^\alpha = \theta^1 = \theta^2 = \theta$. Coincident velocities and temperatures have been used elsewhere in constrained mixture theories [74,75,114,115].

The solution procedure is similar to that for single fluids, but the constitutive model is now much more complex. The shock response is that of the mixture, where governing and jump equations are in (57)–(65). Both phases are quiescent and at reference $\theta_0 = 310$ K and $p_{R0} = 1$ atm upstream; θ_0 was unreported in Ref. [51], but model results are insensitive to θ_0. From (46) and (47) with $\boldsymbol{\mu}^\alpha = \mathbf{0}$, mixture stress and internal energy are

$$\boldsymbol{\sigma} = \sum_\alpha \boldsymbol{\sigma}^\alpha, \quad U = \sum_\alpha n_0^\alpha \rho_{R0}^\alpha u^\alpha = \sum_\alpha n_0^\alpha U^\alpha. \quad (187)$$

Because all phases deform equally without mass supplies, the mixture density is $\rho = \rho_0/J$. As explained later in the context of (191), $\{\mathbf{z}^\alpha\} \to \{z^\alpha\} = 0$. The analog of (41) for the mixture reduces to (186) with $U_0 = 0$ and $p_0 = \sum_\alpha n_0^\alpha p_{R0}^\alpha$. In calculations, J is reduced incrementally from unity. In each decrement, energy equation (186) and constitutive equations for each phase are solved simultaneously and summed, if appropriate, to give mixture values P, U, and θ. Given θ and J, entropy η^α of each phase is found by inversion of (112). Particle and shock velocities are found from mixture analogs of (39). The response of the fluid phase (ECF, $\alpha = 2$) is calculated as before; its energy and pressure contributions are given fully by U_V^α and p_V^α.

The tissue phase (including intracellular fluids), $\alpha = 1$, has a total internal energy per unit reference volume U^α:

$$U^1 = U_V^1 + \varsigma_S^1 \cdot \left(U_S^1 + U_\Gamma^1\right) + \varsigma_F^1 \circ \left(U_F^1 + U_\Phi^1\right) + U_D^1. \quad (188)$$

The first term on the right is the EOS (noting $\varsigma_V = 1$ for compression), second and third are deviatoric matrix

elasticity and viscoelasticity, third and fourth are deviatoric fiber elasticity and viscoelasticity, and the last is surface energy of soft-tissue degradation (i.e., damage). Only passive states are modeled: $U_A^1 = 0$. Thermal variables θ^1 and η^1 only enter U_V^1, which fully specifies the partial pressure p^1. Notation U and Ψ is interchangeable for remaining terms that only affect deviatoric response.

Matrix viscoelasticity is limited to the shear response, following typical assumptions for nearly incompressible soft materials [16,91,92]. For very rapid loading modeled here, viscous relaxation for all (m) configurational variables $\mathbf{\Gamma}_{Sm}^1$ is assumed negligible with $t/\tau_{Sm}^1 \to 0$, so

$$U_S^1 + U_\Gamma^1 \to U_S^1 + \sum_m \hat{\Psi}_{Sm}^1 = U_S^1 \left(1 + \sum_m \beta_{Sm}^1\right). \quad (189)$$

Thus, $\check{\mu}_S^1 = \mu_S^1(1 + \sum_m \beta_{Sm}^1)$ is the glassy shear modulus of the matrix, with static energy and modulus in (115).

Muscle fibers comprise one family, $k = 1$, of direction $\iota_k^\alpha = \iota$ with $\kappa_1^1 = 0$ in (117). Viscous relaxation for all (n) configurational variables $\mathbf{\Gamma}_{\Phi k,n}^1$ is assumed negligible:

$$U_F^1 + U_\Phi^1 \to U_F^1 + \sum_n \hat{\Psi}_{\Phi 1,n}^1 = U_F^1 \left(1 + \sum_n \beta_{\Phi 1,n}^1\right). \quad (190)$$

Static strain energy of fibers U_F^1 is (119) with $\mu_k^\alpha = \mu_1^1$ and $H(\cdot)$ omitted, supporting compressive stress. A dynamic fiber modulus is $\check{\mu}_1^1 = \mu_1^1(1 + \sum_n \beta_{\Phi 1,n}^1)$. Fiber directions relative to $x = x^1$ are ambiguous in Ref. [51]. Calculations apply loading parallel or transverse to ι, both pure mode directions. In the former, the longitudinal sound speed $\mathcal{C}$ obeys $\rho_0 \mathcal{C}^2 = B_\eta + p_0 + \frac{4}{3} n_0^1 (\check{\mu}_S^1 + \frac{2}{3} \check{\mu}_1^1)$. In the latter, $\rho_0 \mathcal{C}^2 = B_\eta + p_0 + \frac{4}{3} n_0^1 (\check{\mu}_S^1 - \frac{1}{3} \check{\mu}_1^1)$.

Damage order parameters for the matrix, $\bar{D}^\alpha = \bar{D}^1 = \bar{D} \in [0, 1]$, and fibers, $D_k^\alpha = D_1^1 = D_1 \in [0, 1]$, degrade respective deviatoric stress contributions from matrix and fibers in (144). They also supply surface energy $U_D^1 = \Psi_D^1$ in (145). Jumps in $\bar{D}$ and D_k are allowed across the shock front. This necessitates $\bar{\alpha}^\alpha = \alpha_k^\alpha = 0 \Rightarrow \bar{l}_R^\alpha = l_{Rk}^\alpha = 0$ in (145) to avoid infinite energy in the front. Gradient energies and conjugate forces $\bar{\zeta}_D^\alpha$, ζ_{Dk}^α vanish identically, as do $\{\mathbf{z}^\alpha\}$. Treatment of shocks as singular surfaces mandates viscosities $\bar{v}_D^\alpha = v_{Dk}^\alpha = 0$ for fracture to avoid infinite dissipation in the shock front if $\bar{D}$ and D_k are discontinuous across the front. Kinetic equations (168) and (173) therefore reduce as follows, with $\bar{\pi}_D^\alpha$, π_{Dk}^α in (165), (170):

$$\bar{\pi}_D^1 = 0, \quad \pi_{D1}^1 = 0. \quad (191)$$

For each decrement of J, (191) are solved simultaneously for $\bar{D}$ and D_1, affecting P and U in Hugoniot equation (186). Damage can be nonzero, so the generalized Finsler metrics of Sec. III C are nontrivial. Here, $\bar{g}_{ij} = \delta_{ij}$, $\bar{G}_{IJ}^\alpha = \delta_{IJ}$, with $\hat{g}_j^i$ and $(\hat{G}^\alpha)_J^I$ in (149)–(152). Isotropic matrix damage gives (151), anisotropic fiber damage (152). Determinants and their derivatives, (153) and (154), enter (145) and (191). For the present loading and material symmetries, with (149), $\hat{g}_j^i$ and $(\hat{G}^\alpha)_J^I$ do not affect J or tr $\tilde{\mathbf{C}}$. Finsler or osculating Riemannian metrics enter the analysis only through (145) and (191).

Properties for the ECF and tissue phase used in calculations are in Table I. Experimental data on hydrated muscle (e.g., Ref. [51]) furnish properties of the mixture as a whole, not the isolated $\alpha = 1$ phase. Given (187), the mixture density, isentropic bulk modulus, bulk sound speed, volumetric thermal expansion coefficient, specific heat, and Grüneisen parameter are, respectively,

$$\rho_0 = \sum_\alpha n_0^\alpha \rho_{R0}^\alpha, \quad B_\eta = \sum_\alpha n_0^\alpha B_\eta^\alpha, \quad (192)$$

$$c_B = \sqrt{(B_\eta + p_0)/\rho_0}, \quad A = \sum_\alpha n_0^\alpha A^\alpha, \quad (193)$$

$$\rho_0 c_p = \sum_\alpha n_0^\alpha \rho_{R0}^\alpha c_p^\alpha = \rho_0 c_\epsilon (1 + A\gamma_0 \theta_0), \quad (194)$$

$$\gamma_0 = AB_\eta/(\rho_0 c_p) = AB_\theta/(\rho_0 c_\epsilon), \quad (195)$$

where c_p^α is specific heat at constant pressure of phase α. Given properties of the mixture [51,120] and ECF ($\alpha = 2$), (192)–(195) are inverted and solved for thermoelastic properties of the tissue phase ($\alpha = 1$). Ultimately, experimental values [51] of ρ_0 and c_B yield tissue density and bulk modulus. Nonlinear bulk stiffening parameters $B_{\eta p}^1$ and k_V^1 are fit to the shock Hugoniot data [51].

Not all static and dynamic shear properties are fully established from Ref. [51], so order-of-magnitude estimates are used based on literature values [8,16,20,105,124,125] for skeletal, and in some cases cardiac, muscle. A standard scalar measure [69] of shear stress τ of the mixture for uniaxial shock compression is the first of

$$\tau = \frac{3}{4}(P - p); \quad \tau = -\frac{3}{4} \sum_\alpha \left[(\sigma^\alpha)_1^1 + p^\alpha\right]. \quad (196)$$

If a material is isotropic, then τ is half the von Mises stress under uniaxial strain. The second expression in (196) specializes the first. Both phases $\alpha = 1, 2$ contribute to p via each EOS; only the tissue phase contributes to τ via deviatoric matrix and fiber, elastic and viscoelastic, stresses. Low-rate data [8,16,20,105,124,125] suggest μ_S^1 and μ_1^1 should be in the kPa range, with fiber exponential stiffening k_1^1 on the order of 10. Define the sums of glassy viscoelastic stiffening factors $\beta_S^1 = \sum_m \beta_{Sm}^1$ and $\beta_{\Phi 1}^1 = \sum_n \beta_{\Phi 1,n}^1$. Low- to moderate-rate data on cardiac tissue [16] suggest values up to the order of 10^3. Dynamic compression data on porcine muscle [124] show von Mises stresses in the MPa range for strain rates on the order of 10^3/s. Extrapolating, τ is anticipated up to order of 10 MPa for strong shock loading, wherein strain rates appear on the order of 10^5/s given rise times under 1 μs [51]. As such, β_S^1 and $\beta_{\Phi 1}^1$ are estimated for strong shock compression as 10^5, probing very high-frequency modes.

For fracture cohesive energy in (145), the usual phase-field description is invoked for matrix and fibers: $\bar{E}_C^1 = \bar{\Upsilon}^1/\bar{l}^1 = \bar{\mathsf{J}}_C^1/(2\bar{l}^1)$ and $E_{C1}^1 = \Upsilon_1^1/l_1^1 = \mathsf{J}_{C1}^1/(2l_1^1)$. Toughness J_C of muscle is known only for the whole tissue [126], so here the simplest physical choice $n_0^1 \bar{\mathsf{J}}_C^1 = n_0^1 \mathsf{J}_{C1}^1 = \frac{1}{2} \mathsf{J}_C$ is used. Similarly, length constants for each mechanism are both set equal to a value calibrated later for modeling tensile damage: $\bar{l}^1 = l_1^1 = l^1$, on the order of 10–15 single-fiber diameters [51]. Values are about $20\times$ those used elsewhere for modeling skin [52]. Standard phase-field choices $\bar{\vartheta}^1 = \vartheta_1^1 = \vartheta^1 = 2$ [23,52] are used for degradation functions (142) and (143).

Regarding generalized Finsler metrics, $\bar{r}^1 = \tilde{r}_1^1 = 2$ is adopted from prior work on skin [52], and remanent microstructure strain factors are set equal: $\bar{\epsilon}^1 = n_0^1 \bar{\kappa}^1 / \bar{r}^1 = \tilde{\epsilon}_1^1 = n_0^1 \tilde{\kappa}_1^1 / \tilde{r}_1^1 = \epsilon_r^1$. Experimental data on vascular tissue [127] furnish $\epsilon_r^1 = 0.2$, set positive (dilative) here, as in other soft tissues [15,52]. Under uniaxial-stress compression [127], axial shortening is overcompensated by radial and circumferential expansion: the arterial wall tissue is residually stretched. Arterial data [127] suggest ϵ_r^1 is higher (lower) for tissues with more collagen (less elastin), but experimental data on skeletal muscle components do not exist to justify different choices of ϵ_r^1 for matrix and fibers.

Shown in Fig. 2(a) for skeletal muscle is mixture Hugoniot stress P versus mixture density ratio ρ/ρ_0. Experimental data on muscle [51], blood [122], and water [118] are shown for comparison, along with model predictions for the ECF in isolation. The mixture theory captures most of the shock data well, exceptions being several anomalous points in the domain $\rho_0/\rho \in [0.82, 0.87]$. Similar statements apply for mixture $\mathcal{U}$ versus υ data [51] and model results in Fig. 2(b). Muscle is stiffer than blood, ECF, and water. Hugoniot θ predictions in Fig. 2(c) show a substantial temperature rise, with higher temperatures in muscle than ECF in isolation. This could cause burn damage or other structural changes, not modeled here. Crystal structure and properties of collagen immersed in water exhibit changes at temperatures above 335 K [128], far exceeded in predictions of Fig. 2(c) for muscle.

Results in Fig. 2 are for shock compression parallel to the fiber direction ι. Shear stress of the mixture (supplied only by the tissue phase) τ is predicted in Fig. 3(a) for tissue shocked parallel and transverse to the fiber direction. Contributions of matrix and fiber deviatoric stresses are delineated; these simply sum to give τ. For parallel compression, matrix and fibers contribute similarly in magnitude. For transverse compression, fibers support less load, and τ is lower. In both arrangements, τ is at most on the order of $10^{-2}P$, so orientation does not discernibly influence the Hugoniot stress that is dominated by $p = P - \frac{4}{3}\tau$. For $\rho_0/\rho \lesssim 0.95$, damage in matrix and fibers causes a reduction in strength, leading to reduced shear stress τ at high compressions.

Order parameters $\bar{D}$ (matrix) and D_1 (muscle fibers) at Hugoniot states are shown in Fig. 3(b), notably resolved by the present framework. For parallel loading, degradation occurs similarly for matrix and fibers. For transverse loading, less degradation occurs in the fibers; their strain energy is lower in this arrangement, giving smaller elastic driving force in $\pi_{D_1}^1$. Shock-recovered samples [4] show microstructure changes indicative of damage in fibers (myofibrils) and slippage at cellular interfaces, implying matrix damage. Other experiments, including microscopy and histology after static crushing of muscle, show shear-induced damage in fibers, interfaces, and extracellular matrix [129,130]. The current model can reflect these trends. Other phase-field approaches that do not delineate between fiber and matrix fractures [22,23] would be unable to give such insight into microstructure.

Model results for muscle in Figs. 2, 3(a), and 3(b) use the generalized Finsler metric with remnant strain $\epsilon_r^1 = 0.2$ (Table I). Predictions in Figs. 3(c) and 3(d) compare aforementioned results for damage and τ with those obtained
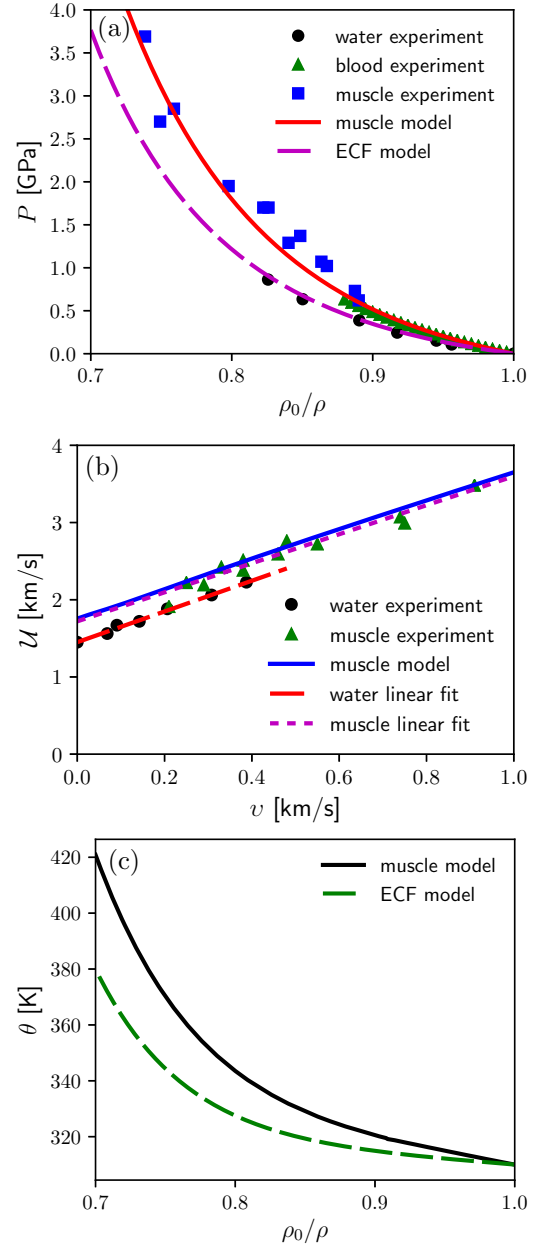
FIG. 2. Model results and/or shock compression data for (a) Hugoniot stress vs mass density, (b) shock velocity vs particle velocity, and (c) temperature. Data in (a) and (b) are for water [118] human blood [122], and porcine skeletal muscle [51].

when $\epsilon_r^1 = 0$, producing Euclidean metrics. Recall $\epsilon_r^1 > 0$ depicts dilatation of the material manifold $\mathfrak{M}^\alpha = \mathfrak{M}^1$ as tearing commences and internal surfaces enlarge. Under shock compression, shear-induced dilatation can occur in solid phases as fracture surfaces slide and open [69]. As a result, area of free surfaces increases, leading to an increase in total fracture surface energy in the model at fixed damage order parameters. As corroborated by Fig. 3(c), damage is suppressed (i.e., more diffuse tearing and rupture) at large deformation when a Finsler metric is used relative to a Euclidean metric. Higher energetic cost of fracture in (145) for the former ($\hat{G}^\alpha > 1$) explains this. Conversely, with higher values of $\bar{D}$ and D_1, τ
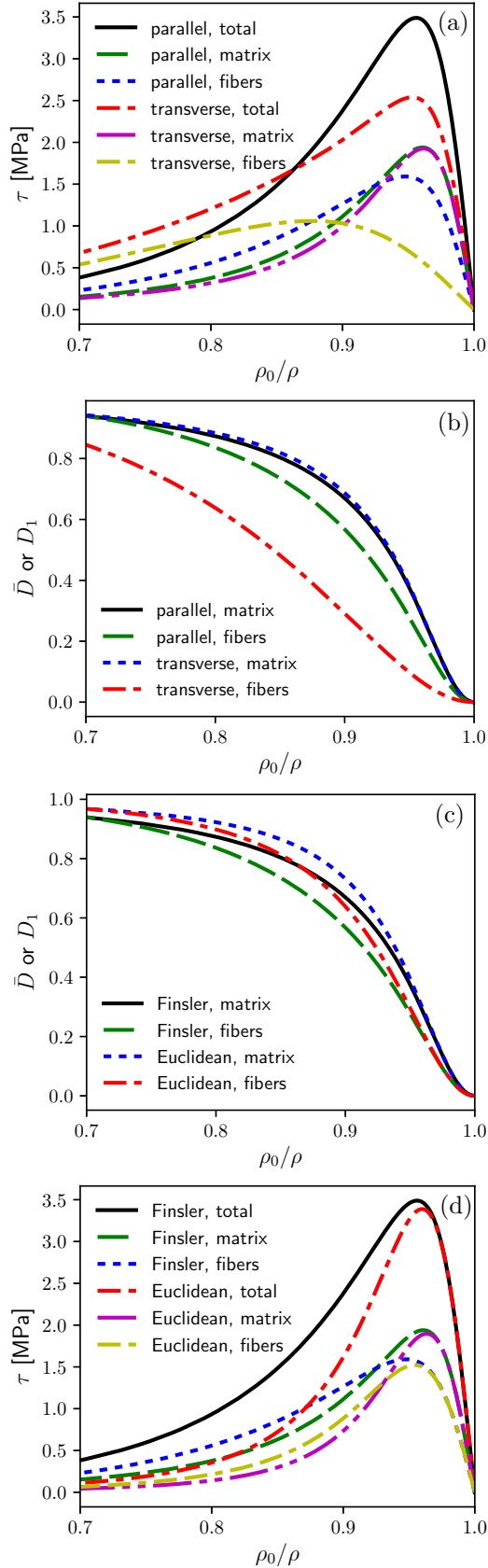
FIG. 3. Predictions for parallel and transverse fiber orientations and Finsler metrics: (a) shear stress vs mass density and (b) damage. Model results for Finsler and Euclidean metrics and parallel orientation: (c) damage and (d) shear stress.

decays more rapidly with increasing compression in Fig. 3(d) when a Euclidean metric ($\hat{G}^\alpha = 1$) is used.

More experimental information (e.g., lateral stress readings of τ [69]) is needed to better validate the choice of metric. Past modeling and experiments on skin tissue [10,52] suggest results from a Finsler metric may generally be more realistic: nonaffine fiber rearrangements and fiber-matrix sliding embodied by $\hat{G}^\alpha > 1$ lead to diffusion of damage, crack blunting, and gradual softening.

For shock stability, $P > 0$, $dP/dJ < 0$, and $d^2P/dJ^2 > 0$ [65]. These, and complementary conditions along isentropes plus $\partial P/\partial \eta > 0$ [64], were verified for $J \in [0.7, 1]$ for all cases in Fig. 3. Damage reduces the tangent shear modulus, but this is more than offset by increasing tangent elastic bulk and shear moduli under compression.

B. Static and dynamic uniaxial stress response

1. Liver

The theory is implemented to model uniaxial-stress compression of bovine liver across a wide range of strain rates as studied experimentally [131], demonstrating efficacy of the model's viscoelastic and damage kinetics. Liver parenchyma is comprised of cells (hepatocytes), blood vessels (sinusoids), lymphatic vessels, bile ducts, and fibrous extracellular matrix (ECM). The organ is encased in a membrane (peritoneum) and connective tissue (Glisson's capsule). In vivo, the liver is internally pressurized, expanded, and perfused with blood, with a fluid volume fraction on the order of 0.5 [7]. Most experimental characterizations, including those modeled here [131], consider excised samples of the parenchyma, initially at ambient pressure (i.e., not perfused), excluding the peritoneum, Glisson's capsule, and major vessels and ligaments. In these cases, initial blood volume is substantially lower, and the response is usually isotropic.

The material is depicted as a mixture of two phases ($N = 2$): a solid tissue phase ($\alpha = 1$) and a fluid phase ($\alpha = 2$) consisting of blood. The EOS used in Sec. IV A is reinvoked, with properties in Table I, any differences between bovine and human blood ignored. In the nonperfused state, the initial fluid fraction is $n_0^2 = 0.12$ [132], the solid fraction $n_0^1 = 0.88$. Effects of intracellular and extracellular fluids other than blood are encompassed by the EOS of the first phase, with free energy of (105) and (106). In addition, free energy of the solid phase ($\alpha = 1$) consists of matrix deviatoric elastic (Ψ_S^1) and viscoelastic (Ψ_Γ^1) terms, fiber elastic (Ψ_{F1}^1) and viscoelastic ($\Psi_{\Phi1}^1$) terms, and damage to matrix and fibers (Ψ_D^1).

A single fiber family is sufficient ($k = 1$), fully dispersed with $\kappa_k^\alpha \to \kappa_1^1 = \frac{1}{3}$ in (117) for isotropy. Damage order parameters for matrix and fibers, $\bar{D}^\alpha \to \bar{D}^1 = \bar{D}$ and $D_k^\alpha \to D_1^1 = D_1$, reduce deviatoric stress in (144) and furnish surface energy in (145). For loading rates up to the order of $10^3/s$ and viscosities $\hat{B}^\alpha$, $\hat{\mu}^\alpha$ in Table I, viscous stress from blood should not exceed tens of Pa. This is negligible relative to total stresses in the kPa to MPa range [131], and thus ignored. For compression, cavitation damage in the fluid is irrelevant.

The sample is a cylindrical annulus [131], deformed uniformly in the longitudinal (i.e., axial) direction to a stretch of $F_1^1(t) = \lambda(t) = 1 - \dot{\epsilon}t \leqslant 1$ at constant "engineering strain" rate of $\dot{\epsilon}$. A Cartesian coordinate frame defines the axial

one-direction and orthogonal (radial) two- and three-directions. Longitudinal velocity history $(v^\alpha)^1(t)$ and axial deformation gradient $(F^\alpha)^1_1(t)$ are identical in each phase. In the initial state, partial pressure in each phase is equilibrated to reference ambient pressure: $p_0^\alpha = n_0^\alpha p_{R0}^\alpha$ with $p_{R0}^\alpha = 1$ atm. At low rates ($\dot\epsilon \lesssim 10^2/\text{s}$), isothermal conditions apply: $\theta^\alpha = \theta_0 = 310$ K. For high rates ($\dot\epsilon \gtrsim 10^2/\text{s}$), macroscopically adiabatic conditions apply: $\mathbf{q}^\alpha = \mathbf{0}$. Interphase mass transfer is excluded: $\hat c^\alpha = 0$.

Two different boundary conditions are considered for transverse (i.e., radial) stress and deformation. First is a "drained" condition, whereby each phase expands or contracts independently to maintain equilibrium with external atmosphere: $(\sigma^\alpha)^2_2 = (\sigma^\alpha)^3_3 = p_0^\alpha$. Transverse velocities $(v^1)^2 = (v^1)^3$ and $(v^2)^2 = (v^2)^3$ are not necessarily equal in each phase, so transverse diffusion velocities $(\mu^\alpha)^2$, $(\mu^\alpha)^3$ need not vanish. Hydraulic conductivity is assumed infinite as a limiting case, so $\lambda^{\alpha\beta} \to 0$ and $\mathbf{h}^\alpha \to \mathbf{0}$ in (176). For the drained case, each α likewise maintains its own temperature $\theta^\alpha(t)$, with $\omega^{\alpha\beta} \to 0$ in (178) as a similarly limiting case, so $\epsilon^\alpha \to 0$. Temperatures are updated by solving (96) separately for $\alpha = 1, 2$.

Second is an "undrained" or "tied" condition, whereby each phase expands or contracts radially with the same transverse velocity history. All diffusion velocities vanish: $\boldsymbol{\mu}^\alpha = \mathbf{0}$. Transverse deformation is obtained by equilibrating the total transverse stress of (46) to atmospheric pressure: $\sigma^2_2 = \sum_{\alpha=1,2}(\sigma^\alpha)^2_2 = p_{R0}^\alpha = 1$ atm. Consistently, for high-rate loading, each phase has the same temperature: $\theta^1(t) = \theta^2(t) = \theta(t)$, updated by integrating the sum of (96) over $\alpha = 1, 2$. Undrained conditions are consistent with limiting very high, yet still finite, $\lambda^{\alpha\beta} \to \infty$ and $\omega^{\alpha\beta} \to \infty$, so $\mathbf{h}^\alpha \to \mathbf{0}$ and $\epsilon^\alpha \to 0$. The tied condition is used elsewhere for biologic solids in "constrained reactive mixture theory" [74,75,114,115].

Axial deformation $\lambda(t)$ is imposed over small time steps Δt. Thermomechanical responses of each phase and the mixture as a whole are obtained by solution and integration of the constitutive (i.e., stress-deformation-temperature) equations, (96) if high-rate loading, and kinetic laws for viscoelasticity and damage. For viscoelasticity, two relaxation modes are sufficient for the deviatoric matrix [$m = 1, 2$ in (121)] and one for fiber [$n = 1$ in (132)] contributions to stress, with volumetric (pressure) contributions omitted for reasons explained in Sec. IV A. The algorithm of Refs. [16,92] is used to solve (124) and (134). Damage is absent in the fluid and spatially homogeneous in the solid: $\nabla \bar D = \nabla D_1 = \mathbf{0}$, ensuring stress fields are homogeneous within each phase, consistent with momentum conservation in the absence of acceleration waves. Gradient energies in (145) and conjugate forces $\bar\zeta_D^\alpha$, ζ_{Dk}^α in (166) and (171) vanish. Order parameters and dissipated energies are obtained by integrating (168), (169), (173), and (174) over the load history with nonzero fracture viscosities $\bar v_D^1$ and v_{D1}^1.

Properties for the isolated solid tissue phase ($\alpha = 1$) of bovine liver are given in Table II. EOS properties, namely ρ_{R0}^α, B_η^α, γ_0^α, and c_ϵ^α, are calculated from mixture rules in (192)–(195) using known values for the fluid ($\alpha = 2$) phase (i.e., blood in Table I), $n_0^1 = 0.88$ [132], and available properties for the liver as a whole (solid + fluid) [120,133,134]. Bulk nonlinear stiffening coefficients k_V^α and $B_{\eta p}^\alpha = B_{\theta p}^\alpha$ are

TABLE II. Physical properties or model parameters ($\alpha = k = 1$) for bovine liver ($n_0^1 = 0.88$) and rabbit muscle ($n_0^1 = 0.9$).

Property	Bovine liver	Rabbit muscle
ρ_{R0}^α (g/cm^3)	1.06	1.10
B_η^α (GPa)	2.67	3.28
c_ϵ^α (J/g K)	3.51	3.25
γ_0^α (–)	0.114	0.313
$B_{\eta p}^\alpha$ (–)	8.0	8.0
k_V^α (–)	6.0	6.0
μ_S^α (kPa)	1.0	1.0
μ_k^α (kPa)	100	600
k_k^α (–)	1.0×10^{-6}	2.1
β_{S1}^α (–)	20	900
β_{S2}^α (–)	150	…
$\beta_{\Phi k,1}^\alpha$ (–)	1.0	0.1
τ_{S1}^α (s)	0.05	0.05
τ_{S2}^α (s)	1.0×10^{-3}	…
$\tau_{\Phi k,1}^\alpha$ (s)	1.0×10^{-3}	0.05
$\hat v_D^\alpha$ (s)	0.05	0
J_C^α (kJ/m^2)	0.08	0.84
l^α (mm)	1.00	0.88
ϑ^α (–)	2.0	2.0
ϵ_r^α (–)	0.2	0.2
$\bar r^\alpha = \tilde r_k^\alpha$ (–)	2.0	2.0

assumed identical to those of skeletal muscle in Table I since high-pressure data are not available for their determination. Values are inconsequential for pressures obtained here under uniaxial-stress compression, wherein $|J^\alpha - 1| < 10^{-4}$.

Total first Piola-Kirchhoff or "engineering" stress magnitude for this purpose, noting $J^1 \approx 1$ and $(\sigma^\alpha)^1_1 \leqslant -n_0^\alpha p_{R0}^\alpha$, is measured relative to ambient pressure p_{R0}^α:

$$P = \frac{J^1\left|(\sigma^1_1 + p_{R0}^1)\right|}{(F^1)^1_1} = \frac{J^1}{\lambda}\left|\sum_\alpha \left[(\sigma^\alpha)^1_1 + n_0^\alpha p_{R0}^\alpha\right]\right|. \quad (197)$$

Shear moduli μ_S^α and μ_k^α, stiffening k_k^α, viscoelastic factors β_{Sm}^α and $\beta_{\Phi k,n}^\alpha$, and relaxation times τ_{Sm}^α and $\tau_{\Phi k,n}^\alpha$ for $\alpha = k = 1$, $m = 1, 2$ and $n = 1$ are fit to data [131] in Figs. 4(a) and 4(b) at rates $\dot\epsilon = 0.01/\text{s}$, $\dot\epsilon = 10/\text{s}$, and $\dot\epsilon = 2000/\text{s}$.

Fracture toughness of the mixture, J_C, is obtained from Ref. [135], presumed similar for porcine and bovine liver. Procedures of Sec. IV A give $n_0^1 \bar{\mathsf{J}}_C^1 = n_0^1 \mathsf{J}_{C1}^1 = \frac{1}{2}\mathsf{J}_C$. Length constants for matrix and fibers are set equal to the value in Table II to best represent data in Figs. 4(a) and 4(b): $\bar l^1 = l_1^1 = l^1 = 1$ mm. Recalling $\bar E_C^1 = \bar\Upsilon^1/\bar l^1 = \bar{\mathsf{J}}_C^1/(2\bar l^1)$ and $E_{C1}^1 = \Upsilon_1^1/l_1 = \mathsf{J}_{C1}^1/(2l_1^1)$, for homogeneous damage, (145) and evolution of order parameters depend only on the ratio of toughness to length (i.e., cohesive energies $\bar E_C^1$, E_{C1}^1) and not toughness and length independently. If gradient regularization lengths $\bar l_R^1$, l_{R1}^1 must be chosen in (145) based on mesh size constraints rather than physical observations (e.g., the smaller value of 0.1 mm used for arterial rupture in Ref. [23]), then $\bar\alpha^1 = \bar l_R^1/\bar l^1$ and $\alpha_1^1 = l_{R1}^1/l_1^1$ can be invoked independently without affecting the cohesive energy. Standard values $\bar\vartheta^1 = \vartheta_1^1 = \vartheta^1 = 2$ [23,52] enter (142) and (143). The same rate dependence of damage, $\hat v_D^\alpha$, normalized by cohesive energy $E_C^\alpha = \bar E_C^\alpha = E_{Ck}^\alpha$ and with units of time, is used for matrix and fibers ($\alpha = k = 1$): $n_0^\alpha \bar v_D^\alpha = n_0^\alpha v_{Dk}^\alpha = E_C^\alpha \hat v_D^\alpha$. The value in
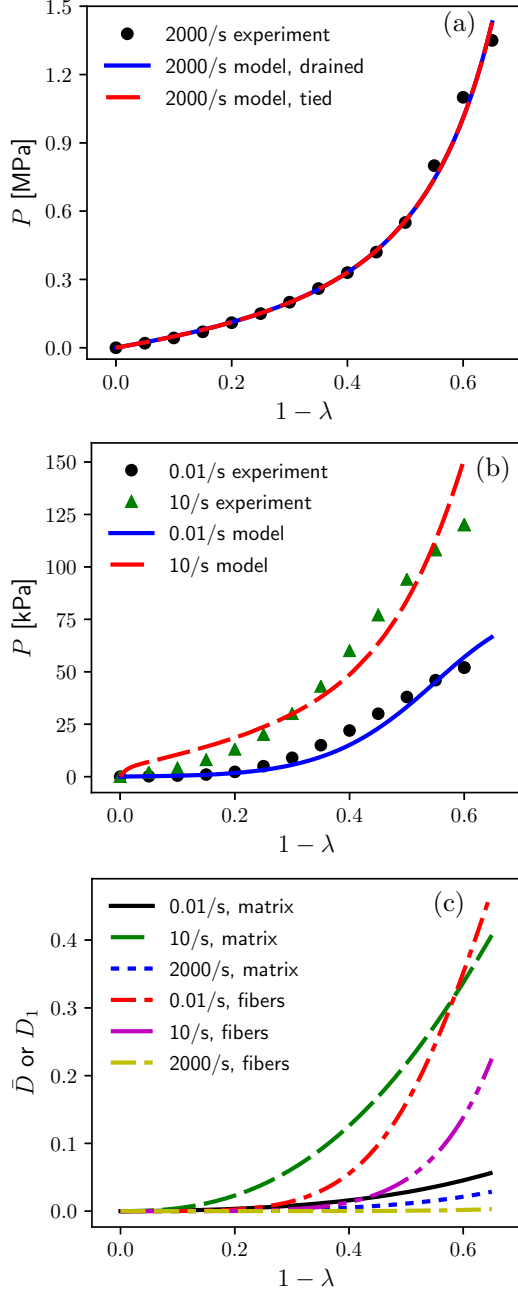
FIG. 4. Model results and experimental data [131] for bovine liver compressed to stretch λ: (a) axial stress P at strain rate $\dot{\epsilon} = 2000/s$, (b) P at $\dot{\epsilon} = 0.01/s$ and $\dot{\epsilon} = 10/s$, and (c) predicted matrix and fiber damage $\bar{D}$ and D_1 at all three rates.

Table II produces credible results in the context of Fig. 4(c). The same parameters for generalized Finsler metrics $\mathbf{G}^\alpha$ are used for liver and muscle, explained in Sec. IV A.

The high-rate response of compressed liver is shown in Fig. 4(a). Model results assume adiabatic conditions, but predicted temperature change is negligible. Damage order parameters attained small maxima at high rates [i.e., $\bar{D} \lesssim 0.03$ and $D_1 \lesssim 0.003$ in Fig. 4(c)] due to the viscosity $\hat{v}_D^\alpha$ preventing notable degradation over the brief time period of deformation. This is consistent with data [131] that show continuously increasing stiffness at this loading rate, with no

evidence of material failure. Differences between drained and undrained conditions are indiscernible because the solid tissue is nearly incompressible.

Low- and moderate-rate stress histories are reported in Fig. 4(b). Model results are isothermal and for drained conditions only; results for undrained, not shown, are nearly identical. This theory captures the mechanical response of liver spanning five decades in strain rate. Previous viscoelastic modeling has been limited to much lower rates [136]. Fits to data are reasonable but not as close as those for high-rate loading in Fig. 4(a).

At low rates, data show reduction in the degree of stiffening at large compression, indicative of strength degradation [2,10]. This phenomenon is captured by damage kinetics, Fig. 4(c). Strength deterioration increases monotonically with compressive strain $1 - \lambda$, and at moderate to high rates is more severe in matrix than fibers. Histological analysis after dynamic blunt impact [137] showed fractures in liver parenchyma avoid fibers and interlobular septa and more often propagate along interfaces, consistent with higher levels of "matrix" damage $\bar{D}$ relative to fiber damage D_1 in Fig. 4(c). Conversely, at the lowest strain rate (0.01/s), fiber damage overtakes matrix damage at large compression ($\lambda \lesssim 0.77$) and is more pronounced due to longer load times for relaxation to ensue. The present theory notably addresses liver tissue damage, resolving that in cellular matrix and collagen fiber network seen experimentally [137]. Models for liver damage at high strain rates appear scarce; one study applies a cohesive zone model for relatively slow extension and tearing [138].

2. Skeletal muscle

The theory is now implemented to study uniaxial-stress tensile behavior of rabbit skeletal muscle at low and moderate strain rates, with and without activation from electrical stimulation. Model results seek to depict experiments reported in Refs. [20,109].

Calculations proceed in the same manner as just described for modeling liver, with a few exceptions. First, tension is modeled rather than compression, with stretch ratio $F_1^1(t) = \lambda(t) = 1 + \dot{\epsilon} t \geqslant 1$ at two rates [109]: $\dot{\epsilon} = 0.17/s$ and $\dot{\epsilon} = 15/s$. Engineering tensile stress is P of (197), where now $(\sigma^\alpha)_1^1 \geqslant -n_0^\alpha p_{R0}^\alpha$. Both drained and undrained conditions are considered, all isothermal. Second, the data do not indicate any consistent rate sensitivity of damage or failure stretch [20], so equilibrium equations (191) used in Sec. IV A for porcine muscle still apply. These correspond to (168) and (173) with null viscosities $\bar{v}_D^\alpha = v_{Dk}^\alpha \to 0$, giving zero dissipation in (169) and (174). Last, active tension, irrelevant for liver, is considered for muscle. The form of free energy Ψ_A^α and Cauchy stress term $\boldsymbol{\sigma}_A^\alpha$ in (140) and (141) are adapted directly from Ref. [20] since they reproduce the overstress from activation recorded in isometric experiments [109]:

$$\Psi_A^1 = \frac{2}{3} \Delta_A \mu_A (\lambda_{A1} - \lambda_{A0})[\bar{\Lambda}^{p_A}/p_A - \bar{\Lambda}^{r_A}/r_A], \quad (198)$$

$$\boldsymbol{\sigma}_A^1 = \frac{2}{3} \frac{\rho^\alpha}{\rho_{R0}^\alpha} \frac{\Delta_A \mu_A}{\lambda_1^1} \bar{\Lambda}^{p_A-1}[1 - \bar{\Lambda}^{q_A-1}]\tilde{\mathbf{h}}_1^1, \quad (199)$$

$$\bar{\Lambda} = \begin{cases} \frac{\lambda_1^1 - \lambda_{A0}}{\lambda_{A1} - \lambda_{A0}} & \forall \lambda_1^1 \in (\lambda_{A0}, \lambda_{A1}), \\ 0 & \text{(otherwise)}. \end{cases} \quad (200)$$

Active tension vanishes for $\bar{\Lambda}$ outside domain [0,1]. Recall fiber stretch obeys $(\lambda_k^\alpha)^2 = I_k^\alpha = \tilde{\mathbf{C}}^\alpha : \mathbf{H}_k^\alpha$ with $\alpha = k = 1$. Parameters are μ_A (stress units) and dimensionless set $(\lambda_{A0}, \lambda_{A1}, p_A, q_A)$, with $r_A = p_A + q_A - 1$. A dimensionless internal variable for activation is $\{\Delta_k^\alpha(t)\} \to \Delta_1^1(t) = \Delta_A$. Only discrete states are considered: $\Delta_A = 1$ in the fully active state and $\Delta_A = 0$ in the fully passive state. Transient switching between states and partial activation are not addressed here or in the experiments [20,109]. Energy χ_k^α in (140) and kinetic law (162) need not be prescribed; no contribution to dissipation arises since $D_t^1 \Delta_A = 0$ in (164). The $\frac{2}{3}$ in (198) is omitted in Ref. [20] where compressibility is ignored.

As prescribed in Sec. IV A for porcine muscle, rabbit muscle consists of solid tissue $\alpha = 1$ and ECF ($\alpha = 2$), where parameters for ECF are in Table I. The initial solid volume fraction remains $n_0^1 = 0.9$. Parameters for rabbit skeletal muscle are compiled in Table II. Thermophysical properties entering the EOS are identical to those for porcine tissue in Table I. Shear properties μ_S^α, μ_k^α, and k_k^α are calibrated to the data [20,109], with $k = 1$ sufficient. Fibers are fully aligned, $\kappa_k^\alpha \to \kappa_1^1 = 0$ in (117), giving anisotropic response. The glassy viscoelastic assumption used for modeling shocks in Sec. IV A is inappropriate for low and moderate strain rates. Instead, viscoelastic strength factors β_{Sm}^α and $\beta_{\Phi k,n}^\alpha$ and relaxation times τ_{Sm}^α and $\tau_{\Phi k,n}^\alpha$ are fit to experimental data; here, a single mode suffices: $m = n = 1$. The activation parameters in (198) are verbatim from Ref. [20]: $\mu_A = 962$ kPa, $\lambda_{A0} = 0.9$, $\lambda_{A1} = 1.32$, $p_A = 1.65$, and $q_A = 2.0$. Assumptions for properties modulating matrix and fiber damage are the same as those explained for porcine tissue in Sec. IV A, with matching toughness J_C [126]. Length $l^1 = \bar{l}^1 = l_1^1$ provides cohesive energies $E_C = \bar{E}_C = E_{C1}$ in (145). The value in Table II best fits softening and failure in test data [20,109] at the lowest loading rate. Finsler metric parameters in Table II match those of porcine muscle in Table I; none are adjusted when fitting the data.

For tensile loading, cavitation of the fluid ($\alpha = 2$) is not impossible. Calibration of the theory for water under isentropic expansion to its 8.7 MPa cavitation stress [139] gives $\bar{E}_C^\alpha = 0.1818$ MPa. Using the same cohesive energy for ECF gives a cavitation stress of 8.9 MPa, and $J^\alpha \gtrsim 1.001$ ($\alpha = 2$) is needed to initiate discernible damage $\bar{D}^\alpha$. Such fluid expansion is never reached in the present modeling of muscle: damage in ECF is negligible here.

Model outcomes and experimental stress-stretch data are compared in Fig. 5(a) for active states and Fig. 5(b) for passive states, at engineering strain rates of $\dot{\epsilon} = 0.17$/s and $\dot{\epsilon} = 15$/s. The fiber direction $\iota = \iota_1^1$ is aligned with the direction of elongation. Model results in Fig. 5 are for drained lateral boundaries; predictions for undrained conditions are nearly indiscernible from drained and thus not shown. For active and passive states, the material is stiffer at the higher rate, with larger peak (failure) stress. Predicted failure stretch is similar at both strain rates. The material supports larger P in the active state over domain $1 \leqslant \lambda \lesssim 1.32$, including an initial stress of $P = 0.192$ MPa at $\lambda(t = 0) = 1$ that matches experiments.

The model closely depicts the majority of data points [20,109], an exception under-prediction of large P-λ data at $\dot{\epsilon} = 15$/s for the passive state in Fig. 5(b). An overprediction of peak stress for active loading at the higher rate was obtained
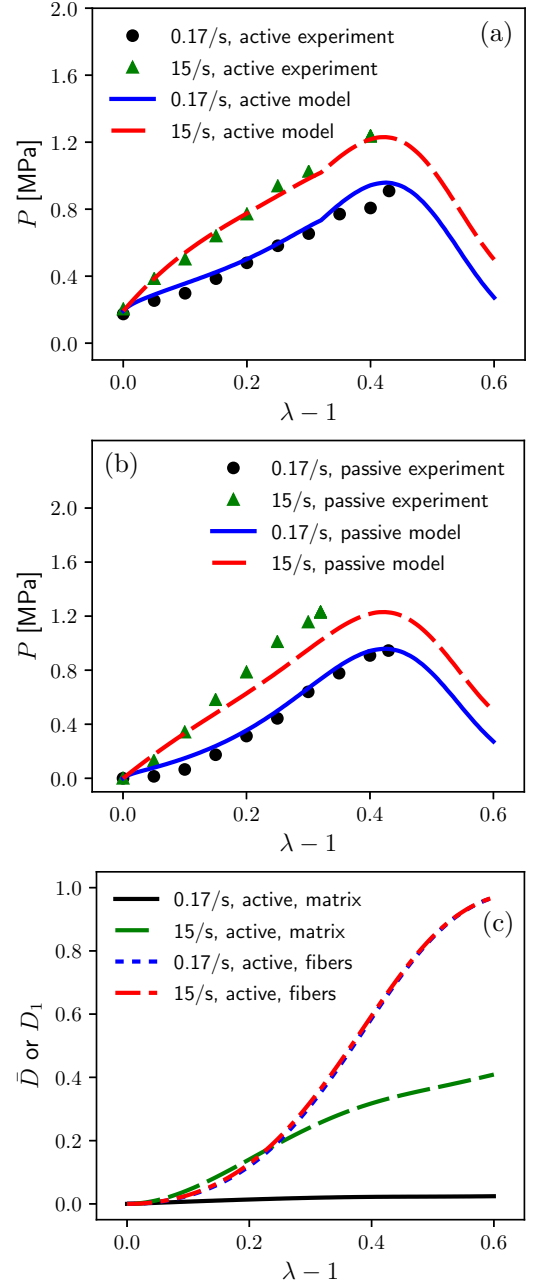
FIG. 5. Model results and experimental data [20,109] for rabbit skeletal muscle to tensile stretch λ at rates of $\dot{\epsilon} = 0.17$/s and $\dot{\epsilon} = 15$/s: (a) axial stress P in active state ($\Delta_A = 1$), (b) P in passive state ($\Delta_A = 0$), and (c) predicted matrix and fiber damage $\bar{D}$ and D_1, active state (passive nearly identical).

from a phenomenological model [20]. That model, however, contained five adjustable parameters, whereas only length parameter l^1 was adjusted for damage modeling in application of the present theory.

More elaborate coupling among viscoelastic and damage kinetics, albeit with more parameters, could improve agreement, but such an exercise is unjustified for closer fitting of relatively few data points. Unlike results for compression in Sec. IV A where the matrix and fibers supported similar stress, here, under tensile loading, the fibers bear the majority

of the load P, with the ratio of fiber to matrix stress increasing as stretch increases and rate decreases. The correspondingly larger strain energy in the fibers provides a larger driving force for fiber damage D_1 than matrix damage $\bar{D}$, which is nearly negligible at $\dot{\epsilon} = 0.17/\text{s}$, as shown in Fig. 5(c).

The model of Ref. [20], which contains more calibrated parameters, does not specifically delineate between matrix and fiber fractures, though it does feature a transversely isotropic representation for fiber failure versus fiber detachment. As discussed in Ref. [140], under tensile loading at low rates, damage to muscle fibers is prominently observed over delamination and damage to the endomysium (i.e., the matrix including connective tissue in which fibers are embedded). The current predictions concur with these observations. At the higher rate of $\dot{\epsilon} = 15/\text{s}$, viscoelastic energy of the matrix is sufficient to induce matrix damage, though it remains less severe than fiber damage for $\lambda \gtrsim 1.23$, which is nearly the same at both rates. The damage model is decoupled from Ψ_A, so order parameters $\bar{D}$ and D_1 have indistinguishable histories for active versus passive states.

C. Shock evolution

1. Analytical solution

Growth and decay of planar shock waves are studied, with shock fronts treated as singular surfaces per theory of Sec. II B. An analytical solution is derived for solid-fluid mixtures with viscoelastic and damage mechanisms, extending Ref. [50] that considered nonlinear elastic solid-fluid mixtures without internal variables and Ref. [65] that considered fluids with internal state variables. To streamline notation, let internal variables $\{\boldsymbol{\xi}^\alpha\} \rightarrow (\mathbf{a}^\alpha, \mathbf{b}^\alpha)$. Generic internal variable class $\mathbf{a}^\alpha$ obeys kinetic laws of form (77) specialized to

$$D_t^\alpha \mathbf{a}^\alpha = D_t^\alpha \mathbf{a}^\alpha (\mathbf{F}^\alpha, \eta^\alpha(\mathbf{F}^\alpha, \theta^\alpha, \mathbf{a}^\alpha, \mathbf{b}^\alpha), \mathbf{a}^\alpha, \mathbf{b}^\alpha). \quad (201)$$

Generic class $\mathbf{b}^\alpha$ obeys equilibrium conditions of form

$$\boldsymbol{\pi}_b^\alpha = \rho^\alpha \partial u^\alpha / \partial \mathbf{b}^\alpha = \mathbf{0}. \quad (202)$$

Type $\mathbf{a}^\alpha$ include dissipative variables for viscoelasticity and order parameters for rate-dependent fracture; $\mathbf{b}^\alpha$ include rate-insensitive order parameter(s). Now excluding gradient regularization and explicit $\mathbf{X}^\alpha$ dependence,

$$u^\alpha = u^\alpha (\mathbf{F}^\alpha, \eta^\alpha, \mathbf{a}^\alpha, \mathbf{b}^\alpha), \quad \theta^\alpha = \theta^\alpha (\mathbf{F}^\alpha, \eta^\alpha, \mathbf{a}^\alpha, \mathbf{b}^\alpha) \quad (203)$$

are internal energy and temperature of (87) and (88). Unless $[\![\boldsymbol{\xi}^\alpha]\!] = \mathbf{0}$, gradient regularization yields infinite energy density in the shock front as its width approaches zero. It also introduces complexity in Rankine-Hugoniot equations via $\boldsymbol{\zeta}^\alpha$, precluding analytical solutions without undue assumptions on shock structure [86] not used here.

From (149), $\hat{g} = \hat{G}^\alpha \Rightarrow g/G^\alpha = 1$. Then 1D kinematics, continuum balance laws, and entropy production are, with $\hat{c}^\alpha = 0, \mathbf{q}^\alpha = \mathbf{0}, r^\alpha = 0, h^\alpha = \mathbf{h}^\alpha \cdot \mathbf{n}$, and $P^\alpha = -t^\alpha$,

$$F^\alpha = \partial \chi^\alpha / \partial X^\alpha = J^\alpha, \quad D_t^\alpha J^\alpha = \partial \upsilon^\alpha / \partial X^\alpha, \quad (204)$$

$$\rho_0^\alpha = J^\alpha \rho^\alpha, \quad \rho_0^\alpha D_t^\alpha \upsilon^\alpha = -(\partial P^\alpha / \partial X^\alpha) + J^\alpha h^\alpha, \quad (205)$$

$$\rho_0^\alpha D_t^\alpha u^\alpha = -P^\alpha (\partial \upsilon^\alpha / \partial X^\alpha) + J^\alpha \epsilon^\alpha, \quad (206)$$

$$\rho_0^\alpha \theta^\alpha D_t^\alpha \eta^\alpha = J^\alpha (\epsilon^\alpha - \boldsymbol{\pi}_a^\alpha \cdot D_t^\alpha \mathbf{a}^\alpha), \quad (207)$$

$$\sum_\alpha (J^\alpha / \theta^\alpha)(\epsilon^\alpha - \boldsymbol{\pi}_a^\alpha \cdot D_t^\alpha \mathbf{a}^\alpha + c^\alpha \theta^\alpha \eta^\alpha) \geqslant 0. \quad (208)$$

A single shock propagates in the (x, X^α)-direction at Lagrangian speed $\mathcal{U}^\alpha$. Ahead of the shock front Σ^α, each phase α obeys equilibrium and uniformity conditions:

$$J^{\alpha+} = 1, \quad \upsilon^{\alpha+} = 0, \quad \theta^{\alpha+} = \theta_0, \quad \eta^{\alpha+} = \text{constant}$$
$$\Rightarrow \rho^{\alpha+} = \rho_0^\alpha, \quad h^{\alpha+} = 0, \quad \epsilon^{\alpha+} = 0, \quad \mathcal{U}^\alpha = \mathcal{U}; \quad (209)$$

$$\mathbf{a}^{\alpha+} = \mathbf{a}_0^\alpha = \text{const}, \quad \mathbf{b}^{\alpha+} = \mathbf{b}_0^\alpha = \text{const}. \quad (210)$$

Rankine-Hugoniot equations ($P^\alpha > 0 \Leftrightarrow$ compression) are

$$[\![\upsilon^\alpha]\!] = -\mathcal{U}[\![J^\alpha]\!], \quad [\![P^\alpha]\!] = -\rho_0^\alpha \mathcal{U}^2 [\![J^\alpha]\!], \quad (211)$$

$$\rho_0^\alpha [\![u^\alpha]\!] = -\langle P^\alpha \rangle [\![J]\!], \quad \sum_\alpha \rho_0^\alpha [\![\eta^\alpha]\!] \geqslant 0. \quad (212)$$

To avoid infinite dissipation in the shock front [65,121],

$$[\![\mathbf{a}^\alpha]\!] = \mathbf{0} \Rightarrow \mathbf{a}^{\alpha-} = \mathbf{a}_0^\alpha. \quad (213)$$

Jumps $[\![\mathbf{b}^\alpha]\!]$ in nondissipative variables can be nonzero across Σ^α so long as (202) holds. However, it is assumed that (202) can be solved, at least implicitly, at any (X^α, t) with the first of each of (203), (205), and then via (213),

$$\mathbf{b}^\alpha = \bar{\mathbf{b}}^\alpha (J^\alpha, \eta^\alpha, \mathbf{a}^\alpha), \quad \mathbf{b}^{\alpha-} = \bar{\mathbf{b}}^{\alpha-}(J^{\alpha-}, \eta^{\alpha-}, \mathbf{a}_0^\alpha). \quad (214)$$

Now with (213) and (214) at a given $(\cdot)^+$ state, the first of (212) can be written $H(J^{\alpha-}, \eta^{\alpha-}, \bar{\mathbf{b}}^{\alpha-}(J^{\alpha-}, \eta^{\alpha-})) = 0$. Again, at least implicitly, this can be solved for entropy along the Hugoniot and then the other state variables:

$$[\![\eta^\alpha]\!] = \eta_H^\alpha([\![J^\alpha]\!]), \quad [\![\mathbf{b}^\alpha]\!] = \mathbf{b}_H^\alpha([\![J^\alpha]\!]), \quad (215)$$

$$[\![P^\alpha]\!] = P_H^\alpha([\![J^\alpha]\!]), \quad [\![u^\alpha]\!] = u_H^\alpha([\![J^\alpha]\!]). \quad (216)$$

Hugoniot states do not depend explicitly on $h^{\alpha-}$ or $\epsilon^{\alpha-}$. From (89) with $\mathbf{F}^\alpha = \text{diag}(J^\alpha, 1, 1)$, note, then define

$$P^\alpha = -\rho_0^\alpha \partial u^\alpha / \partial J^\alpha, \quad \theta^\alpha = \partial u^\alpha / \partial \eta^\alpha; \quad (217)$$

$$\mathsf{C}^\alpha = -\partial P^\alpha / \partial J^\alpha = \rho_0^\alpha \partial^2 u^\alpha / \partial (J^\alpha)^2, \quad (218)$$

$$\mathsf{G}^\alpha = -\partial P^\alpha / \partial \eta^\alpha = -\rho_0^\alpha J^\alpha \theta^\alpha (\gamma^\alpha)_1^1, \quad (219)$$

$$\mathbf{A}^\alpha = -\partial P^\alpha / \partial \mathbf{a}^\alpha, \quad \mathbf{B}^\alpha = -\partial P^\alpha / \partial \mathbf{b}^\alpha, \quad (220)$$

$$\mathbf{b}'^\alpha = \partial \bar{\mathbf{b}}^\alpha / \partial J^\alpha, \quad \mathbf{b}''^\alpha = \partial^2 \bar{\mathbf{b}}^\alpha / \partial (J^\alpha)^2, \quad (221)$$

$$\hat{\mathsf{C}}^\alpha = \mathsf{C}^\alpha + \mathbf{B}^\alpha \cdot \mathbf{b}'^\alpha, \quad \mathbf{B}'^\alpha = \partial \mathbf{B}^\alpha / \partial J^\alpha, \quad (222)$$

$$\mathsf{C}'^\alpha = \partial \mathsf{C}^\alpha / \partial J^\alpha = \rho_0^\alpha \partial^3 u^\alpha / \partial (J^\alpha)^3, \quad (223)$$

$$\hat{\mathsf{C}}'^\alpha = \mathsf{C}'^\alpha + \mathbf{B}'^\alpha \cdot \mathbf{b}'^\alpha + \mathbf{B}^\alpha \cdot \mathbf{b}''^\alpha, \quad (224)$$

$$\hat{\mathsf{G}}^\alpha = \mathsf{G}^\alpha + \mathbf{B}^\alpha \cdot \mathbf{b}_\eta^\alpha. \quad (225)$$

Weak shocks are analyzed in the limit $[\![J^\alpha]\!] \to 0$. Applying theorems [64] relating isentropic and tangent moduli, (215) and (216) are expanded from a $(\cdot)^+$ state:

$$[\![P^\alpha]\!] = -\hat{\mathsf{C}}^{\alpha+}[\![J^\alpha]\!] - \frac{1}{2}\hat{\mathsf{C}}'^{\alpha+}[\![J^\alpha]\!]^2 + O([\![J^\alpha]\!]^3), \quad (226)$$

$$[\![\rho_0^\alpha u^\alpha]\!] = -P^{\alpha+}[\![J^\alpha]\!] + \frac{1}{2}\hat{\mathsf{C}}^{\alpha+}[\![J^\alpha]\!]^2 + O([\![J^\alpha]\!]^3), \quad (227)$$

$$[\![\rho_0^\alpha \theta^\alpha]\!] = \hat{\mathsf{G}}^{\alpha+}[\![J^\alpha]\!] + \frac{1}{2}\left(\frac{\partial\hat{\mathsf{G}}}{\partial J}\right)^{\alpha+}[\![J^\alpha]\!]^2 + O([\![J^\alpha]\!]^3),$$
$$(228)$$

$$[\![\mathbf{b}^\alpha]\!] = \mathbf{b}'^{\alpha+}[\![J^\alpha]\!] + \frac{1}{2}\mathbf{b}''^{\alpha+}[\![J^\alpha]\!]^2 + O([\![J^\alpha]\!]^3), \quad (229)$$

$$[\![\eta^\alpha]\!] = \frac{1}{12}\{\hat{\mathsf{C}}'^{\alpha+}/(\rho_0^\alpha\theta_0)\}[\![J^\alpha]\!]^3 + O([\![J^\alpha]\!]^4). \quad (230)$$

From (230), $[\![\eta^\alpha]\!]$ is of order three in $[\![J^\alpha]\!]$, and $[\![J^\alpha]\!] \leqslant 0$ when $\hat{\mathsf{C}}'^{\alpha+} < 0$ to satisfy the second of (212) for a single α. Interactions $\mathbf{h}^\alpha$ and ϵ^α are respectively odd and even functions of υ^β [50,66], so from (209), (211), and (228),

$$h^{\alpha-} = -\mathcal{U}\sum_\beta(\partial h^\alpha/\partial\upsilon^\beta)^+[\![J^\beta]\!] + O([\![J^\beta]\!]^2), \quad (231)$$

$$\epsilon^{\alpha-} = \sum_\beta(\partial\epsilon^\alpha/\partial\theta^\beta)^+(\hat{\mathsf{G}}^\beta/\rho_0^\beta)^+[\![J^\beta]\!] + O([\![J^\beta]\!]^2). \quad (232)$$

From (212) and (226), $\mathcal{U}^\beta$ approaches the sound speed:

$$(\mathcal{U}^\beta)^2 = (\mathcal{C}^\beta)^2 + \frac{1}{2}(\hat{\mathsf{C}}'^\beta/\rho_0^\beta)^+[\![J^\beta]\!] + O([\![J^\beta]\!]^2),$$
$$\mathcal{C}^\beta = \sqrt{\hat{\mathsf{C}}^{\beta+}/\rho_0^\beta}. \quad (233)$$

Considering $\alpha \neq \beta$ and $\mathcal{C}^\alpha \neq \mathcal{C}^\beta$, (233) implies [50,66]

$$\{(\mathcal{C}^\alpha)^2 - (\mathcal{C}^\beta)^2\}[\![J^\beta]\!] + O([\![J^\alpha]\!][\![J^\beta]\!]) + O([\![J^\beta]\!]^2) = 0$$
$$\Rightarrow \mathcal{U}^2 = (\mathcal{C}^\alpha)^2 + O([\![J^\alpha]\!]) \quad \text{(for one } [\![J^\alpha]\!] \neq 0\text{)},$$
$$[\![J^\beta]\!] = 0 \ (\forall \beta = 1, 2, \dots, \alpha - 1, \alpha + 1, \dots, N). \quad (234)$$

Each distinct wave speed $\mathcal{C}^\alpha$ corresponds to isolated jump $[\![J^\alpha]\!]$. From (226)–(230), a weak shock in phase α does not induce jumps $[\![P^\beta]\!]$, $[\![u^\beta]\!]$, $[\![\theta^\beta]\!]$, etc. in other phases β. Since $[\![J^\beta]\!] = 0$ for $\beta \neq \alpha$, (231) and (232) become

$$h^{\alpha-} = -\mathcal{C}^\alpha(\partial h^\alpha/\partial\upsilon^\alpha)^+[\![J^\alpha]\!] + O([\![J^\alpha]\!]^2), \quad (235)$$

$$\epsilon^{\alpha-} = (\partial\epsilon^\alpha/\partial\theta^\alpha)^+(\hat{\mathsf{G}}^\alpha/\rho_0^\alpha)^+[\![J^\alpha]\!] + O([\![J^\alpha]\!]^2), \quad (236)$$

that also apply for $h^{\beta-}, \epsilon^{\beta-}$, $\beta \neq \alpha$ with $(\partial h^\alpha/\partial\upsilon^\alpha)^+ \to (\partial h^\beta/\partial\upsilon^\alpha)^+$ and $(\partial\epsilon^\alpha/\partial\theta^\alpha)^+ \to (\partial\epsilon^\alpha/\partial\theta^\alpha)^+$ [66].

Resuming analysis of the nonlinear (i.e., strong-shock) regime, denote by f^α any of $(J^\alpha, P^\alpha, \eta^\alpha, \theta^\alpha, \rho^\alpha, \upsilon^\alpha, u^\alpha, \mathbf{b}^\alpha)$. Recall that across surface Σ^α, f^α, $D_t^\alpha f^\alpha$, and $\nabla_0^\alpha f^\alpha = \partial f^\alpha/\partial X^\alpha$ can be discontinuous. From (213), $\mathbf{a}^\alpha$ is continuous; however, $D_t^\alpha\mathbf{a}^\alpha$ and $\nabla_0^\alpha\mathbf{a}^\alpha$ need not be so. Recall (9) in 1D is $D_t^\alpha J^\alpha = \nabla_0^\alpha\upsilon^\alpha$ via (204). Applying (42) with the last of (209) gives [65]

$$\delta_t[\![f^\alpha]\!] = [\![D_t^\alpha f^\alpha]\!] + \mathcal{U}[\![\nabla_0^\alpha f^\alpha]\!], \quad (237)$$

$$[\![D_t^\alpha\mathbf{a}^\alpha]\!] = -\mathcal{U}[\![\nabla_0^\alpha\mathbf{a}^\alpha]\!]. \quad (238)$$

Intermediate steps of the derivation of the nonlinear solution are given in Appendix C, equations (C1)–(C13). Solving (C11) and (C13) for $\delta_t\mathcal{U}$ and $\delta_t[\![\eta^\alpha]\!]$, then insertion in (C6) with (209) and (C10) yields the fully nonlinear shock evolution equations for $\delta_t[\![J^\alpha]\!]$ and $\delta_t[\![P^\alpha]\!]$:

$$\delta_t\mathcal{U} = \mathcal{U}\frac{(1 - \hat{\xi}^\alpha)}{(2 - \hat{\zeta}^\alpha)\hat{\xi}^\alpha[\![J^\alpha]\!]}\delta_t[\![J^\alpha]\!], \quad (239)$$

$$\delta_t[\![\eta^\alpha]\!] = \frac{\hat{\mathsf{C}}^{\alpha-}}{\hat{\mathsf{G}}^{\alpha-}}\frac{\hat{\zeta}^\alpha(1 - \hat{\xi}^\alpha)}{(2 - \hat{\zeta}^\alpha)}\delta_t[\![J^\alpha]\!], \quad (240)$$

$$\delta_t[\![J^\alpha]\!] = \mathcal{U}\frac{(1 - \hat{\xi}^\alpha)(2 - \hat{\zeta}^\alpha)\{\Lambda^\alpha - (\nabla_0^\alpha J^\alpha)^-\}}{(3\hat{\xi}^\alpha + 1) - \hat{\zeta}^\alpha(3\hat{\xi}^\alpha - 1)}, \quad (241)$$

$$\delta_t[\![P^\alpha]\!] = -\hat{\mathsf{C}}^{\alpha-}\mathcal{U}\frac{\{3 - \hat{\xi}^\alpha(1 + \hat{\zeta}^\alpha)\}\{\Lambda^\alpha - (\nabla_0^\alpha J^\alpha)^-\}}{(3\hat{\xi}^\alpha + 1) - \hat{\zeta}^\alpha(3\hat{\xi}^\alpha - 1)},$$
$$(242)$$

$$\Lambda^\alpha = \frac{1 + [\![J^\alpha]\!]}{(1 - \hat{\xi}^\alpha)\hat{\mathsf{C}}^{\alpha-}}\left\{\frac{\rho_0^\alpha}{J^{\alpha-}}[\mathbf{L}^{\alpha-} \cdot (D_t^\alpha\mathbf{a}^\alpha)^-]\right.$$
$$\left. - h^{\alpha-} + [\hat{\mathsf{G}}^{\alpha-}/(\rho_0^\alpha\mathcal{U}\theta^{\alpha-})]\epsilon^{\alpha-}\right\}. \quad (243)$$

When $(\nabla_0^\alpha J^\alpha)^-$ equals a critical strain gradient Λ^α (a function of $(\cdot)^-$ conditions immediately behind the wave front), (239)–(242) vanish so the shock is steady.

Preceding derivations are for phase α. Now let $\mathcal{U}$ for phase α be imposed simultaneously on $\beta \neq \alpha$. The trivial solution to (211) is $[\![J^\beta]\!] = 0$. Noting (C13) and (240) still apply with $\alpha \to \beta$, substitution of (239) into the former gives a nontrivial solution (i.e., a shock interaction law) for the strain jump amplitude in other constituent(s) β:

$$\delta_t[\![J^\beta]\!] = \frac{(2 - \hat{\zeta}^\beta)\hat{\xi}^\beta(1 - \hat{\xi}^\beta)}{(2 - \hat{\zeta}^\alpha)\hat{\xi}^\alpha(1 - \hat{\xi}^\beta)}\frac{[\![J^\beta]\!]}{[\![J^\alpha]\!]}\delta_t[\![J^\alpha]\!]. \quad (244)$$

In the weak limit, $\mathcal{U} = \mathcal{U}^\alpha \to \mathcal{C}^\alpha = \text{const}$ and shock evolution depends only on $(\cdot)^+$ states. As $[\![J^\alpha]\!] \to 0$, from (211), (212), (226), (228), (231), (232), (241), and (243),

$$\hat{\xi}^\alpha = 1 - \frac{1}{2}(\hat{\mathsf{C}}'^{\alpha+}/\hat{\mathsf{C}}^{\alpha+})[\![J^\alpha]\!] + O([\![J^\alpha]\!]^2), \quad (245)$$

$$\hat{\zeta}^\alpha = \{\hat{\mathsf{G}}^{\alpha+}/(\rho_0^\alpha\theta_0)\}[\![J^\alpha]\!] + O([\![J^\alpha]\!]^2), \quad (246)$$

$$\Lambda^\alpha = -4\mathcal{C}^\alpha\rho_0^\alpha\omega^\alpha/\hat{\mathsf{C}}'^{\alpha+} + O([\![J^\alpha]\!]), \quad (247)$$

$$\omega^\alpha = -\frac{1}{2\rho_0^\alpha}\left\{\frac{1}{(\mathcal{C}^\alpha)^2}\left[\mathbf{A}^{\alpha+} + \mathbf{B}^{\alpha+} \cdot \mathbf{b}_\mathbf{a}^{\alpha+} - \frac{\hat{\mathsf{G}}^{\alpha+}}{\rho_0^\alpha\theta_0}\pi_\mathbf{a}^{\alpha+}\right]\right.$$
$$\cdot\left[\left(\frac{\partial(D_t^\alpha\mathbf{a}^\alpha)}{\partial J^\alpha}\right)^+ + \left(\frac{\partial(D_t^\alpha\mathbf{a}^\alpha)}{\partial\mathbf{b}^\alpha} \cdot \mathbf{b}'^\alpha\right)^+\right]$$
$$\left. + \left(\frac{\partial h^\alpha}{\partial\upsilon^\alpha}\right)^+ + \frac{1}{\theta_0}\left(\frac{\hat{\mathsf{G}}^{\alpha+}}{\rho_0^\alpha\mathcal{C}^\alpha}\right)^2\left(\frac{\partial\epsilon^\alpha}{\partial\theta^\alpha}\right)^+\right\}, \quad (248)$$

$$\delta_t[\![J^\alpha]\!] = -\omega^\alpha[\![J^\alpha]\!] + O([\![J^\alpha]\!][\![\nabla_0^\alpha J^\alpha]\!]; [\![J^\alpha]\!]^2). \quad (249)$$

Omitting higher-order products on the right of (249) [66],

$$[\![J^\alpha]\!](t) = \Delta J_0^\alpha\exp(-\omega^\alpha t), \quad \Delta J_0^\alpha = [\![J^\alpha]\!](t = 0). \quad (250)$$

For small $[\![J^\alpha]\!]$, if $\nabla_0^\alpha J^\alpha$ remains negligible behind wave front Σ^α, then shock amplitude evolves at a rate determined by

$\omega^\alpha = \text{const}$. Jumps $[\![P^\alpha]\!]$, $[\![u^\alpha]\!]$, $[\![\theta^\alpha]\!]$, and $[\![\mathbf{b}^\alpha]\!]$ evolve proportionally via (226)–(229); $[\![\eta^\alpha]\!] \to 0$ by (230).

Derivations of Sec. IV C apply trivially for a single-phase material ($\alpha = N = 1$, $h^\alpha \to 0$, $\epsilon^\alpha \to 0$). They can also describe a shock moving with velocity $\mathcal{U}$ through the mixture as a whole per Sec. II C. Assuming $\upsilon^\alpha = \upsilon$ and $\theta^\alpha = \theta$ for all constituents, then $J^\alpha = J$, diffusion velocities $\boldsymbol{\mu}^\alpha = \mathbf{0}$, and thus $h^\alpha = 0$ and $\epsilon^\alpha = 0$. Then from Sec. II C, mixture quantities include $\psi = u - \theta\eta$ and

$$P = \sum_\alpha P^\alpha, \quad \rho_0 = \sum_\alpha n_0^\alpha \rho_{R0}^\alpha, \quad \rho_0 u = \sum_\alpha \rho_0^\alpha u^\alpha,$$

$$\hat{\mathsf{C}} = \sum_\alpha \hat{\mathsf{C}}^\alpha, \quad \hat{\mathsf{G}} = \sum_\alpha \frac{\partial P^\alpha}{\partial \eta}, \quad \eta = -\frac{\partial \psi}{\partial \theta}. \tag{251}$$

Since u^α is independent of $(\mathbf{a}^\beta, \mathbf{b}^\beta) \, \forall \, \beta \neq \alpha$ per (203),

$$\mathbf{L} \cdot [\![\dot{\mathbf{a}}]\!] = \sum_\alpha \mathbf{L}^\alpha \cdot [\![D_t^\alpha \mathbf{a}^\alpha]\!]. \tag{252}$$

2. Biologic tissue

Quantities entering Λ^α and ω^α of (247) and (248) are now evaluated for constitutive frameworks of Sec. III. First, consider an ideal gas. Variables $(\mathbf{a}^\alpha, \mathbf{b}^\alpha)$ are irrelevant, $\rho_0^\alpha = n_0^\alpha \rho_{R0}^\alpha$, and (102) and (104) give

$$P^{\alpha+} = n_0^\alpha p_{R0}^\alpha, \quad \hat{\mathsf{C}}^{\alpha+} = n_0^\alpha p_{R0}^\alpha (1 + \gamma_0^\alpha), \tag{253}$$

$$\hat{\mathsf{C}}'^{\alpha+} = -n_0^\alpha p_{R0}^\alpha (1 + \gamma_0^\alpha)(2 + \gamma_0^\alpha), \tag{254}$$

$$\hat{\mathsf{G}}^{\alpha+} = -\rho_0^\alpha \theta_0 \gamma_0^\alpha, \quad \mathcal{C}^\alpha = \left[n_0^\alpha p_{R0}^\alpha (1 + \gamma_0^\alpha) / \rho_0^\alpha \right]^{1/2}, \tag{255}$$

$$(\partial \hat{\mathsf{G}}^\alpha / \partial J^\alpha)^+ = -\hat{\mathsf{G}}^{\alpha+}(1 + \gamma_0^\alpha). \tag{256}$$

Next, consider a compressible fluid obeying the EOS in (109)–(112). With null cavitation for compression, $(\mathbf{a}^\alpha, \mathbf{b}^\alpha)$ are again irrelevant, $\rho_0^\alpha = n_0^\alpha \rho_{R0}^\alpha$, (256) holds, and

$$P^{\alpha+} = n_0^\alpha p_{R0}^\alpha, \quad \hat{\mathsf{C}}^{\alpha+} = n_0^\alpha (p_{R0}^\alpha + B_\eta^\alpha), \tag{257}$$

$$\hat{\mathsf{C}}'^{\alpha+} = -n_0^\alpha \{ 2 p_{R0}^\alpha + B_\eta^\alpha (1 + B_{\eta p}^\alpha) \}, \tag{258}$$

$$\hat{\mathsf{G}}^{\alpha+} = -\rho_0^\alpha \theta_0 \gamma_0^\alpha, \quad \mathcal{C}^\alpha = \left[n_0^\alpha (p_{R0}^\alpha + B_\eta^\alpha) / \rho_0^\alpha \right]^{1/2}. \tag{259}$$

Last, a solid constituent with EOS (109)–(112), viscoelastic matrix, viscoelastic fibers, matrix- and fiber-damage is addressed. Bulk and shear viscoelasticity and fiber family $k = 1$ furnish internal variables $\mathbf{a}^\alpha \to \{\boldsymbol{\Gamma}_{Vl}^\alpha, \boldsymbol{\Gamma}_{Sm}^\alpha, \boldsymbol{\Gamma}_{\Phi k,n}^\alpha\}$ with initial conditions $\{\boldsymbol{\Gamma}_{Vl}^{\alpha+} = \boldsymbol{\Gamma}_{Sm}^{\alpha+} = \boldsymbol{\Gamma}_{\Phi k,n}^{\alpha+} = \mathbf{0}\}$. Rate-insensitive damage supplies order parameters $\mathbf{b}^\alpha \to \{\bar{D}^\alpha, D_k^\alpha\}$ with initial conditions $\{\bar{D}^{\alpha+} = D_k^{\alpha+} = 0\}$. Fibers are either aligned, $\kappa_k^\alpha = 0$ parallel to (x, X^α), or isotropic, $\kappa_k^\alpha = \frac{1}{3}$. Constant active tension is permitted, affecting energy, stress $(\sigma_A)_1^1$, and stiffness via (140) and (141); since $\Delta_k^\alpha = \text{const}$, this does not affect dissipation nor need enter $\mathbf{a}^\alpha$. As usual, $\rho_0^\alpha = n_0^\alpha \rho_{R0}^\alpha$ and $(\mathcal{C}^\alpha)^2 = \hat{\mathsf{C}}^{\alpha+} / \rho_0^\alpha$. Lengthy, yet routine, derivations yield the material response coefficients listed in Appendix D.

For rate-insensitive damage, from $\bar{\pi}_D^\alpha = 0$ and $\pi_{Dk}^\alpha = 0$ via (202) and using (229) and (D17) with $\bar{\vartheta}^\alpha = \vartheta_k^\alpha = 2$,

$$\bar{D}^{\alpha-} = \frac{1}{n_0^\alpha \bar{E}_C^\alpha} (\mathsf{C}_S^{\alpha+} + \mathsf{C}_\Gamma^{\alpha+}) [\![J^\alpha]\!]^2 + O([\![J^\alpha]\!]^3), \tag{260}$$

$$D_k^{\alpha-} = \frac{1}{n_0^\alpha E_{Ck}^\alpha} (\mathsf{C}_F^{\alpha+} + \mathsf{C}_\Phi^{\alpha+}) [\![J^\alpha]\!]^2 + O([\![J^\alpha]\!]^3). \tag{261}$$

Notice $D_k^{\alpha-} \to 0$ in (261) if $\kappa_k^\alpha = \frac{1}{3}$. To at least $O([\![J^\alpha]\!]^2)$, (260) and (261) are unaffected by Finsler versus Euclidean metrics $(\mathbf{g}, \mathbf{G}^\alpha)$ for current prescriptions $\bar{r}^\alpha \geqslant 2$ and $\tilde{r}_k^\alpha \geqslant 2$. From $\mathbf{b}^{\alpha+} \to \mathbf{0}$ and (D17), rate-insensitive fractures do not affect weak-shock evolution (247)–(250).

If fractures are rate dependent, then $\mathbf{b}^\alpha \to \mathbf{0}$ and $\mathbf{a}^\alpha \to \{\boldsymbol{\Gamma}_{Vl}^\alpha, \boldsymbol{\Gamma}_{Sm}^\alpha, \boldsymbol{\Gamma}_{\Phi k,n}^\alpha, \bar{D}^\alpha, D_k^\alpha\}$. Then (213) yields $\bar{D}^{\alpha-} = 0$ and $D_k^{\alpha-} = 0$ in lieu of (260) and (261). From (168) and (173), damage kinetics do not contribute to $\mathbf{A}^{\alpha+}$ or $\boldsymbol{\pi}_a^{\alpha+}$ nor Λ^α or ω^α in (247), (248); (D18)–(D20) are unchanged. Importantly, damage, regardless of rate (in)dependence, can still affect strong-shock evolution in (239)–(243) even if its effects on weak shock decay are negligible.

Phase interactions affect Λ^α and ω^α, from (176)–(179),

$$\left(\frac{\partial h^\alpha}{\partial \upsilon^\alpha} \right)^+ = -\sum_{\beta \neq \alpha} \bar{\lambda}^{\alpha\beta+}, \quad \left(\frac{\partial \epsilon^\alpha}{\partial \theta^\alpha} \right)^+ = -\sum_{\beta \neq \alpha} \bar{\omega}^{\alpha\beta+}. \tag{262}$$

Consider now a two-phase mixture of solid ($\alpha = 1 \to$ s) and fluid ($\alpha = 2 \to$ f). Adopting physics in Refs. [41,42],

$$\bar{\lambda}^{12+} = (n_0^f)^2 \hat{\mu}^f / \Xi, \quad \bar{\omega}^{12+} = \alpha_v \kappa^{\text{fs}}, \tag{263}$$

with fluid viscosity $\hat{\mu}^f$, system permeability Ξ, interfacial area per unit volume α_v, and heat transfer coefficient κ^{fs}. Although macroscopic Newtonian viscosity and Fourier conduction are excluded for singular shocks [121], microscopic h^α and ϵ^α include viscosity and heat transfer.

Recall from (234) that the weak-shock solution (250) for a multi-phase material corresponds to strain jump ΔJ_0^α and resulting discontinuities in P^α and θ^α applied as a loading condition for one phase α, with all other phase $\beta = 1, 2, \ldots \alpha - 1, \alpha + 1, \ldots, N$ witnessing no discontinuities in J^β, P^β, or θ^β. This shock moves through all phases at speed $\mathcal{C}^\alpha$; phase interactions h^α and ϵ^α induce decay in amplitude $[\![J^\alpha]\!](t)$ so long as $\bar{\lambda}^{\alpha\beta} > 0$ and $\bar{\omega}^{\alpha\beta} > 0$. Velocities υ^β and temperatures θ^β ($\beta \neq \alpha$) can evolve continuously in space-time behind the wave front from such interactions, their values indeterminate.

In contrast, if the mixture is idealized as homogeneous with matching υ^α and θ^α, then h^α and ϵ^α do not explicitly affect shock evolution. In this "tied" case, ΔJ_0^α is applied simultaneously at $t = 0$ to all phases $\alpha = 1, \ldots, N$ as a loading condition. Speed $\mathcal{C} = (\hat{\mathsf{C}} / \rho_0)^{1/2}$ results from stiffness and density of the whole mixture in (251), and

$$\hat{\mathsf{C}}'^+ = \sum_\alpha \hat{\mathsf{C}}'^{\alpha+}, \quad \hat{\mathsf{G}}^+ = -\rho_0 \theta_0 \frac{\sum_\alpha \gamma_0^\alpha \rho_0^\alpha c_\epsilon^\alpha}{\sum_\alpha \rho_0^\alpha c_\epsilon^\alpha}. \tag{264}$$

3. Predictions

The analytical solution for weak shock evolution, namely (247)–(250), is applied to three biologic systems at $\theta_0 = 310$ K, each comprised of one solid tissue phase and one fluid: skeletal muscle with interstitial fluid, liver with blood,

TABLE III. Shock evolution parameters for rabbit muscle (ECF and solid, $n_0^1 = 0.9$), bovine liver (blood and solid, $n_0^1 = 0.88$), and canine lung (air and solid, $n_0^1 = 0.336$). "Mixture" invokes same shock simultaneously to each phase. $(\Delta P)_0^\alpha$, $(\Delta\theta)_0^\alpha$, $(\Delta\bar{D})_0^\alpha$, and $(\Delta D_1)_0^\alpha$ are initial stress, temperature, and matrix and fiber damage jumps for initial strain change $\Delta J_0^\alpha = [\![J^\alpha]\!](t=0) = -0.1$.

Property or model prediction	Muscle			Liver			Lung		
	ECF	Solid	Mixture	Blood	Solid	Mixture	Air	Solid	Mixture
ρ_0^α (g/cm^3)	0.103	0.990	1.093	0.127	0.933	1.060	7.56×10^{-4}	0.337	0.338
$\hat{\mathbf{C}}^{\alpha+}$ (GPa)	0.220	2.954	3.174	0.317	2.350	2.667	9.42×10^{-5}	9.26×10^{-5}	1.87×10^{-4}
$\hat{\mathbf{C}}'^{\alpha+}$ (GPa)	-1.751	-26.57	-28.32	-4.118	-21.15	-25.27	-2.26×10^{-4}	-2.42×10^{-4}	-4.68×10^{-4}
$\mathcal{C}^\alpha$ (km/s)	1.462	1.727	1.704	1.578	1.587	1.586	0.353	1.66×10^{-2}	2.35×10^{-2}
$\hat{\mathbf{G}}^{\alpha+}$ (g·K/cm^3)	-4.215	-96.06	-99.15	-6.309	-32.97	-39.31	-9.38×10^{-2}	-11.91	-11.95
ω^α (1/s)	8.69×10^9	9.05×10^8	7.01×10^{-3}	1.89×10^7	2.57×10^6	6.62×10^{-2}	2.97×10^4	1.13×10^2	2.95×10^{-2}
Λ^α (1/m)	2.99×10^6	2.33×10^5	1.84×10^{-6}	3.68×10^3	7.21×10^2	1.76×10^{-5}	1.40×10^2	1.04×10^1	2.01×10^{-3}
$(\Delta P)_0^\alpha$ (MPa)	30.8	428	459	52.3	341	393	1.06×10^{-2}	1.05×10^{-2}	2.10×10^{-2}
$(\Delta\theta)_0^\alpha$ (K)	4.32	10.3	9.66	5.25	3.73	3.92	13.3	3.73	3.74
$(\Delta\bar{D})_0^\alpha$ (–) matrix	…	0.045	0.045	…	0.100	0.100	…	5.03×10^{-3}	5.03×10^{-3}
$(\Delta D_1)_0^\alpha$ (–) fibers	…	0.022	0.022	…	0	0	…	0	0

and lung with air. Physical properties or parameters, ω^α, and Λ^α are given in Table III for each component, and for the homogeneous idealization of (251), (252), and (264) labeled "Mixture."

Constitutive and metric-tensor parameters are those for rabbit skeletal muscle and bovine lung of Sec. IV B, Table I (ECF, blood) and Table II (solids). For muscle, active tension from (199) affects initial stress but does not appreciably change tabulated results (not shown).

Air is modeled as an ideal gas [50] with $\mathfrak{R}^\alpha = 287\,\mathrm{J/kg \cdot K}$ and $\gamma_0^\alpha = 0.4$. Viscosity for air in (263) is $\hat{\mu}^f = 18.3\,\mu\mathrm{Pa\,s}$ [41]. Solid properties are for canine lung [6,50,100] with bulk and shear viscoelasticity ($l = m = 1$), isotropic fibers ($\kappa_k^\alpha = \frac{1}{3}$), solid fraction $n_0^1 = 0.336$, $B_\eta^\alpha = 164\,\mathrm{kPa}$, $\mu_S^\alpha = 2.98\,\mathrm{kPa}$, $\beta_{Vl}^\alpha = 0.009$, $\beta_{Sm}^\alpha = 1.5$, $\tau_{Vl}^\alpha = \tau_{Sm}^\alpha = 0.5\,\mathrm{s}$. Values $\gamma_0^\alpha = 0.114$ and $\bar{E}_C^\alpha = 22.7\,\mathrm{kPa}$, unmeasured for lung parenchyma, are borrowed from liver parenchyma. This value of γ_0^α for lung is approximately twice that of Ref. [50], with the latter estimate $10^3 \times$ that of classical thermodynamics [141] using the low B_θ^α of the highly porous structure.

In (263), $\Xi = 6.7 \times 10^{-18}\mathrm{m}^2$ for muscle [142], $\Xi = 1.5 \times 10^{-14}\mathrm{m}^2$ for liver [43], and $\Xi = 1.83 \times 10^{-10}\mathrm{m}^2$ for lung [41]. For heat transfer, $\kappa^{\mathrm{fs}} = 6\,\mathrm{W/m}^2 \cdot \mathrm{K}$ in muscle and liver [113], and $\kappa^{\mathrm{fs}} = 41.2\,\mathrm{W/m}^2 \cdot \mathrm{K}$ in lung [143]. From idealized microstructure geometries [1,132,142], a contact area estimate for muscle is $\alpha_v = \pi/R_0$ with $R_0 = 30\,\mu\mathrm{m}$ the fiber radius [51], for liver $\alpha_v = 2n_0^f/R_0$ with $R_0 = 4\,\mu\mathrm{m}$ the capillary radius [113], and for lung $\alpha_v = \pi/(2R_0)$ with $R_0 = 30\,\mu\mathrm{m}$ the alveolar radius [100].

The lower four rows of Table III contain initial jumps in stress of (226), temperature of (228), matrix damage of (260), and fiber fracture of (261), each to $O([\![J^\alpha]\!]^2)$ for initial strain jump $\Delta J_0^\alpha = -0.1$. If damage is modeled as rate dependent, then its jumps must vanish instead in the infinitesimal-width shock approximation of (213).

Normalized exponential decay of $[\![P^\alpha]\!]$ and $[\![\theta^\alpha]\!]$ arising from (250) is shown for both components of each two-phase system in Fig. 6. In each system, a shock applied to the fluid decays over a much shorter distance than one applied to the solid. From Fig. 6, decay distance is shortest in muscle and longest in lung. When mixtures are shocked uniformly, decay

from viscoelastic dissipation alone manifests over much larger distances (not shown).

From Table III and Fig. 6, when ΔJ_0^α is applied to one constituent alone, then $|\Lambda^\alpha|$ and $|\omega^\alpha|$ are relatively large, with $\omega^\alpha > 0$ for transient decay. For $dP_H^\alpha/d[\![J^\alpha]\!] \approx -\hat{\mathbf{C}}^{\alpha-} < 0$ and since $\Lambda^\alpha > 0$, a negative stress gradient $\nabla_0 P^{\alpha-}$ is needed for a steady shock (i.e, no decay). In a steady shock, P^α should decrease steeply as Σ^α is approached from the $(\cdot)^-$ side. For muscle and liver, $(\partial h^\alpha/\partial \upsilon^\alpha)^+$ is the dominant contribution to ω^α due to relatively small Ξ and large $\hat{\mu}^f$ in (263). For lung, both $(\partial h^\alpha/\partial \upsilon^\alpha)^+$ and $(\partial \epsilon^\alpha/\partial \theta^\alpha)^+$ have significant influence on shock decay, the latter due to a comparatively low $\mathcal{C}^\alpha$. Viscoelastic dissipation embodied in $\mathcal{A}_{\Gamma V}$, $\mathcal{A}_{\Gamma S}$, and $\mathcal{A}_\Phi$ has relatively small effects, negligible compared to interphase drag and heat exchange. Nearly incompressible viscoelastic responses of these soft biologic tissues, also typical of soft polymers at high rates [144], leads to small glassy shear moduli relative to bulk moduli, the latter (bulk) modeled here having little or no viscoelastic relaxation. From Table III, stress rises $(\Delta P)_0^\alpha$ are greatest in solid phases of muscle and liver having largest tangent moduli. Temperature $(\Delta\theta)_0^\alpha$ is highest in air in the lung.

Table IV compares decay distances for shocks applied to isolated solid constituents (albeit with nonzero fluid-solid interactions h^α and ϵ^α) in skeletal muscle, liver, and lung. Denote by $\varphi^\alpha(t)$ the normalized shock amplitude in constituent α with speed $\mathcal{C}^\alpha$ and decay constant ω^α. Inverting (250), decay distance $X^\alpha = \mathcal{C}^\alpha t$ from a shock applied at $t = 0$ is

$$X^\alpha = -(\mathcal{C}^\alpha/\omega^\alpha)\ln\varphi^\alpha. \tag{265}$$

TABLE IV. Decay distance X^α to attain fraction of initial shock strength φ^α for weak shocks in solid tissue phase ($\alpha = 1$).

Soft tissue	Decay distance X^α (units)		
	$\varphi^\alpha = 0.9$	$\varphi^\alpha = 0.5$	$\varphi^\alpha = 0.1$
Muscle	0.20 μm	1.32 μm	4.40 μm
Liver	0.07 mm	0.43 mm	1.42 mm
Lung	1.55 cm	10.18 cm	33.81 cm
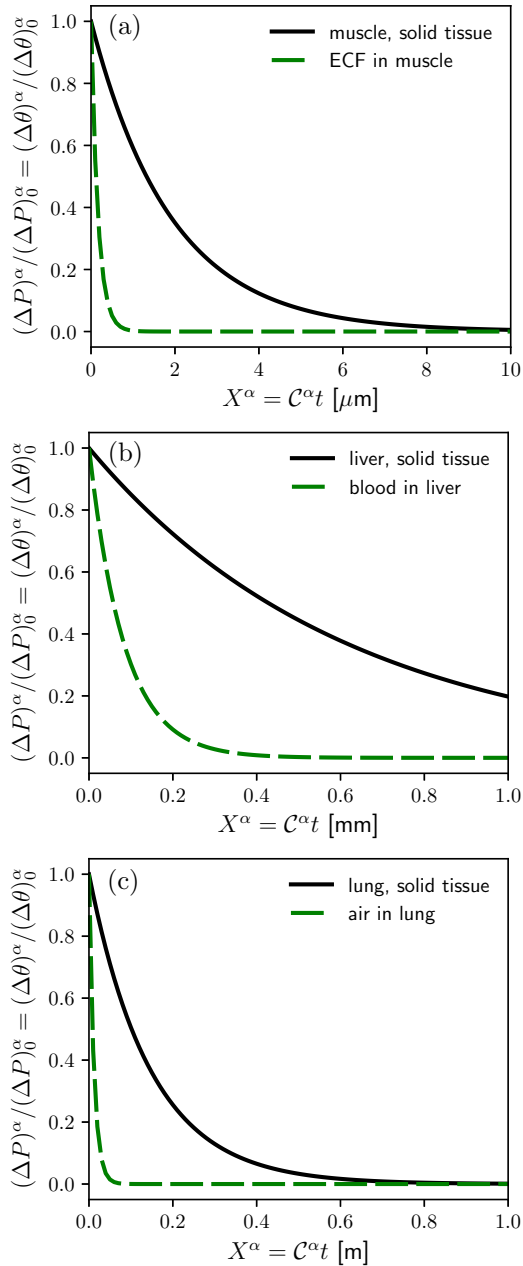
FIG. 6. Predicted ratio of jump in shock stress $(\Delta P)^\alpha$ or temperature $(\Delta \theta)^\alpha$ normalized by initial magnitude $(\Delta P)^\alpha_0$ or $(\Delta \theta)^\alpha_0$, for shock amplitude ΔJ^α_0 applied individually to phase α, vs propagation distance X^α in the weak shock limit: (a) rabbit muscle, (b) bovine liver, and (c) canine lung. Wave speed is $\mathcal{C}^\alpha$; different scales (i.e., μm, mm, or m) used for X^α.

Substantial decay requires distances on the order of μm in solid tissue of skeletal muscle. Decay takes place over distances of mm in liver. Significant shock evolution requires the largest distances in lung, on the order of cm. If isolated shocks degenerate over distances small relative to microstructure dimensions, then a physically rational assumption is that macroscopic shock propagation can be modeled using the homogenized mixture approximation (i.e., a constrained mixture theory [74,75,114,115]). From results in Table IV, this "locally undrained" assumption, wherein fluid and solid phases

move in concert with the same local velocity (i.e., fluid is entrapped or immobile with respect to the solid) and temperature, appears most-to-least appropriate in the following order: skeletal muscle, liver parenchyma, and lung parenchyma.

V. CONCLUDING REMARKS

A theoretical framework is posited for modeling multiphase soft biologic materials over wide ranges of loading rate and pressure. Classical continuum mixture theory of Bowen and Truesdell is augmented with internal variables that can address viscoelasticity, activation, growth and remodeling, and tissue degradation (e.g., the opposite of growth and remodeling). Dependence of free energy and external working on state variable gradients leads to Ginzburg-Landau type kinetics for these state variables. The phase-field fracture theory distinguishes among order parameters associated with matrix and fiber damage, providing more physical insight than prior models that used only single damage order parameter. Permitting non-Euclidean metric tensors to depend on internal state can resolve residual (i.e., remnant) strain from growth, remodeling, or degradation. Fracture resistance increases in concert with remnant strain, similar to toughening seen in structural materials in concert with plastic strain.

Results for uniaxial-stress and shock loading agree with experimental data on biologic fluids and soft tissues. Fluids include water, ECF, and blood. Soft tissues in include skeletal muscle infused with ECF, liver infused with blood, and lung permeated with air. Usual incompressibility assumptions of soft-tissue mechanics and poromechanics are abandoned to permit modeling of shock waves and large (volumetric) compressions, the latter unrestricted by initial porosity of the drained solid medium.

Uniaxial-stress calculations confirm that damage, represented by order parameters for matrix rupture and fiber fractures, is strain-rate insensitive in muscle fibers but rate dependent in liver. Stress results closely match most experimental data on these fluid-rich tissues. Since solids and fluids have similar bulk compressibility, with null or small ratios of shear to bulk modulus, uniaxial stresses supported by the mixture are nearly indistinguishable whether the fluids are equilibrated to partial atmospheric pressures or tied to deform laterally with the solid.

An analytical solution has been derived for shock evolution including phase interactions, viscoelasticity, and tissue damage. Previous derivations have not considered all phenomena simultaneously, so are unable to quantify relative effects of each mechanism on shock decay. Closed-form results are obtained in the weak-shock limit. Calculations consider one or the other phase shock-compressed independently (albeit still interacting with the other initially quiescent phase) or a single shock wave applied simultaneously to a homogenized material system. Predictions reveal dominance of interphase momentum and energy exchange over viscoelastic dissipation and effects of matrix and fiber damage for all two-phase materials. For muscle and liver, effects of interphase heat transfer on shock decay are small versus interphase viscous drag. For lung, thermal effects are not insignificant.

Decay distances for shocks in solid constituents are around one order of magnitude larger than for fluid constituents.

Weak shock decay in isolated constituents occurs over μm in muscle, mm in liver, and cm in lung. An assumption that the mixture can be idealized as a single-phase material with homogenized properties appears to be most valid for dynamic shock-wave responses of skeletal muscle, less valid for liver, and least valid for lung.

APPENDIX A: STEADY WAVES

Jump equations are derived for mass, momentum, and energy between two points in a structured steady wave [69,80]. In a 1D Lagrangian setting, let $\mathcal{D}^\alpha$ be a constant wave speed; for a differentiable function $f(X^\alpha, t)$,

$$f(X^\alpha, t) = f(X^\alpha - \mathcal{D}^\alpha t) = f(Y^\alpha), \tag{A1}$$

$$\partial f/\partial X^\alpha = df/dY^\alpha, \quad D_t^\alpha f = -\mathcal{D}^\alpha df/dY^\alpha. \tag{A2}$$

Applying (A2) to 1D equations $D_t^\alpha F^\alpha = \partial \upsilon^\alpha/\partial X^\alpha$ and

$$\rho_0^\alpha D_t^\alpha \upsilon^\alpha = \partial t^\alpha/\partial X^\alpha + \rho_0^\alpha b^\alpha + (\partial \chi^\alpha/\partial X^\alpha)h^\alpha, \tag{A3}$$

which is the first of (16), gives

$$d\upsilon^\alpha/dY = -\mathcal{D}^\alpha dF^\alpha/dY, \tag{A4}$$

$$dt^\alpha/dY = -\rho_0^\alpha \mathcal{D}^\alpha d\upsilon^\alpha/dY - \rho_0^\alpha b^\alpha - F^\alpha h^\alpha. \tag{A5}$$

Select two points at steady-wave coordinates $Y^\pm$, and define the jump in a quantity between these points as in (23): $[\![f(Y)]\!] = f(Y^-) - f(Y^+)$. Direct integration of (A4) over $Y^- \to Y^+$ and substitution into (A5) gives

$$[\![\upsilon^\alpha]\!] = -\mathcal{D}^\alpha [\![F^\alpha]\!], \tag{A6}$$

$$[\![t^\alpha]\!] = \rho_0^\alpha (\mathcal{D}^\alpha)^2 [\![F^\alpha]\!] + \int_-^+ (\rho_0^\alpha b^\alpha + F^\alpha h^\alpha) dY. \tag{A7}$$

Using the same procedure for 1D continuum laws of energy conservation and entropy production, (17) and (19),

$$\rho_0^\alpha D_t^\alpha u^\alpha = t^\alpha \partial \upsilon^\alpha/\partial X^\alpha + \partial(\{z\}^\alpha\{D_t^\alpha \xi^\alpha\})/\partial X^\alpha$$
$$- \partial q^\alpha/\partial X^\alpha + \rho_0^\alpha r^\alpha + (\partial \chi^\alpha/\partial X^\alpha)\epsilon^\alpha, \tag{A8}$$

$$\sum_\alpha \Big[\rho_0^\alpha D_t^\alpha \eta^\alpha + \partial(q^\alpha/\theta^\alpha)/\partial X^\alpha - \rho_0^\alpha r^\alpha/\theta^\alpha$$
$$+ (\partial \chi^\alpha/\partial X^\alpha)c^\alpha \eta^\alpha \Big] \geqslant 0; \tag{A9}$$

$$\rho_0^\alpha \mathcal{D}^\alpha \left[\!\!\left[u^\alpha + \frac{1}{2}|\upsilon^\alpha|^2 \right]\!\!\right]$$
$$= -\left[\!\!\left[t^\alpha \upsilon^\alpha + \{z^\alpha\}\{D_t^\alpha \xi^\alpha\} - q^\alpha \right]\!\!\right]$$
$$+ \int_-^+ \{ \rho_0^\alpha(r^\alpha + b^\alpha \upsilon^\alpha) + F^\alpha(\epsilon^\alpha + h^\alpha \upsilon^\alpha) \} dY, \tag{A10}$$

$$\sum_\alpha \left(\rho_0^\alpha \mathcal{D}^\alpha [\![\eta^\alpha]\!] - [\![q^\alpha/\theta^\alpha]\!] \right)$$
$$- \int_-^+ (\rho_0^\alpha r^\alpha/\theta^\alpha - F^\alpha c^\alpha \eta^\alpha) dY \Big\} \geqslant 0. \tag{A11}$$

Relation (A6) is identical to the mass conservation law for a singular surface in the first of (40) when $\mathcal{D}^\alpha \to \mathcal{U}^\alpha$. Relation (A7) is identical to the momentum conservation law in the second of (40) when the integral on the right of (A7) vanishes

(e.g., constant body force and null drag). Relation (A10) is identical to the energy conservation law in (37) when its integral terms vanish, and (A11) is identical to entropy inequality (38) when its integral terms involving heat and mass supplies vanish. In such cases, Eulerian jump conditions in (28) and (29) can be recovered for a steady wave of Eulerian speed $\mathcal{D}$ where $f(x, t) = f(x - \mathcal{D}t)$ when $\mathcal{D} = F^\alpha \mathcal{D}^\alpha + \upsilon^\alpha = $ const.

Given (53), (54), (56), (64), and (65), the treatment of steady Lagrangian waves can be applied to the mixture as a whole. Let $f(X, t) = f(X - \mathcal{D}t) = f(Y)$ in a steady wave, with $\mathcal{D}$ the constant speed. Using relations akin to (A1) and (A2), the local compatibility and linear momentum equations (64) and (53) (in 1D) are

$$d\upsilon/dY = -\mathcal{D}dF^\alpha/dY, \tag{A12}$$

$$d\sigma/dY = -\rho_0 \mathcal{D}d\upsilon/dY - \rho_0 b. \tag{A13}$$

Integrating from $Y^+ \to Y^-$ gives conditions like (61):

$$[\![\upsilon]\!] = -\mathcal{D}[\![F]\!] = -\mathcal{D}\rho_0[\![1/\rho]\!], \tag{A14}$$

$$[\![\sigma]\!] = -\rho_0 \mathcal{D}[\![\upsilon]\!] + \int_-^+ \rho_0 b \, dY. \tag{A15}$$

APPENDIX B: METRIC PARTITION AND ALTERNATIVE STRAIN

Decompositions of metrics of (2) and (3) into symmetric position-dependent (i.e., classical) and dimensionless, invertible, space-time-dependent parts are [52,54,57]

$$\mathbf{g}(\mathbf{x}, t) = \bar{\mathbf{g}}(\mathbf{x})\hat{\mathbf{g}}(\{\boldsymbol{\xi}^\alpha(\mathbf{x}, t)\}), \tag{B1}$$

$$\mathbf{G}^\alpha(\mathbf{X}^\alpha, t) = \bar{\mathbf{G}}^\alpha(\mathbf{X}^\alpha)\hat{\mathbf{G}}^\alpha(\{\boldsymbol{\Xi}^\alpha(\mathbf{X}^\alpha, t)\}). \tag{B2}$$

A deformation $\bar{\mathbf{C}}^\alpha$ and Jacobian $\bar{J}^\alpha$ based on $(\bar{\mathbf{g}}, \bar{\mathbf{G}}^\alpha)$ are

$$(\bar{C}^\alpha)_J^K = \bar{G}^{KI}(F^\alpha)_I^i \bar{g}_{ij}(F^\alpha)_J^j (\mathbf{G}^\alpha)_K \otimes (\mathbf{G}^\alpha)^J, \tag{B3}$$

$$\bar{J}^\alpha = \sqrt{\det \bar{\mathbf{C}}^\alpha} = J^\alpha \sqrt{\hat{G}^\alpha/\hat{g}}, \tag{B4}$$

with dimensionless $\hat{g} = \det \hat{\mathbf{g}}$ and $\hat{G}^\alpha = \det \hat{\mathbf{G}}^\alpha$. Alternative constitutive equations [52], also energetically objective, are obtained by positing dependence of ψ^α, η^α, u^α, and θ^α through $\bar{\mathbf{C}}^\alpha(F^\alpha)$ rather than $\mathbf{C}^\alpha$, whereby

$$\partial \psi^\alpha/\partial \mathbf{F}^\alpha = 2\mathbf{F}^\alpha \partial \psi^\alpha/\partial \bar{\mathbf{C}}^\alpha$$
$$\leftrightarrow \partial \psi^\alpha/\partial(F^\alpha)_J^i = 2\bar{g}_{ik}(F^\alpha)_L^k \partial \psi^\alpha/\partial(\bar{C}^\alpha)_{JL}. \tag{B5}$$

Derivations in (81)–(96) continue to apply for $\psi^\alpha(\bar{\mathbf{C}}^\alpha, \cdot)$, $\eta^\alpha(\bar{\mathbf{C}}^\alpha, \cdot)$, etc. with several changes manifested by (B5):

$$(\bar{\sigma}^\alpha)_i^j = 2\rho^\alpha \bar{g}_{ik}(F^\alpha)_L^k(F^\alpha)_J^j \partial \psi^\alpha/\partial(\bar{C}^\alpha)_{JL}$$
$$= 2\rho^\alpha \bar{g}_{ik}(F^\alpha)_L^k(F^\alpha)_J^j \partial u^\alpha/\partial(\bar{C}^\alpha)_{JL}, \tag{B6}$$

$$\bar{\boldsymbol{\beta}}^\alpha = \rho^\alpha c_\epsilon^\alpha \bar{\boldsymbol{\gamma}}^\alpha = -2\rho^\alpha \partial^2 \psi^\alpha/\partial \theta^\alpha \partial \bar{\mathbf{C}}^\alpha, \tag{B7}$$

$$\rho^\alpha c_\epsilon^\alpha D_t^\alpha \theta^\alpha = \mathfrak{D}^\alpha - \frac{1}{2}\theta^\alpha \bar{\boldsymbol{\beta}}^\alpha : D_t^\alpha \bar{\mathbf{C}}^\alpha$$
$$+ \rho^\alpha \theta^\alpha \big[(\partial^2 \psi/\partial \theta^\alpha \partial\{\boldsymbol{\xi}^\alpha\}) \cdot \{D_t^\alpha \boldsymbol{\xi}^\alpha\}$$
$$+ (\partial^2 \psi/\partial \theta^\alpha \partial\{\boldsymbol{\nabla}\boldsymbol{\xi}^\alpha\}) : \{\boldsymbol{\nabla}(D_t^\alpha \boldsymbol{\xi}^\alpha)\} \big]$$
$$- \boldsymbol{\nabla} \cdot \mathbf{q}^\alpha + \rho^\alpha r^\alpha + \epsilon^\alpha. \tag{B8}$$

Mixed-variant $\bar{\boldsymbol{\sigma}}^\alpha$ in (B6) excludes $\hat{\mathbf{g}}(\mathbf{x}, t)$. Contravariant stress defined as $(\bar{\sigma}^\alpha)^{ij} = \frac{1}{2}[g^{ik}(\bar{\sigma}^\alpha)^j_k + g^{jk}(\bar{\sigma}^\alpha)^i_k]$ or $(\bar{\sigma}^\alpha)^{ij} = \bar{g}^{ik}(\bar{\sigma}^\alpha)^j_k$ must be symmetric. The former depends on $\hat{\mathbf{g}}(\mathbf{x}, t)$ implicitly from g^{ik}. This choice presumes, *a priori*, that skew contributions from (B6) perform no work in the energy balance so can thus be redefined as zero. The latter prescription either redefines raising or lowering indices on Cauchy stress or presumes that $\mathbf{d}^\alpha$ is defined in covariant form by lowering of $\mathbf{l}^\alpha$ with $\bar{g}_{ij}$, rather than the typical g_{ij} prior to symmetrization.

APPENDIX C: DERIVATION OF SHOCK EVOLUTION LAW

Using (237) on $[\![J^\alpha]\!]$ and $[\![\upsilon^\alpha]\!]$, then (42) on $\mathcal{U}$ in (211),

$$2\mathcal{U}\delta_t[\![J^\alpha]\!] + [\![J^\alpha]\!]\delta_t\mathcal{U} = \mathcal{U}^2[\![\boldsymbol{\nabla}^\alpha_0 J^\alpha]\!] - [\![D^\alpha_t\upsilon^\alpha]\!]. \quad \text{(C1)}$$

From (205), (207), (209), (211), and (217)–(220),

$$\rho^\alpha_0[\![D^\alpha_t\upsilon^\alpha]\!] = \mathsf{C}^{\alpha-}[\![\boldsymbol{\nabla}^\alpha_0 J^\alpha]\!] + \mathsf{G}^{\alpha-}[\![\boldsymbol{\nabla}^\alpha_0\eta^\alpha]\!] + J^{\alpha-}[\![h^\alpha]\!]$$
$$+ \mathbf{A}^{\alpha-}\cdot[\![\boldsymbol{\nabla}^\alpha_0\mathbf{a}^\alpha]\!] + \mathbf{B}^{\alpha-}\cdot[\![\boldsymbol{\nabla}^\alpha_0\mathbf{b}^\alpha]\!], \quad \text{(C2)}$$

$$\rho^\alpha_0\theta^{\alpha-}[\![D^\alpha_t\eta^\alpha]\!] = J^{\alpha-}([\![\epsilon^\alpha]\!] - \boldsymbol{\pi}^{\alpha-}_\mathsf{a}\cdot[\![D^\alpha_t\mathbf{a}^\alpha]\!]), \quad \text{(C3)}$$

where $\boldsymbol{\pi}^\alpha_\mathsf{a} = \rho^\alpha\partial u^\alpha/\partial\mathbf{a}^\alpha$. With $f^\alpha\to\eta^\alpha$, putting (C3) into (237) gives $[\![\boldsymbol{\nabla}^\alpha_0\eta^\alpha]\!]$ in terms of $\delta_t[\![\eta^\alpha]\!]$ and jumps on the right of (C3). This $[\![\boldsymbol{\nabla}^\alpha_0\eta^\alpha]\!]$ is inserted in (C2). The fourth term on the right of (C2) is $-\frac{1}{\mathcal{U}}\mathbf{A}^{\alpha-}\cdot[\![D^\alpha_t\mathbf{a}^\alpha]\!]$ via (238). From this, (221), and (C3), the fifth term includes

$$[\![\boldsymbol{\nabla}^\alpha_0\mathbf{b}^\alpha]\!] = \mathbf{b}^{\prime\alpha-}[\![\boldsymbol{\nabla}^\alpha_0 J^\alpha]\!] - (1/\mathcal{U})\,\mathbf{b}^{\alpha-}_\mathsf{a}\cdot[\![D^\alpha_t\mathbf{a}^\alpha]\!]$$
$$+ \frac{\mathbf{b}^{\alpha-}_\eta}{\mathcal{U}}\left\{\delta_t[\![\eta^\alpha]\!] - \frac{J^{\alpha-}([\![\epsilon^\alpha]\!] - \boldsymbol{\pi}^{\alpha-}_\mathsf{a}\cdot[\![D^\alpha_t\mathbf{a}^\alpha]\!])}{\rho^\alpha_0\theta^{\alpha-}}\right\}, \quad \text{(C4)}$$

$$\mathbf{b}^\alpha_\mathsf{a} = \partial\bar{\mathbf{b}}^\alpha/\partial\mathbf{a}^\alpha, \quad \mathbf{b}^\alpha_\eta = \partial\bar{\mathbf{b}}^\alpha/\partial\eta^\alpha. \quad \text{(C5)}$$

Putting (C4) into (C2), the latter is inserted into (C1):

$$\delta_t[\![J^\alpha]\!] = \frac{1}{2\mathcal{U}}\left\{\left(\mathcal{U}^2 - \frac{\hat{\mathsf{C}}^{\alpha-}}{\rho^\alpha_0}\right)[\![\boldsymbol{\nabla}^\alpha_0 J^\alpha]\!] - \frac{\hat{\mathsf{G}}^{\alpha-}}{\rho^\alpha_0\mathcal{U}}\delta_t[\![\eta^\alpha]\!]\right.$$
$$- \delta_t\mathcal{U}[\![J^\alpha]\!] - \frac{J^{\alpha-}}{\rho^\alpha_0}[\![h^\alpha]\!] + \frac{J^{\alpha-}\hat{\mathsf{G}}^{\alpha-}}{(\rho^\alpha_0)^2\mathcal{U}\theta^{\alpha-}}[\![\epsilon^\alpha]\!]$$
$$\left. + \mathbf{L}^{\alpha-}\cdot[\![D^\alpha_t\mathbf{a}^\alpha]\!]\right\}, \quad \text{(C6)}$$

$$\mathbf{L}^\alpha = \frac{1}{\rho^\alpha_0\mathcal{U}}\left\{\mathbf{A}^\alpha + \mathbf{B}^\alpha\cdot\mathbf{b}^\alpha_\mathsf{a} - \frac{J^\alpha\hat{\mathsf{G}}^\alpha}{\rho^\alpha_0\theta^\alpha}\boldsymbol{\pi}^\alpha_\mathsf{a}\right\}. \quad \text{(C7)}$$

From (202), (211), (212), (217), (222), (238), and (225),

$$\rho^\alpha_0\delta_t[\![u^\alpha]\!] = -(P^{\alpha-} + \rho^\alpha_0\mathcal{U}^2[\![J^\alpha]\!])\delta_t[\![J^\alpha]\!]$$
$$- [\![J^\alpha]\!]\delta_t P^{\alpha-} - \rho^\alpha_0\mathcal{U}[\![J^\alpha]\!]^2\delta_t\mathcal{U}, \quad \text{(C8)}$$

$$\rho^\alpha_0\delta_t[\![u^\alpha]\!] = -P^{\alpha-}\delta_t[\![J^\alpha]\!] + \rho^\alpha_0\theta^{\alpha-}\delta_t[\![\eta^\alpha]\!], \quad \text{(C9)}$$

$$\delta_t P^{\alpha-} = \delta_t[\![P^\alpha]\!] = -\hat{\mathsf{C}}^{\alpha-}\delta_t[\![J^\alpha]\!] - \hat{\mathsf{G}}^{\alpha-}\delta_t[\![\eta^\alpha]\!]. \quad \text{(C10)}$$

Eliminating $\delta_t[\![u^\alpha]\!]$ and $\delta_t P^{\alpha-}$, then differentiating (211),

$$\rho^\alpha_0[\![J^\alpha]\!]^2\mathcal{U}\delta_t\mathcal{U} = \mathsf{G}^{\alpha-}[\![J^\alpha]\!](1 - 1/\hat{\zeta}^\alpha)\delta_t[\![\eta^\alpha]\!]$$
$$+ \hat{\mathsf{C}}^{\alpha-}(1 - \hat{\xi}^\alpha)[\![J^\alpha]\!], \quad \text{(C11)}$$

$$\hat{\xi}^\alpha = \rho^\alpha_0\mathcal{U}^2/\hat{\mathsf{C}}^{\alpha-}, \quad \hat{\zeta}^\alpha = \hat{\mathsf{G}}^{\alpha-}[\![J^\alpha]\!]/(\rho^\alpha_0\theta^{\alpha-}); \quad \text{(C12)}$$

$$2\rho^\alpha_0[\![J^\alpha]\!]\mathcal{U}\delta_t\mathcal{U} = \hat{\mathsf{C}}^{\alpha-}(1 - \hat{\xi}^\alpha)\delta_t[\![J^\alpha]\!] + \hat{G}^{\alpha-}\delta_t[\![\eta^\alpha]\!]. \quad \text{(C13)}$$

APPENDIX D: COEFFICIENTS FOR WEAK SHOCK EVOLUTION

For solid phases, (245)–(250) and Table III utilize

$$P^{\alpha+} = n^\alpha_0\{p^\alpha_{R0} - (\sigma^\alpha_A)^{1+}_1\}, \quad \mathsf{G}^{\alpha+} = -\rho^\alpha_0\theta_0\gamma^\alpha_0; \quad \text{(D1)}$$

$$(\partial\hat{\mathsf{G}}^\alpha/\partial J^\alpha)^+ = -\hat{\mathsf{G}}^{\alpha+}(1 + \gamma^\alpha_0), \quad \text{(D2)}$$

$$\hat{\mathsf{C}}^{\alpha+} = \mathsf{C}^{\alpha+}, \quad \hat{\mathsf{C}}^{\prime\alpha+} = \mathsf{C}^{\prime\alpha+}, \quad \hat{\mathsf{G}}^{\alpha+} = \mathsf{G}^{\alpha+}, \quad \text{(D3)}$$

$$\mathsf{C}^{\alpha+} = \mathsf{C}^{\alpha+}_V + \mathsf{C}^{\alpha+}_S + \mathsf{C}^{\alpha+}_\Gamma + \mathsf{C}^{\alpha+}_A + \mathsf{C}^{\alpha+}_F + \mathsf{C}^{\alpha+}_\Phi, \quad \text{(D4)}$$

$$\mathsf{C}^{\prime\alpha+} = \mathsf{C}^{\prime\alpha+}_V + \mathsf{C}^{\prime\alpha+}_S + \mathsf{C}^{\prime\alpha+}_\Gamma + \mathsf{C}^{\prime\alpha+}_A + \mathsf{C}^{\prime\alpha+}_F + \mathsf{C}^{\prime\alpha+}_\Phi; \quad \text{(D5)}$$

$$\mathsf{C}^{\alpha+}_V = n^\alpha_0(p^\alpha_{R0} + B^\alpha_\eta), \quad \mathsf{C}^{\alpha+}_S = \frac{4}{3}n^\alpha_0\mu^\alpha_S, \quad \text{(D6)}$$

$$\mathsf{C}^{\alpha+}_\Gamma = n^\alpha_0\left(B^\alpha_\theta\sum_l\beta^\alpha_{Vl} + \frac{4}{3}\mu^\alpha_S\sum_m\beta^\alpha_{Sm}\right), \quad \text{(D7)}$$

$$\mathsf{C}^{\alpha+}_A = n^\alpha_0(\partial^2\Psi^\alpha_{Ak}/\partial(J^\alpha)^2)^+ \quad (k = 1), \quad \text{(D8)}$$

$$\mathsf{C}^{\alpha+}_F = \begin{cases} \frac{8}{9}n^\alpha_0\mu^\alpha_k & (\kappa^\alpha_k = 0), \\ 0 & (\kappa^\alpha_k = \frac{1}{3}), \end{cases} \quad \text{(D9)}$$

$$\mathsf{C}^{\alpha+}_\Phi = \begin{cases} \frac{8}{9}n^\alpha_0\mu^\alpha_k\sum_n\beta^\alpha_{\Phi k,n} & (\kappa^\alpha_k = 0), \\ 0 & (\kappa^\alpha_k = \frac{1}{3}); \end{cases} \quad \text{(D10)}$$

$$\mathsf{C}^{\prime\alpha+}_V = -n^\alpha_0\{2p^\alpha_{R0} + B^\alpha_\eta(1 + B^\alpha_{\eta p})\}, \quad \text{(D11)}$$

$$\mathsf{C}^{\prime\alpha+}_S = -\frac{28}{9}n^\alpha_0\mu^\alpha_S, \quad \text{(D12)}$$

$$\mathsf{C}^{\prime\alpha+}_\Gamma = -3n^\alpha_0\left(B^\alpha_\theta\sum_l\beta^\alpha_{Vl} + \frac{28}{27}\mu^\alpha_S\sum_m\beta^\alpha_{Sm}\right), \quad \text{(D13)}$$

$$\mathsf{C}^{\prime\alpha+}_A = n^\alpha_0(\partial^3\Psi^\alpha_{Ak}/\partial(J^\alpha)^3)^+ \quad (k = 1), \quad \text{(D14)}$$

$$\mathsf{C}^{\prime\alpha+}_F = \begin{cases} \frac{24}{27}n^\alpha_0\mu^\alpha_k & (\kappa^\alpha_k = 0), \\ 0 & (\kappa^\alpha_k = \frac{1}{3}), \end{cases} \quad \text{(D15)}$$

$$\mathsf{C}^{\prime\alpha+}_\Phi = \begin{cases} \frac{24}{27}n^\alpha_0\mu^\alpha_k\sum_n\beta^\alpha_{\Phi k,n} & (\kappa^\alpha_k = 0), \\ 0 & (\kappa^\alpha_k = \frac{1}{3}); \end{cases} \quad \text{(D16)}$$

$$\mathbf{B}^{\alpha+}\to\mathbf{0}, \quad \mathbf{b}^{\alpha+}_\mathsf{a}\to\mathbf{0}, \quad \mathbf{b}^{\prime\alpha+}\to\mathbf{0}, \quad \mathbf{b}^{\alpha+}_\eta\to\mathbf{0}, \quad \text{(D17)}$$

$$\mathbf{A}^{\alpha+} \rightarrow -n_0^\alpha \left\{ \frac{\partial \mathbf{Q}_{Vl}^\alpha}{\partial J^\alpha}, \frac{\partial \mathbf{Q}_{Sm}^\alpha}{\partial J^\alpha}, \frac{\partial \mathbf{Q}_{\Phi k,n}^\alpha}{\partial J^\alpha} \right\}^+ , \tag{D18}$$

$$\left(\frac{\partial \left(D_t^\alpha \mathbf{a}^\alpha \right)}{\partial J^\alpha} \right)^+ \rightarrow \left\{ \frac{\partial \mathbf{Q}_{Vl}^\alpha / \partial J^\alpha}{\beta_{Vl}^\alpha B_\theta^\alpha \tau_{Vl}^\alpha}, \frac{\partial \mathbf{Q}_{Sm}^\alpha / \partial J^\alpha}{\beta_{Sm}^\alpha \mu_S^\alpha \tau_{Sm}^\alpha}, \left(\partial \mathbf{Q}_{\Phi k,n}^\alpha / \partial J^\alpha \right) / \left(\beta_{\Phi k,n}^\alpha \mu_k^\alpha \tau_{\Phi k,n}^\alpha \right) \right\}^+ , \quad \boldsymbol{\pi}_{\mathsf{a}}^{\alpha+} \rightarrow \mathbf{0}, \tag{D19}$$

$$\mathbf{A}^{\alpha+} \cdot \left(\partial \left(D_t^\alpha \mathbf{a}^\alpha \right) / \partial J^\alpha \right)^+ \rightarrow \mathcal{A}_{\Gamma V}^\alpha + \mathcal{A}_{\Gamma S}^\alpha + \mathcal{A}_\Phi^\alpha , \tag{D20}$$

$$\mathcal{A}_{\Gamma V}^\alpha = -3 n_0^\alpha B_\theta^\alpha \sum_l \frac{\beta_{Vl}^\alpha}{\tau_{Vl}^\alpha}, \quad \mathcal{A}_{\Gamma S}^\alpha = -\frac{8}{3} n_0^\alpha \mu_S^\alpha \sum_m \frac{\beta_{Sm}^\alpha}{\tau_{Sm}^\alpha},$$

$$\mathcal{A}_\Phi^\alpha = \begin{cases} -\frac{32}{27} n_0^\alpha \mu_k^\alpha \sum_n \beta_{\Phi k,n}^\alpha / \tau_{\Phi k,n}^\alpha & (\kappa_k^\alpha = 0), \\ 0 & (\kappa_k^\alpha = \frac{1}{3}). \end{cases} \tag{D21}$$

[1] Y.-C. Fung, *Biomechanics: Motion, Flow, Stress, and Growth* (Springer, New York, 1990).

[2] Y.-C. Fung, *Biomechanics: Mechanical Properties of Living Tissues*, 2nd ed. (Springer, New York, 1993).

[3] H. Saraf, K. T. Ramesh, A. M. Lennon, A. C. Merkle, and J. C. Roberts, J. Biomech. **40**, 1960 (2007).

[4] J. M. Wilgeroth, P. Hazell, and G. J. Appleby-Thomas, in *Shock Compression of Condensed Matter - 2011*, edited by M. L. Elert, W. T. Buttler, J. P. Borg, J. L. Jordan, and T. J. Vogler, AIP Conf. Proc. Vol. 1426 (AIP, Melville, NY, 2012), p. 139.

[5] J. D. Clayton, Biomech. Model. Mechanobiol. **19**, 2603 (2020).

[6] J. D. Clayton, R. J. Banton, and A. D. Freed, in *Shock Compression of Condensed Matter - 2019*, edited by J. M. D. Lane, T. C. Germann, M. R. Armstrong, R. Wixom, D. Damm, and J. Zaug, AIP Conf. Proc. Vol. 2272 (AIP, Melville, NY, 2020), p. 040001.

[7] T. Ricken, U. Dahmen, and O. Dirsch, Biomech. Model. Mechanobiol. **9**, 435 (2010).

[8] G. A. Holzapfel and R. W. Ogden, Phil. Trans. R. Soc. A **367**, 3445 (2009).

[9] D. Sachs, A. Wahlsten, S. Kozerke, G. Restivo, and E. Mazza, Biomech. Model. Mechanobiol. **20**, 969 (2021).

[10] W. Yang, V. R. Sherman, B. Gludovatz, E. Schaible, P. Stewart, R. O. Ritchie, and M. A. Meyers, Nat. Commun. **6**, 6649 (2015).

[11] A. Zubelewicz, Sci. Rep. **3**, 1323 (2013).

[12] P. Van Liedekerke, E. Tijskens, H. Ramon, P. Ghysels, G. Samaey, and D. Roose, Phys. Rev. E **81**, 061906 (2010).

[13] G. A. Holzapfel, T. C. Gasser, and R. W. Ogden, J. Elast. **61**, 1 (2000).

[14] G. Chagnon, M. Rebouah, and D. Favier, J. Elast. **120**, 129 (2015).

[15] M. B. Rubin and S. R. Bodner, Int. J. Solids Struct. **39**, 5081 (2002).

[16] O. Gültekin, G. Sommer, and G. A. Holzapfel, Comp. Methods Biomech. Biomed. Eng. **19**, 1647 (2016).

[17] T. C. Gasser, R. W. Ogden, and G. A. Holzapfel, J. R. Soc. Interface **3**, 15 (2006).

[18] J. Planas, G. V. Guinea, and M. Elices, Phys. Rev. E **76**, 041903 (2007).

[19] M. Kalhöfer-Köchling, E. Bodenschatz, and Y. Wang, Phys. Rev. Appl. **13**, 064039 (2020).

[20] D. Ito, E. Tanaka, and S. Yamamoto, J. Mech. Behav. Biomed. Mater. **3**, 85 (2010).

[21] W. Li, J. Med. Biol. Eng. **36**, 285 (2016).

[22] A. Raina and C. Miehe, Proc. Appl. Math. Mech. **15**, 103 (2015).

[23] O. Gültekin, S. Hager, H. Dal, and G. A. Holzapfel, Biomech. Model. Mechanobiol. **18**, 1607 (2019).

[24] V. I. Levitas, V. A. Levin, K. M. Zingerman, and E. I. Freiman, Phys. Rev. Lett. **103**, 025702 (2009).

[25] L. Yang and K. Dayal, Appl. Phys. Lett. **96**, 081916 (2010).

[26] J. D. Clayton and J. Knap, Physica D **240**, 841 (2011).

[27] A. Acharya and J. Vinals, Phys. Rev. B **102**, 064109 (2020).

[28] A. Karma, D. A. Kessler, and H. Levine, Phys. Rev. Lett. **87**, 045501 (2001).

[29] V. I. Marconi and E. A. Jagla, Phys. Rev. E **71**, 036110 (2005).

[30] R. Spatschek, C. Muller-Gugenberger, E. Brener, and B. Nestler, Phys. Rev. E **75**, 066111 (2007).

[31] J. D. Clayton and J. Knap, Int. J. Fract. **189**, 139 (2014).

[32] V. I. Levitas, J. Mech. Phys. Solids **70**, 154 (2014).

[33] V. I. Levitas, A. V. Idesman, and A. K. Palakala, J. Appl. Phys. **110**, 033531 (2011).

[34] D. Santillan, J.-C. Mosquera, and L. Cueto-Felgueroso, Phys. Rev. E **96**, 053002 (2017).

[35] M. A. Biot, J. Appl. Phys. **12**, 155 (1941).

[36] C. A. Truesdell and R. A. Toupin, The classical field theories, in *Handbuch der Physik*, edited by S. Flugge (Springer, Berlin, 1960), Vol. III, pp. 226–793.

[37] R. M. Bowen, Theory of mixtures, in *Continuum Physics*, edited by A. C. Eringen (Academic Press, New York, 1976), Vol. 3, pp. 1–127.

[38] R. M. Bowen, Int. J. Eng. Sci. **20**, 697 (1982).

[39] M. Yang and L. A. Taber, J. Biomech. **24**, 587 (1991).

[40] J. M. Huyghe, T. Arts, D. H. V. Campen, and R. S. Reneman, Am. J. Physiol. **262**, H1256 (1992).

[41] R. A. Regueiro, B. Zhang, and S. L. Wozniak, Comp. Mod. Eng. Sci. **98**, 1 (2014).

[42] H. S. Suh and W. Sun, Comput. Methods Appl. Mech. Eng. **387**, 114182 (2021).

[43] Y. Zheng, Y. Jiang, and Y. Cao, J. Mech. Phys. Solids **150**, 104339 (2021).

[44] K. Terzaghi, *Theoretical Soil Mechanics* (John Wiley & Sons, New York, 1943).

[45] S. M. Fielding, J. O. Cochran, J. Huang, D. Bi, and M. C. Marchetti, Phys. Rev. E **108**, L042602 (2023).

[46] Y. Mulla, G. Oliveri, J. T. B. Overvelde, and G. H. Koenderink, Phys. Rev. Lett. **120**, 268002 (2018).

[47] M. R. Baer and J. W. Nunziato, Int. J. Multiphase Flow **12**, 861 (1986).

[48] D. Madjarevic and S. Simic, Phys. Rev. E **100**, 023119 (2019).

[49] A. Grillo, M. Carfagna, and S. Federico, J. Eng. Math. **109**, 139 (2018).

[50] J. D. Clayton, Int. J. Eng. Sci. **175**, 103675 (2022).

[51] J. M. Wilgeroth, P. J. Hazell, and G. J. Appleby-Thomas, Int. J. Impact Eng. **50**, 83 (2012).

[52] J. D. Clayton, Symmetry **15**, 1828 (2023).

[53] K. Takamizawa and T. Matsuda, J. Appl. Mech. **57**, 321 (1990).

[54] A. Yavari, J. Nonlin. Sci. **20**, 781 (2010).

[55] S. Sadik, A. Angoshtari, A. Goriely, and A. Yavari, J. Nonlin. Sci. **26**, 929 (2016).

[56] J. D. Clayton, J. Geom. Phys. **112**, 118 (2017).

[57] J. D. Clayton, Z. Angew. Math. Phys. **68**, 9 (2017).

[58] A. Bejancu, *Finsler Geometry and Applications* (Ellis Horwood, New York, 1990).

[59] Y. Takano and H. Koibuchi, Phys. Rev. E **95**, 042411 (2017).

[60] S. Ikeda, Tensor, N.S. **27**, 361 (1973); J. Math. Phys. **22**, 1211 (1981).

[61] V. A. Eremeyev and V. Konopinska-Zmyslowska, Symmetry **12**, 1632 (2020).

[62] J. D. Clayton, Int. J. Geom. Methods Mod. Phys. **15**, 1850113 (2018).

[63] J. D. Clayton, Math. Mech. Solids **27**, 910 (2022).

[64] B. D. Coleman and M. E. Gurtin, Proc. R. Soc. Lond. A **292**, 562 (1966).

[65] P. J. Chen and M. E. Gurtin, Phys. Fluids **14**, 1091 (1971).

[66] R. M. Bowen and P. J. Chen, Arch. Ration. Mech. Anal. **53**, 277 (1974).

[67] H. Rund, *The Differential Geometry of Finsler Spaces* (Springer-Verlag, Berlin, 1959).

[68] S. Amari, A theory of deformations and stresses of ferromagnetic substances by Finsler geometry, in *RAAG Memoirs*, edited by K. Kondo (Gakujutsu Bunken Fukyu-Kai, Tokyo, Japan, 1962), Vol. 3, pp. 257–278.

[69] J. D. Clayton, *Nonlinear Elastic and Inelastic Models for Shock Compression of Crystalline Solids* (Springer, Cham, 2019).

[70] C. A. Truesdell, *Rational Thermodynamics*, 2nd ed. (Springer-Verlag, New York, 1984).

[71] K. R. Rajagopal and L. Tao, *Mechanics of Mixtures* (World Scientific, Singapore, 1995).

[72] R. Hall and K. Rajagopal, Exp. Mech. **60**, 591 (2020).

[73] A. C. Hansen, R. L. Crane, M. H. Damson, R. P. Donovan, D. T. Horning, and J. L. Walker, Int. J. Eng. Sci. **29**, 561 (1991).

[74] J. D. Humphrey and K. R. Rajagopal, Math. Models Methods Appl. Sci. **12**, 407 (2002).

[75] G. A. Ateshian and B. K. Zimmerman, J. Biomech. Eng. **144**, 041011 (2022).

[76] T. Ruggeri and S. Simic, Phys. Rev. E **80**, 026317 (2009).

[77] M. E. Gurtin, Physica D **92**, 178 (1996).

[78] H. Rund, Monatshefte fur Math. **79**, 233 (1975).

[79] J. D. Clayton, *Differential Geometry and Kinematics of Continua* (World Scientific, Singapore, 2014).

[80] J. D. Clayton, J. Mech. Phys. Solids **157**, 104633 (2021).

[81] A. E. Green and R. S. Rivlin, Zeit. Angew. Math. Phys. **15**, 290 (1964).

[82] J. E. Marsden and T. J. R. Hughes, *Mathematical Foundations of Elasticity* (Prentice-Hall, New Jersey, 1983).

[83] C. A. Truesdell, Rend. Accad. Lincei **44**, 381 (1968).

[84] Misprints in Eqs. (2.15), (4.1), $(4.19)_1$, $(4.30)_3$, (4.45), (4.63), $(5.2)_2$, and $(5.13)_2$ of Ref. [50] are corrected herein.

[85] J. Casey, Int. J. Struct. Changes Solids **3**, 61 (2011).

[86] J. D. Clayton, Int. J. Fract. **208**, 53 (2017).

[87] E. Kuhl and P. Steinmann, Proc. R. Soc. Lond. A **459**, 2547 (2003).

[88] K. Y. Volokh, Acta Biomater. **2**, 493 (2006).

[89] J. E. Dunn and J. Serrin, Arch. Ration. Mech. Anal. **88**, 95 (1985).

[90] R. M. Bowen and R. L. Rankin, Arch. Ration. Mech. Anal. **51**, 261 (1973).

[91] G. A. Holzapfel and J. C. Simo, Int. J. Solids Struct. **33**, 3019 (1996).

[92] G. A. Holzapfel, Int. J. Numer. Meth. Eng. **39**, 3903 (1996).

[93] A. Menzel, Biomech. Model. Mechanobiol. **3**, 147 (2005).

[94] V. A. Lubarda and A. Hoger, Int. J. Solids Struct. **39**, 4627 (2002).

[95] B. D. Coleman and W. Noll, Arch. Ration. Mech. Anal. **13**, 167 (1963).

[96] B. D. Coleman and M. E. Gurtin, J. Chem. Phys. **47**, 597 (1967).

[97] Z. T. Irwin, J. D. Clayton, and R. A. Regueiro, Int. J. Numer. Meth. Eng. **125**, e7411 (2024).

[98] J.-P. Poirier and A. Tarantola, Phys. Earth Planet. Inter. **109**, 1 (1998).

[99] J. D. Clayton, Int. J. Eng. Sci. **79**, 1 (2014).

[100] J. D. Clayton and A. D. Freed, Mech. Soft Mater. **2**, 3 (2020).

[101] D. Balzani, P. Neff, J. Schroder, and G. A. Holzapfel, Int. J. Solids Struct. **43**, 6052 (2006).

[102] G. A. Holzapfel, T. C. Gasser, and M. Stadler, Eur. J. Mech. A Sol. **21**, 441 (2002).

[103] J. D. Clayton and A. D. Freed, Acta Mech. **231**, 3319 (2020).

[104] J. Stålhand, R. M. McMeeking, and G. A. Holzapfel, J. Mech. Phys. Solids **94**, 490 (2016).

[105] J. A. C. Martins, E. B. Pires, R. Salvado, and P. B. Dinis, Comput. Methods Appl. Mech. Eng. **151**, 419 (1998).

[106] G. Franchini, I. D. Breslavsky, F. Giovanniello, A. Kassab, G. A. Holzapfel, and M. Amabili, Proc. Natl. Acad. Sci. USA **119**, e2117232119 (2022).

[107] A. Kumar and A. Yavari, J. Mech. Phys. Solids **181**, 105449 (2023).

[108] G.-J. Guo and Y.-G. Zhang, Mol. Phys. **99**, 283 (2001).

[109] T. Taniguchi, S. Yamamoto, A. Hayakawa, E. Tanaka, H. Kimpara, and K. Miki, Strain-rate and muscle-tonus dependence of mechanical properties of rabbit tibialis anterior muscle, in *Proceedings of the International Conference on Advanced Technology in Experimental Mechanics: Second Asian Conference in Experimental Mechanics*, edited by K. Tanaka (The Japan Society of Mechanical Engineers, Nagoya, Japan, 2003), p. OS07W0228.

[110] J. D. Clayton, D. L. McDowell, and D. J. Bammann, Int. J. Eng. Sci. **42**, 427 (2004).

[111] M. Epstein and G. Maugin, Int. J. Plast. **16**, 951 (2000).

[112] F. Xu, T. J. Lu, and K. A. Seffen, J. Mech. Phys. Solids **56**, 1852 (2008).

[113] J. C. Chato, J. Biomech. Eng. **102**, 110 (1980).

[114] R. J. Nims and G. A. Ateshian, J. Elast. **129**, 69 (2017).

[115] J. D. Humphrey, J. Elast. **145**, 49 (2021).

[116] J. Zhu, L.-Q. Chen, J. Shen, and V. Tikare, Phys. Rev. E **60**, 3564 (1999).

[117] G. S. Kell, J. Chem. Eng. Data **20**, 97 (1975).

[118] K. Nagayama, Y. Mori, K. Shimada, and M. Nakahara, J. Appl. Phys. **91**, 476 (2002).

[119] D.-K. Yao, C. Zhang, K. Maslov, and L. V. Wang, J. Biomed. Opt **19**, 017007 (2014).

[120] K. C. Jones, W. Nie, J. Hu, J. Turian, A. Kassaee, C. Sehgal, and S. Avery, Phys. Med. Biol. **63**, 025018 (2018).

[121] A. Morro, Arch. Mech. **32**, 145 (1980); **32**, 193 (1980).

[122] H. Nagoya, T. Obara, and K. Takayama, Underwater shock propagation and focusing in inhomogeneous media, in *Shockwaves at Marseille*, edited by R. Brun (Springer-Verlag, Berlin, 1995), Vol. 3, pp. 439–444.

[123] M. Neville and R. Mathias, J. Physio. **288**, 45 (1979).

[124] B. Song, W. Chen, Y. Ge, and T. Weerasooriya, J. Biomech. **40**, 2999 (2007).

[125] D. A. Morrow, T. Donahue, G. Odegard, and K. Kaufman, J. Mech. Behav. Biomed. Mater. **3**, 124 (2010).

[126] O. J. Aryeetey, M. Frank, A. Lorenz, and D. H. Pahr, J. Mech. Behav. Biomed. Mater. **135**, 105429 (2022).

[127] E. Maher, M. Early, A. Creane, C. Lally, and D. J. Kelly, J. Biomech. **45**, 1393 (2012).

[128] P. J. Flory and O. K. Spurr, J. Am. Chem. Soc. **83**, 1308 (1961).

[129] R. A. Sanderson, R. Foley, G. McIvor, and W. Kirkaldy-Willis, Clin. Ortho. Rel. Res. **113**, 27 (1975).

[130] T. Winkler, P. Roth, G. Matziolis, M. Schumann, S. Hahn, P. Strube, G. Stoltenburg-Didinger, C. Perka, G. Duda, and S. Tohtz, Acta Orthopaed. **82**, 102 (2011).

[131] F. Pervin, W. W. Chen, and T. Weerasooriya, J. Mech. Behav. Biomed. Mater. **4**, 76 (2011).

[132] A. Bonfiglio, K. Leungchavaphongse, R. Repetto, and J. H. Siggers, J. Biomech. Eng. **132**, 111011 (2010).

[133] Z. Gao, K. Lister, and J. P. Desai, Ann. Biomed. Eng. **38**, 505 (2010).

[134] B. Soroushian, W. M. Whelan, and M. C. Kolios, J. Biomed. Opt. **15**, 065002 (2010).

[135] T. Azar and V. Hayward, Estimation of the fracture toughness of soft tissue from needle insertion, in *Proceedings of 4th International Symposium on Biomedical Simulation - 2008*, Lecture Notes in Computer Science, edited by F. Bello and E. Edwards (Springer-Verlag, Berlin, 2008), Vol. 5104, pp. 166–175.

[136] E. Roan and K. Vemaganti, Med. Biol. Eng. Comput. **49**, 497 (2011).

[137] A. Malečková, P. Kochova, R. Palek, V. Liska, P. Mik, T. Bonkowski, M. Horak, and Z. Tonar, Physiol. Meas. **42**, 025008 (2021).

[138] C. Untaroiu, Y. Lu, S. Siripurapu, and A. Kemper, J. Mech. Behav. Biomed. Mater. **41**, 280 (2015).

[139] J. M. Boteler and G. T. Sutherland, J. Appl. Phys. **96**, 6919 (2004).

[140] J. Lamsfuss and S. Bargmann, J. Mech. Behav. Biomed. Mater. **134**, 105386 (2022).

[141] J. D. Clayton, *Nonlinear Mechanics of Crystals* (Springer, Dordrecht, 2011).

[142] Q. Wang, S. Pei, X. L. Lu, L. Wang, and Q. Wu, J. Mech. Behav. Biomed. Mater. **102**, 103504 (2020).

[143] S. C. Saha, I. Francis, X. Huang, and A. R. Paul, Phys. Fluids **34**, 061906 (2022).

[144] P. Khandagale, T. Breitzman, C. Majidi, and K. Dayal, Phys. Rev. E **107**, 064501 (2023).